Crack detection in frames using natural frequency degradations

Amr Labib

Thesis submitted to Cardiff University for the award of PhD

December 2015

Form: PGR_Submission_2012_01

NOTICE OF SUBMISSION OF THESIS FORM: POSTGRADUATE RESEARCH

CARDIFF UNIVERSITY
PRIFYSGOL CAERDYDD

DECLARATION

This work has not been submitted in substance for any other degree or award at this or any other university or place of learning, nor is being submitted concurrently in candidature for any degree or other award.

Signed ..... (candidate) Date 23/12/2015

STATEMENT 1

This thesis is being submitted in partial fulfillment of the requirements for the degree of PhD (insert MCh, MD, MPhil, PhD etc, as appropriate)

Signed ..... (candidate) Date 23/12/2015

STATEMENT 2

This thesis is the result of my own independent work/investigation, except where otherwise stated. Other sources are acknowledged by explicit references. The views expressed are my own.

Signed ..... (candidate) Date 23/12/2015

STATEMENT 3

I hereby give consent for my thesis, if accepted, to be available for photocopying and for inter-library loan, and for the title and summary to be made available to outside organisations.

Signed ..... (candidate) Date 23/12/2015

Acknowledgments

I would like to express my deep appreciation and gratitude to my supervisors, Prof. David Kennedy and Prof. Carol Featherston, for their tremendous support and guidance during the past three years. I would also like to sincerely thank my parents for their patience and encouragement.

Summary

Crack detection at an early stage can prevent catastrophic structural failures. In this thesis, the inverse problem of crack detection in frames is studied. The direct problem of calculating the natural frequencies of beams and frames with multiple cracks is first tackled. A new method for natural frequency calculation is devised. The cracks are modelled as rotational springs. 4×4 dynamic stiffness matrices for beams are evaluated in a recursive manner, according to the number of cracks, by applying partial Gaussian eliminations. The resulting transcendental eigenvalue problem is solved using the Wittrick–Williams algorithm to extract the natural frequencies. Additional sign counts resulting from the partial Gaussian eliminations must be accounted for when applying the algorithm. The dynamic stiffness matrix of a frame with multiply cracked members is then assembled. The natural frequency calculation method forms a basis for detecting a single crack in a frame using only natural frequency measurements. Each frame member is discretised into a number of points. Selected natural frequencies are calculated accurately in the uncracked case and when the crack is placed individually at each discretisation point. The variation between the uncracked and cracked frequencies is normalised giving a number of curves corresponding to the selected frequencies. The normalisation is then applied on the measured frequencies. For noise free measurements, point crack locations are obtained. Applying the principles of interval arithmetic, noisy measurements give crack location ranges. Empirical probability distributions are used to graphically represent these ranges and their relative probabilities. Crack severity ranges are then obtained. The detection method is validated experimentally on a frame with scaled down dimensions. The fast Fourier transform is used to convert the time domain vibration signal into the frequency domain. Using higher order natural frequencies, two enhancement procedures for the detection method are devised and applied theoretically.

Contents

List of figures

List of tables

Notation

A	cross-sectional area
A, B	labels for beam elements
a	point on a frame satisfying $\hat{G}_i(a) = 0$
a_0, $a_1 \ldots a_n$	coefficients of the function $C(d/h)$
a_m, b_m, c_m, d_m, e_m, f_m, α_m, β_m, γ_m, z_m, $\overline{z}_m$	terms of the 6 × 6 dynamic stiffness matrix of an uncracked or cracked beam
b_i, c_i	coefficients of the function $\hat{G}_i$
$C(d/h)$	dimensionless function of the crack depth to section height ratio
C_m, S_m, $C_m^{'}$, $S_m^{'}$,	cosine, sine, coshine, and shine of λL_m
d^*	randomly assumed crack depth (≤ 0.4) for the calculation of the normalised frequency variations $\overline{\delta}_i$
D_m	denominator in the expansion of the dynamic stiffness matrix terms corresponding to shear and bending
d	crack depth
E	Young's modulus
$F(a, \{b_i, c_i\})$	least squares residual function used in the calculation of a
F_1, F_2, F_3, F_i, F_j	external shear forces at nodes 1, 2, 3, i, and j
f	highest mode number within a selected natural frequency group
$f_i(x/l)$	function of the dimensionless crack location x/l
$f_{1i}(x_1/l)$, $f_{2i}(x_2/l)$,…	function of the dimensionless crack locations corresponding to cracks 1, 2,…, and natural frequency i
f^*	compliance of the rotational spring equal to $1/k^*$

$\bar{f}^*$	compliance of the axial spring equal to $1/\bar{k}^*$
g	gravitational acceleration
G_i	difference between the normalised natural frequency variation $\overline{\delta}_i$ and the normalised simulated or measured natural frequency variation $\overline{\delta}_{im}$
G_{ij}	values of G_i when the crack is present at separate locations x_j in a frame, where $j = 1, 2, 3$
$\hat{G}_i(x/l)$	parabolic least squares fitted function corresponding to G_i
g_{ij}	gradient of the triangular distribution assumed for crack location range j corresponding to natural frequency i
h	cross-sectional height
$h(t)$	a continuous function in time
h_k	discrete value of $h(t)$ at time instant k, where $k = 0, 1,\ldots, N_s - 1$
$\tilde{h}_i$	common triangle height corresponding to natural frequency i, used in the calculation of the empirical probability distribution
$H(\omega)$	Fourier transform of the function $h(t)$
H_n	discrete value of $H(\omega)$ at time instant n, where $n = 0, 1,\ldots, N_s - 1$
I	second moment of area
J	number of natural frequencies lying below a trial frequency ω^*
J_m	number of fixed end natural frequencies lying below ω^* for each beam element $m = \mathrm{A}, \mathrm{B}, \mathrm{C},\ldots$
$\mathbf{K}(\omega)$	6 × 6 dynamic stiffness matrix of an uncracked or cracked beam vibrating at frequency ω
$\mathbf{K}_{\mathrm{Axial}}$	2 × 2 dynamic stiffness matrix of an uncracked or cracked

	beam considering only axial vibrations
$\mathbf{K}_{\text{local}}$	stiffness matrix of a beam in the local coordinate system
$\mathbf{K}_{\text{global}}$	stiffness matrix of a beam in the global coordinate system
$k_{1,1} \ldots k_{N,N}$	$N \times N$ dynamic stiffness matrix terms for mode shape calculation
k^*	stiffness of rotational spring
$\bar{k}^*$	stiffness of axial spring
l	beam or column length
L_{ij}, U_{ij}	lower and upper limits of the crack location range j corresponding to natural frequency i
L_{cj}, U_{cj}	lower and upper limits of the combined crack location range j
M_{1A}, M_{1B}, M_2, M_3, M_i, M_j	external bending moments at nodes 1, 2, 3, i, and j
m	beam elements A, B, AB, ABC…
m_{ij}	half the length of the crack location range j corresponding to natural frequency i
N	number of assumed degrees of freedom in the beam or frame for mode shape calculation
N_s	number of time samples used in the fast Fourier transform, usually taken as a power of 2
$P(x)$	empirical probability distribution function corresponding to all natural frequencies combined
P_o	critical buckling load
$p_i(x)$	probability distribution function corresponding to natural frequency i
P_{1A}, P_{1B}, P_2, P_3	external axial forces at nodes 1, 2, and 3

p_1, p_2, p_3, p_4	functions of the dynamic stiffness matrix terms corresponding to two beam elements connected together with a rotational spring, along with q_1, q_2, and q_3
q_1, q_2, q_3	functions of the dynamic stiffness matrix terms corresponding to two beam elements connected together with a rotational spring, along with Δ_1, and Δ_2
r_i	total number of crack location ranges corresponding to natural frequency i
S_2, S_3, S_4	summations given by $\sum_{j=1}^{3}(x_j/l-a)^2$, $\sum_{j=1}^{3}(x_j/l-a)^3$, $\sum_{j=1}^{3}(x_j/l-a)^4$, used in the calculation of a
$s\{\mathbf{K}\}$	sign count of $\mathbf{K}$, which is the number of negative leading diagonal elements of the upper triangular matrix obtained from $\mathbf{K}$ by standard Gaussian elimination without row interchange
s_c	additional sign counts to be taken into account for each crack c
$\tilde{s}$	functions of the crack severity which do not depend on the mode number
$\tilde{s}_c$	severity function corresponding to crack c
$sn(\sigma_m)$	$= 1$ if $\sigma_m > 0$, and $=$ -1 if $\sigma_m < 0$
$sg\{\Delta_j\}$	$= 1$ if $\Delta_j < 0$, and $= 0$ otherwise, for $j = 1, 2, 3$
$\mathbf{T}$	6 × 6 transformation matrix formed from $\mathbf{t}$
T	total sampling period related to vibration measurements and the fast Fourier transform
T_{i1}, T_{i2}	summations given by $\sum_{j=1}^{3}(x_j/l-a)G_{ij}$, $\sum_{j=1}^{3}(x_j/l-a)^2 G_{ij}$, used in the calculation of a
$\mathbf{t}$	3 × 3 transformation matrix
u_{1A}, u_{1B}, u_2, u_3	axial deformations at nodes 1, 2, and 3

w_1, w_2, w_3, w_i, w_j	shear deformations at nodes 1, 2, 3, i, and j
X, Y	ranges of positive real numbers
X_{LL}, Y_{LL}	lower limits of X and Y
X_{UL}, Y_{UL}	upper limits of X and Y
x	crack location measured along the longitudinal axis of a beam or frame member
x_A, x_I	crack location in frame members A, and I
x_c	location of crack c in a frame member
ΔT	temperature change
$\Delta\omega$	frequency resolution related to the fast Fourier transform
$\Delta\omega_i$	change in the i^{th} natural frequency between the uncracked and cracked case
Δ_1, Δ_2, Δ_3	functions of the dynamic stiffness matrix terms corresponding to two beam elements connected together with a rotational spring
Δ_4, Δ_5	functions of the dynamic stiffness matrix terms corresponding to two beam elements connected together with an axial spring
$\boldsymbol{\delta}_i$	set of natural frequency variations δ_i corresponding to each higher order mode $i \neq$ 1, 2, 3 calculated when a crack having $D/h =$ 0.4 is placed individually at the frame discretisation points
$\boldsymbol{\delta}_{\max}$	set of maximum variations of all selected higher order modes
$\delta_{4\max}, \delta_{7\max}, \ldots, \delta_{f\max}$	maximum natural frequency variations corresponding to modes 4, 7,…, f
δ_i	variation between the uncracked and cracked natural frequencies, equal to $1 - (\omega_{ic}/\omega_{io})$

δ_i^t	combined natural frequency variations due to a series of cracks and also due to temperature change
$\overline{\delta}_i$	normalised frequency variation corresponding to mode i
$\overline{\delta}_{im}$	normalised simulated or measured natural frequency variation
$\overline{\delta}_{im}^L$, $\overline{\delta}_{im}^U$	lower and upper limits of $\overline{\delta}_{im}$
η	frequency function equal to $\omega\sqrt{\mu/EA}$
θ	inclination angle of a beam longitudinal axis from an arbitrary global axis
θ_{1A}, θ_{1B}, θ_2, θ_3, θ_i, θ_j	rotational deformations at nodes 1, 2, 3, i, and j
λ	frequency function equal to $\sqrt[4]{\mu\omega^2/EI}$
λ^*	dimensionless local compliance
μ	mass per unit length
ν	Poisson's ratio
$\xi_1, \xi_2, \xi_3, \xi_4$	fractions of the column and beam lengths in the frame of Section 2.3.2.1
σ_m	denominator of the terms a_m, b_m, c_m, d_m, e_m, f_m, α_m, β_m, γ_m equal to $1 - C_m C_m^{'}$
$\emptyset_i$	constant relating the change in the i^{th} natural frequency to that of the temperature change
ψ_j	displacement (or rotation) corresponding to degree of freedom j
ω	frequency of vibration
ω_i	natural frequency corresponding to mode i
ω_{ia}	natural frequency of the axially loaded member

$\omega_{i\mathrm{u}}$	natural frequency of the unloaded member
ω_{icm}	simulated or measured natural frequency in the cracked case
ω_{icm}^{L}, ω_{icm}^{U}	lower and upper limits of ω_{icm}
ω_{io}	natural frequency in the uncracked case, corresponding to mode i
ω_{iom}	simulated or measured natural frequency in the uncracked case
$\omega_{iom}^{L}, \omega_{iom}^{U}$	lower and upper limits of ω_{iom}
ω_{ic}	natural frequency in the cracked case, corresponding to mode i
$\omega_{\max}$	Nyquist frequency
ω_{s}	sampling frequency
ω^{*}	trial frequency in the application of the Wittrick–Williams algorithm

Chapter 1 – Introduction

1.1. Crack detection

Structures and machinery require regular assessment of their serviceability. Non-destructive testing can be performed in a scheduled and repetitive manner as required, to detect cracks or defects in structural elements. Examples of these elements include aircraft components suffering barely visible impact damage or fatigue cracks, and bridge and building structures suffering earthquake damage, amongst others (Escobar et al. 2005; Fang et al. 2005; Ge and Lui 2005; Caddemi and Greco 2006; Wang and Ong 2008; Chatzi et al. 2011). The onset of small cracks, such as fatigue cracks, in many cases invisible to the naked eye, has been the cause of some serious accidents, especially in the aviation industry. In 1988, an Aloha Airlines Boeing 737-200 suffered a decompression due to the separation of a 5 m section of the upper cabin fuselage, with one loss of life as a result (Werfelman 2011). A similar incident occurred in 2011 to a Southwest Airlines Boeing 737-300 with a 1.5 m gap in the fuselage, although with no loss of life (Berger and Wilson 2011). It is, therefore, of great importance to detect cracks at an early stage to ensure safety and avoid catastrophic failure.

The crack detection process involves determining the presence of cracks, their locations and severities. Together with estimating the remaining service life of the structure, these steps form what is called Structural Health Monitoring (Rytter 1993; Wang and Ong 2008). A robust structural health monitoring technique should allow the efficient evaluation of the monitored structure, in terms of time and accuracy. Repair work can then be carried out in an economic manner and without incurring any loss of life (Wang and Ong 2008).

Different types of non-destructive testing can be used to determine the presence of cracks, their locations and severities. These include visual inspection, ultrasound, acoustic emission, magnetic field, eddy current, and radiography tests. However, these procedural initiatives require a preliminary estimation of the crack locations before performing the test and are, therefore, not applicable to inaccessible members in a structure (Rytter 1993; Teughels et

al. 2002; Caddemi and Greco 2006; Wang and Ong 2008; Chatzi et al. 2011; Danai et al. 2012). If a preliminary estimation is not available or cannot be made, then the whole structure must be inspected, rendering these tests more time and cost consuming. To overcome this limitation, two other types of non-destructive techniques can be used to detect structural cracks in situ. The first is the measurement of static deflections (Caddemi and Morassi 2007). The other is the measurement of vibration characteristics, mainly the natural frequencies and mode shapes. The presence of cracks in a structural element changes its static deflections and vibration characteristics, together with those of the assembled structure. Discontinuities are induced in the static deflections and mode shapes, while degradations occur in the natural frequencies (Teughels et al. 2002; Escobar et al. 2005; Fang et al. 2005; Ge and Lui 2005; Caddemi and Greco 2006; Caddemi and Morassi 2007; Wang and Ong 2008; Chatzi et al. 2011; Danai et al. 2012). In practice, measuring static deflections and mode shapes requires sensors located at more than one point in the structure. In contrast, natural frequencies can be measured at any chosen point of the structure and are independent of the location of measurements (Hassiotis and Jeong 1993). Natural frequencies are thus more easily obtained than static deflection measurements and mode shapes, especially when taking into consideration the accessibility limitations of some structural members.

This thesis is concerned with the inverse problem of crack identification in plane frames using only one type of vibration characteristic, the natural frequencies, which are easily extractable. However, the highly pertinent direct problem of calculating the natural frequencies of beams and frames with predefined cracks should be first tackled. The word ‘crack’ is used to denote any type of cracks (such as fatigue cracks), or a notch.

1.2. Literature review

1.2.1. Direct problem

Before attempting to solve the inverse problem of crack detection in plane frames using natural frequency measurements, the direct problem should be first studied. That is the calculation of the natural frequencies in the presence of cracks. As frames are assemblies of beams (and columns), connected together

at the joints, it is highly pertinent to study the natural frequency calculation of beams, with which much of the literature in the area of crack detection is concerned.

Solving the boundary value problem, researchers have deduced implicit expressions for the natural frequencies of damaged Bernoulli-Euler beams with open cracks from the equations of motion. Applying the Rayleigh–Ritz method, Christides and Barr (1984) deduced a frequency equation for simply supported beams with symmetric double-edge mid-span cracks. The study was extended by Shen and Pierre (1990) who proposed a Galerkin solution. Ostachowicz and Krawczuk (1991) derived the natural frequencies of a cantilever beam with two single-edge and double-edge cracks. Liang et al. (1992) formulated equations for the change in natural frequencies when single cracks are introduced in simply supported and cantilever beams. Morassi (1993) generalised the equations for any boundary condition such that the natural frequency changes are functions of the square of the uncracked mode shape curvature, together with the crack severity. A review paper by Dimarogonas (1996) is a useful collective reference for previous publications concerned with similar solution methods. A recent study by Banerjee and Guo (2009) used the well-established dynamic stiffness matrix for an undamaged beam (Błaszkowiak and Kączkowski 1966) as a basis for assembling the global stiffness matrix for a beam with a single crack, adding six degrees of freedom to the undamaged beam.

The studies described so far are based on the solution of differential equations for obtaining the natural frequencies in the case of one crack. As the number of cracks increases, the solution becomes much more difficult. Shifrin and Ruotolo (1999) used the Dirac's delta distribution functions in their simplified solution in the case of multiple cracks. Khiem and Lien (2001), along with Lin et al. (2002), proposed more simplified solutions using transfer matrix methods. More recent studies used Heaviside and Dirac's delta functions in a different manner compared with that of Shifrin and Ruotolo (1999), to solve beam vibration problems with multiple open cracks (Caddemi and Caliò 2009; Caddemi and Morassi 2013). Based on these functions, dynamic stiffness matrices for cracked frames were deduced (Caddemi and Caliò 2013).

In terms of modelling cracks, the majority of the published literature assumes either a reduction in stiffness extending over the damaged length, or else rotational springs representing single cracks (Cerri and Vestroni 2000; Vestroni and Capecchi 2000; Friswell 2007). In the first instance, the stiffness reduction is the result of a decrease in cross-sectional area or Young's modulus of the material. Alternatively, the rotational spring model relates the crack depth to an equivalent spring stiffness (or compliance). Using fracture mechanics methods, different relations have been formulated experimentally according to the strain energy density function (Rizos et al. 1990; Ostachowicz and Krawczuk 1991; Dimarogonas 1996; Chondros et al. 1998; Caddemi and Caliò 2009). The crack model used by Gounaris and Dimarogonas (1988) incorporates rotational, shear, axial and torsional springs, along with the couplings between them. A simpler model used by Banerjee and Guo (2009) incorporates only rotational, shear and axial springs. Chondros et al. (1998) developed a continuous cracked beam vibration theory which assumes the distribution of the added flexibility due to a crack over the damaged length of the beam.

1.2.2. Inverse problem

Given a solution to the direct problem relating the natural frequencies of a cracked beam to the characteristics of the crack, the inverse problem must next be examined in order to determine the location and severity of a crack from the detected degradations in the natural frequencies. Different approaches were used in tackling the inverse problem of crack detection. Rizos et al. (1990) devised a crack detection method for beams using one of its natural frequencies and two vibration amplitude measurements, all corresponding to one mode. The crack is modelled as a rotational spring and the boundary value problem is solved iteratively using the Newton–Raphson method to obtain the crack location and severity. The method was experimentally applied on a cantilever beam with two accelerometers mounted. A harmonic exciter was used. The detection method showed good accuracy for crack depth to section height ratios greater than 0.10. The method was improved by Liang et al. (1991), eliminating the need for vibration amplitude (mode shape) measurements and iterations but requiring three natural frequencies as inputs. Cerri and Vestroni (2000) applied

first principles and optimality criteria to detect damage in beams where cracks are concentrated in a zone. Two methods were formulated; the first was based on solving at least three simultaneous non-linear equations, while the other was based on minimising the difference between the analytical and experimental natural frequencies. The second method was refined to utilise the natural frequency variations between the uncracked and cracked cases, instead of the frequency values. Based on this refinement, experimental investigations were carried out on cracked reinforced concrete beams (Cerri and Vestroni 2003) and it was concluded that at least three frequencies are required to identify the location and severity of the cracked zone. Vestroni and Capecchi (2000) studied crack detection based on the spring model and finite elements separately. Chinchalkar (2001) devised a method for detecting a single crack using the rotational spring model in conjunction with finite elements. The method was applied on tapered and stepped beams. Explicit expressions for crack locations and magnitudes corresponding to different beam boundary conditions were deduced by Morassi (2008). Gillich and Praisach (2014) detected single cracks in cantilever beams using the first ten natural frequencies and the corresponding mode shapes calculated in the uncracked case. Their method does not require a crack model, but relies on pattern recognition. A method for single crack detection in multi-span beams was formulated by Sharma et al. (2015) by solving the boundary value problem. Experimental investigations were carried out on a two span beam (clamped-pinned-clamped and pinned-pinned-pinned boundary conditions) where the introduced crack covered half the cross-section height. The detection results showed good accuracy compared with the actual crack size and location.

A number of crack detection techniques are based on finite elements represented by stiffness and mass matrices, with the cracks modelled as reductions in the stiffnesses of specific elements. Kam and Lee (1992) devised a method for locating single cracks in beams using natural frequency and mode shape measurements, by applying an optimality criterion on the stiffness and mass matrices. The crack sizes were estimated based on strain energy equilibrium. The crack detection method was applied analytically on the beam originally tested and studied by Rizos et al. (1990). The natural frequencies and

mode shapes corresponding to the first ten vibration modes, obtained from finite element analysis, were used. The identified crack depths showed good agreement with the actual depths and also compared well with those obtained by Rizos et al. (1990). However, a comparison between the two identification methods in terms of the crack location accuracy is not possible due to the difference in the crack models of the two methods. A number of quadratic optimality criteria were applied to detect single and multiple simulated damages in beams, with natural frequency simulations as the only modal inputs (Hassiotis and Jeong 1993, 1995). Experimental validation was then carried out using the first six natural frequencies of a cantilever beam, obtained by Yang et al. (1985), where the beam was excited by a hammer and the signals from six accelerometers were analysed to obtain the natural frequencies. The detection method locates the finite element containing the actual crack, in addition to other false elements. The reduction in stiffness of the true element compares well with the actual reduction. Lee and Chung (2000) combined finite element analysis, first principles, and fracture mechanics to detect single cracks in cantilever beams, based on rank ordering of the frequency degradations due to the crack. Using the first four natural frequencies, the method was applied analytically on the cantilever beam originally tested and studied by Rizos et al. (1990). The crack detection results had varying accuracy according to the crack positions and severities.

Other damage detection methods are based on finite element model updating (Teughels et al. 2002; Titurus et al. 2003a, b), mode shape curvatures which are altered in a local manner due to the damage presence (Pandey et al. 1991; Yoon et al. 2009; Ciambella and Vestroni 2015), and wavelet analysis applied on mode shapes (Solís et al. 2013). The wavelet analysis is explained by Solís et al. (2013) in contrast with the fast Fourier transform (outlined in Chapter 4 of this thesis). Methods based on mode shape measurements require a large number of measurement points. Solís et al. (2013) concluded from their free vibration experiments that at least thirteen measurement points are required for their tested beam, while only using three vibration modes. Ratcliffe (2000) developed a detection method relying on frequency response functions covering a wide (broadband) frequency range; a method which requires a large

number of measurement points. Two important papers overviewing the inverse problem have been published by Doebling et al. (1998) and Friswell (2007).

Damage detection methods applying optimality criteria may require the use of advanced numerical techniques such as genetic algorithms (Friswell et al. 1998; Rao et al. 2004; He and Hwang 2006; Perry et al. 2006; Vakil-Baghmisheh et al. 2008), neural networks (Yun and Bahng 2000; Kao and Hung 2003; Fang et al. 2005; Jiang et al. 2011), or bees algorithm (Moradi et al. 2011).

When considering more complex structures such as frames, the majority of published studies model each frame member as one finite element, or two elements to eliminate symmetry. The damage is modelled as a reduction in the stiffnesses of specific finite elements (Hassiotis and Jeong 1993, 1995; Bicanic and Chen 1997; Hassiotis 2000; Escobar et al. 2005; Ge and Lui 2005). The work of Morassi and Rovere (1997) is among a few in the published literature in which frame members are discretised into a large number of elements and an optimisation technique is applied to detect a single crack close to a joint in a one bay, five storey frame. Experimental data acquired from forced vibration tests, was used. Brasiliano et al. (2004) also discretised frame members into a large number of elements and devised a new detection method termed the Residual Error Method in the Movement Equation. The method requires the use of natural frequencies and mode shapes.

Modelling the crack as a set of rotational, axial and shear springs, Nikolakopoulos et al. (1997) utilised contours extracted from 3D plots of the relationship between the natural frequency variation due to a concentrated crack, and the crack parameters, namely location and magnitude, to detect cracks in frames. A cracked beam finite element was used. As a result, the identified crack location was in terms of the finite element number. The method was validated experimentally on a one bay one storey frame using free vibration. Two natural frequencies were used. However, the introduced crack covered half the cross-section height, so the differences in natural frequencies between the uncracked and cracked cases were relatively large, 6.49% and 2.35% for the first and second modes, respectively. Greco and Pau (2012) incorporated the rotational spring stiffness in the exact dynamic stiffness matrix

of a cracked frame. An optimisation criterion was applied, which was the least sum of squares of the differences between the theoretical and pseudo-experimental values of the variation between the uncracked and cracked natural frequencies with respect to the uncracked frequencies. The Wittrick–Williams algorithm (Wittrick and Williams 1971) was used in calculating the theoretical natural frequencies corresponding to different crack locations and magnitudes, which were then used to apply the optimisation criterion, once with respect to the crack magnitude and then with respect to the crack location. It was concluded that a minimum of three natural frequencies are required to detect a single crack, in the absence of experimental noise. The effect of noise in the natural frequency measurements was studied using Monte Carlo simulations. Using contour plots and a slightly modified optimality criterion to that of Greco and Pau (2012), while reverting to finite elements, Diaferio and Sepe (2015) devised a single crack detection method for multi-bay multi-storey plane frames using natural frequencies. However, the natural frequencies were restricted to those corresponding to local modes, where only the beams, as opposed to the columns, show large vibration amplitudes. The detection method was, in return, restricted to single cracks in the beams. The effect of noise was simulated by plotting the average mean error and standard deviation in both the detected crack location and severity, against the number of samples. Lien et al. (2014) applied wavelet analysis on the analytically calculated mode shapes of frames with multiple cracks.

1.3. Thesis structure

This thesis is divided into six chapters including this, the introduction. The remaining chapters describe new work. In the second chapter, the direct problem is tackled. A new advanced method is devised for obtaining the natural frequencies of beams and frames with multiple single-edge cracks, using exact dynamic stiffness matrices, without resorting to finite elements or solving the boundary value problem, thus allowing for faster and accurate calculations. A rotational spring model and the Wittrick–Williams algorithm (Wittrick and Williams 1971) are utilised in the calculations. The orders of the calculated natural frequencies are guaranteed to be correct, contrary to other root searching algorithms, where some natural frequencies can be missed. The

method is applied on a number of example beams and frames. The results are compared with those published in the literature.

The third chapter is concerned with the inverse problem. A new method for single crack localisation in frames is devised, based on normalising the dimensionless variation between the uncracked and cracked natural frequencies. The crack severities are also recovered. The natural frequency calculation procedure described in the second chapter forms a fundamental part of the detection procedure. The effect of noise is studied by simulating a measurement error in the natural frequencies. The principles of interval arithmetic (Moore 1979) are then used to calculate crack location and severity ranges. The detection method is applied on a two bay two storey frame example, considering both types of simulated noise free and contaminated measurements.

The fourth chapter describes the experimental application of the crack detection method devised in the third chapter. Tests were carried out on a two bay, two storey steel frame with scaled down dimensions (bay lengths and storey heights) compared to those of the example in the third chapter. An outline of the fast Fourier transform is explained in order to correctly operate the equipment supplied software controlling all measurement aspects.

The fifth chapter presents refinements to the formulated crack detection procedure. Two refinement methods are described and applied to the frame example used in the third chapter. One method is described as performing a second iteration of the same detection procedure, using more natural frequencies selected based on the arrangement of analytical natural frequency variations corresponding to a group of vibration modes. The other method depends on using a combination of low and higher order natural frequencies showing zero variations when the crack is present anywhere along specific frame members.

The sixth chapter is the conclusions chapter. Some suggestions for future work are presented, along with an outline of research currently being carried out and inspired by the two papers (Labib et al. 2014, 2015) published in relation to this thesis.

1.4. Publications list

Two journal papers have been published, based on Chapters 2 and 3 of this thesis:

- Labib, A., Kennedy, D. and Featherston, C.A. 2014. Free vibration analysis of beams and frames with multiple cracks for damage detection. *Journal of Sound and Vibration*, 333(20), pp. 4991-5003.
- Labib, A., Kennedy, D. and Featherston, C.A. 2015. Crack localisation in frames using natural frequency degradations. *Computers and Structures*, 157(0), pp. 51-59.

Additionally, three conference papers have been presented, based on Chapters 2, 3 and 5:

- Labib, A., Kennedy, D. and Featherston, C.A. 2013. Natural frequencies of beams and frames with concentrated open cracks. In: *The Ninth International Symposium on Vibrations of Continuous Systems.* Courmayeur, Italy, 21-26 July, 2013. pp. 43-45.
- Labib, A., Kennedy, D. and Featherston, C.A. 2015. Crack localisation in frames using natural frequency measurements. In: The Institution of Structural Engineers ed. *17th Young Researchers' Conference.* London, UK, 14 April, 2015. pp. 68-69.
- Labib, A., Kennedy, D. and Featherston, C.A. 2015. Identifying cracked frame members using higher order natural frequencies. In: *International Conference on Structural Engineering Dynamics ICEDyn 2015.* Lagos, Portugal, 22-24 June, 2015.

Chapter 2 – Free vibration analysis of beams and frames

2.1. Introduction

The presence of cracks in a structural element changes its vibration characteristics and those of the assembled structure (Teughels et al. 2002; Escobar et al. 2005; Fang et al. 2005; Ge and Lui 2005; Caddemi and Greco 2006; Wang and Ong 2008; Chatzi et al. 2011; Danai et al. 2012). In order to attempt to solve the inverse problem of damage identification using vibration measurements to detect these changes, the direct problem of calculating the natural frequencies of Bernoulli-Euler beams and frames with predefined cracks is studied in this chapter. The rotational spring model is used and cracks are assumed to be always open, thus, the problem can be described as a linear one (Shen and Chu 1992; Chati et al. 1997; Chondros et al. 2001). Since cracks have a high probability of occurring under large static loads, as in reinforced concrete structures, the open cracks assumption is practically valid in many cases (Rizos et al. 1990). As widely assumed in the literature, the crack covers the whole width of the beam or frame member under consideration, and the loss in mass due to the crack is negligible. Similar to the case of slender arches (Pau et al. 2011), it is assumed that the axial stiffness of the beam at the crack location remains intact. The theoretical derivations, however, are reported. Neglecting structural damping, the dynamic stiffness matrix for undamaged beams (Błaszkowiak and Kączkowski 1966) is used in assembling a 6 × 6 global stiffness matrix for beams with multiple cracks. The Wittrick–Williams algorithm (Wittrick and Williams 1971) is used for calculating the natural frequencies numerically, using a MATLAB (MathWorks 2012) code, given in the appendix. The study is then extended to cracked frames. The results obtained are compared with those reported by Banerjee and Guo (2009), Caddemi and Caliò (2013), along with Caddemi and Morassi (2013). A two bay, two storey frame example is formulated to study the effect of changing the location of a small crack on the natural frequencies of a more complex structure, thus giving an insight into the inverse problem of damage detection.

2.2. Natural frequencies of cracked beams

2.2.1. Cracked beam modelling

A concentrated open crack in a Bernoulli–Euler beam is represented by a rotational spring of stiffness k^*, as shown in Fig. 2.1.

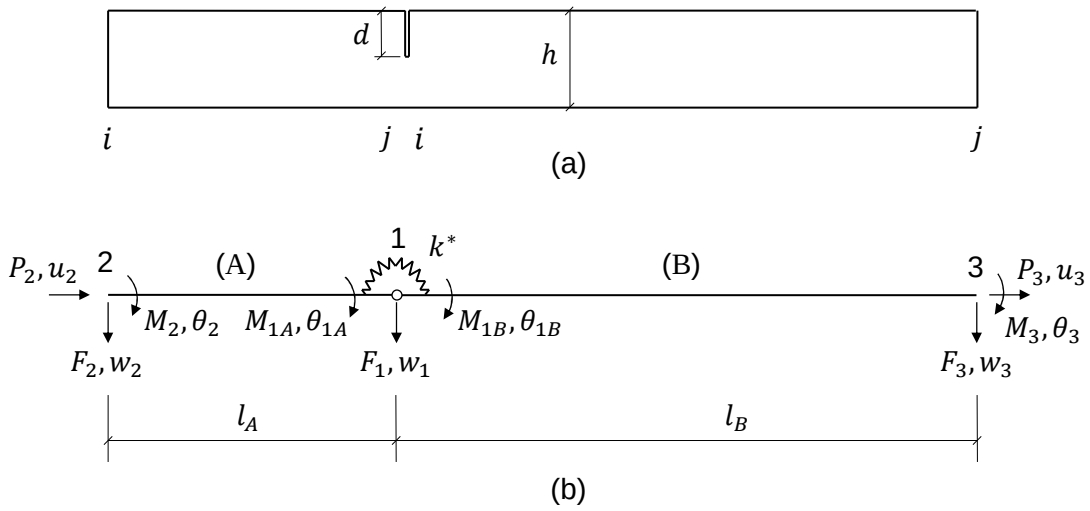

Fig. 2.1. Damaged beam. (a) Beam with a crack of depth d; (b) Rotational spring model and nodal forces.

The spring stiffness is assumed to be related to the crack depth d by the equation (Caddemi and Caliò 2008, 2009, 2014):

$$k^* = \frac{EI}{l}\frac{1}{\lambda^*}, \tag{2.1}$$

in which

$$\lambda^* = \frac{h}{l}C(d/h), \tag{2.2}$$

where λ^* is termed the dimensionless local compliance, EI is the beam bending stiffness, l is the total length of the beam, h is the cross-sectional depth, and $C(d/h)$ is a dimensionless function which can be written in a general form as:

$$C(d/h) = a_0 \sum_{n=1}^{10} a_n (d/h)^n. \tag{2.3}$$

Combinations of a_0 and a_n, representing different formulas for $C(d/h)$ given in the literature, are presented in Table 2.1. An alternative formula implemented by Caddemi and Caliò (2013) is:

$$C(d/h) = \frac{(d/h)[2-(d/h)]}{0.9[(d/h)-1]^2}. \quad (2.4)$$

A comparison between the formulas is illustrated in Fig. 2.2, similar to that presented by Caddemi and Caliò (2008, 2014), but with the addition of the formula implemented by Banerjee and Guo (2009), Eq. (2.3d), in the comparison. It must be noted that Eq. (2.3d) gives only an approximate comparison, as the rotational spring it represents is used with shear and axial springs. For this reason, Eq. (2.3d) generally gives the lowest values for $C(d/h)$, while maintaining similar trends to that of the other formulas for $d/h \leq 0.8$. The irregular behaviour of Eq. (2.3d) when d/h increases beyond 0.8 can be attributed to the curve fitting process involved in the formula derivation, being applied within $d/h \leq 0.5$ (Zheng and Kessissoglou 2004).

Table 2.1. Coefficients a_0 and a_n in different formulas for $C(d/h)$ based on Eq. (2.3).

Coefficients	Formula no.			
	(2.3a)*	(2.3b)**	(2.3c)***	(2.3d)****
a_0	5.346	6π	$6\,\pi(1-\nu^2)$	$\frac{(1-\nu^2)}{12}e^{\frac{1}{1-(d/h)}}$
a_1	0	0	0	-0.219628 x 10^{-4}
a_2	1.86	0.6384	0.6272	52.37903
a_3	-3.95	-1.035	-1.04533	-130.2483
a_4	16.375	3.7201	4.5948	308.442769
a_5	-37.226	-5.1773	-9.9736	-602.445544
a_6	76.81	7.553	20.2948	939.044538
a_7	-126.9	-7.332	-33.0351	-1310.95029
a_8	172	2.4909	47.1063	1406.52368
a_9	-143.97	0	-40.7556	-1067.4998
a_{10}	66.56	0	19.6	391.536356

ν is Poisson's ratio, assumed 0.3.
* Rizos et al. (1990); Dimarogonas (1996); Caddemi and Caliò (2009).
** Ostachowicz and Krawczuk (1991); Caddemi and Caliò (2009).
*** Chondros et al. (1998); Caddemi and Caliò (2009).
**** Banerjee and Guo (2009).

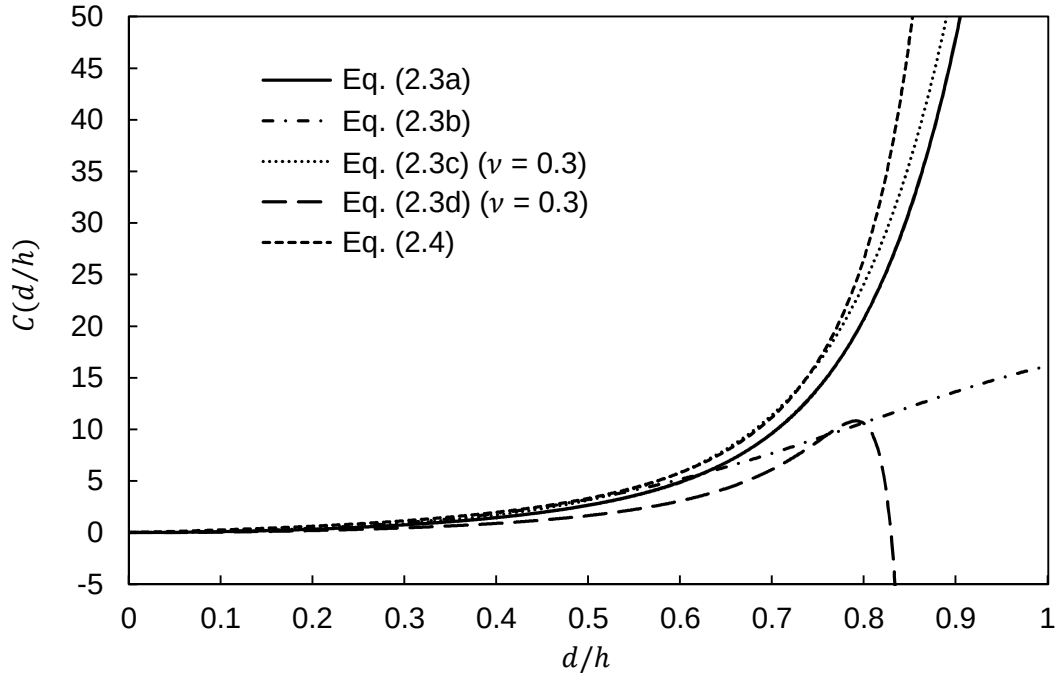

Fig. 2.2. Comparison between the compliance formulae of Eqs. (2.3) and (2.4).

Formulas (2.3c) and (2.3d) are assumed to be valid when $d/h \leq 0.6$ and 0.5, respectively. It is clear that for smaller cracks having $d/h \leq 0.4$, using any of the five formulas does not significantly change the obtained results, despite the wide variation of the coefficients a_0 and a_n. This variation in the coefficients is due to the different strain energy density functions used in the derivation of the formulas (Rizos et al. 1990; Ostachowicz and Krawczuk 1991; Dimarogonas 1996; Chondros et al. 1998; Banerjee and Guo 2009; Caddemi and Caliò 2009). Practically, the rotational spring model is valid for small cracks only (Morassi 2008). In this thesis, the d/h value of 0.4 is taken as an upper limit for small cracks.

2.2.2. Derivation of the dynamic stiffness matrix

A beam portion is considered, containing a single crack and consisting of two elements, labelled A and B, as shown in Fig. 2.1. The beam, vibrating at frequency ω, has cross-sectional area A and mass per unit length μ. Considering the vertical deflections $w_{i,j}$, and rotations $\theta_{i,j}$, the exact dynamic stiffness equations for a single element m (= A, B) with length l_m, connecting nodes i and j, take the form (Błaszkowiak and Kączkowski 1966):

$$\begin{Bmatrix} F_i \\ M_i \\ F_j \\ M_j \end{Bmatrix} = \begin{bmatrix} a_m & b_m & -d_m & e_m \\ b_m & c_m & -\varepsilon_m & f_m \\ -d_m & -\varepsilon_m & \alpha_m & -\beta_m \\ e_m & f_m & -\beta_m & \gamma_m \end{bmatrix} \begin{Bmatrix} w_i \\ \theta_i \\ w_j \\ \theta_j \end{Bmatrix}, \tag{2.5}$$

where $F_{i,j}$ and $M_{i,j}$ are the nodal shear forces and moments, respectively. For a uniform element with no cracks,

$$\left.\begin{aligned} a_m = \alpha_m = EI\lambda^3\left(S_m C_m^{'} + C_m S_m^{'}\right)/\sigma_m\,, \quad & b_m = \beta_m = EI\lambda^2\left(S_m S_m^{'}\right)/\sigma_m\,, \\ c_m = \gamma_m = EI\lambda\left(S_m C_m^{'} - C_m S_m^{'}\right)/\sigma_m\,, \quad & d_m = EI\lambda^3\left(S_m + S_m^{'}\right)/\sigma_m\,, \\ e_m = \varepsilon_m = EI\lambda^2\left(C_m^{'} - C_m\right)/\sigma_m\,, \quad & f_m = EI\lambda\left(S_m^{'} - S_m\right)/\sigma_m\,, \end{aligned}\right\} \tag{2.6}$$

in which

$$\left.\begin{aligned} C_m = \cos\lambda l_m\,, \quad S_m = \sin\lambda l_m\,, \quad C_m^{'} = \cosh\lambda l_m\,, \quad S_m^{'} = \sinh\lambda l_m\,, \\ \lambda = \sqrt[4]{\mu\omega^2/EI}\,, \quad \sigma_m = 1 - C_m C_m^{'}. \end{aligned}\right\} \tag{2.7}$$

Connecting elements A and B, as shown in Fig. 2.1, gives the stiffness equations:

$$\begin{Bmatrix} M_{1A} \\ M_{1B} \\ F_1 \\ F_2 \\ M_2 \\ F_3 \\ M_3 \end{Bmatrix} = \begin{bmatrix} \gamma_A + k^* & -k^* & -\beta_A & e_A & f_A & 0 & 0 \\ -k^* & c_B + k^* & b_B & 0 & 0 & -\varepsilon_B & f_B \\ -\beta_A & b_B & \alpha_A + a_B & -d_A & -\varepsilon_A & -d_B & e_B \\ e_A & 0 & -d_A & a_A & b_A & 0 & 0 \\ f_A & 0 & -\varepsilon_A & b_A & c_A & 0 & 0 \\ 0 & -\varepsilon_B & -d_B & 0 & 0 & \alpha_B & -\beta_B \\ 0 & f_B & e_B & 0 & 0 & -\beta_B & \gamma_B \end{bmatrix} \begin{Bmatrix} \theta_{1A} \\ \theta_{1B} \\ w_1 \\ w_2 \\ \theta_2 \\ w_3 \\ \theta_3 \end{Bmatrix}, \tag{2.8}$$

where the presence of the rotational spring results in separate moments and rotations at either side of Node 1, in addition to the vertical displacement. Applying partial Gaussian elimination to the first three rows and columns of the 7 × 7 matrix in Eq. (2.8), without row interchange, gives the stiffness equations for the combined element (AB) in the form of Eq. (2.5), where the matrix elements are given by:

$$\left.\begin{aligned} a_m = a_A - e_A^2 q_1 - p_1^2\Delta_3, \quad & b_m = b_A - e_A f_A q_1 - p_1 p_2 \Delta_3, \\ c_m = c_A - f_A^2 q_1 - p_2^2\Delta_3, \quad & d_m = -e_A\varepsilon_B\Delta_1\Delta_2 + p_1 p_3\Delta_3, \\ e_m = -e_A f_B\Delta_1\Delta_2 - p_1 p_4\Delta_3, \quad & f_m = -f_A f_B\Delta_1\Delta_2 - p_2 p_4\Delta_3, \\ \alpha_m = \alpha_B - \varepsilon_B^2\Delta_2 - p_3^2\Delta_3, \quad & \beta_m = \beta_B - \varepsilon_B f_B\Delta_2 + p_3 p_4\Delta_3, \\ \gamma_m = \gamma_B - f_B^2\Delta_2 - p_4^2\Delta_3, \quad & \varepsilon_m = -f_A\varepsilon_B\Delta_1\Delta_2 + p_2 p_3\Delta_3, \end{aligned}\right\} \tag{2.9}$$

in which

$$\left.\begin{aligned} &p_1 = -d_A + e_A q_2, && p_2 = -\varepsilon_A + f_A q_2, \\ &p_3 = -d_B + \varepsilon_B q_3, && p_4 = e_B - f_B q_3, \\ &q_1 = \Delta_1(f^* + \Delta_1\Delta_2), && q_2 = \beta_A q_1 - b_B\Delta_1\Delta_2, \\ &q_3 = \Delta_2(b_B - \beta_A\Delta_1), && \Delta_1 = 1/(1+\gamma_A f^*), \\ &\Delta_2 = 1/(c_B + \gamma_A\Delta_1), && \Delta_3 = 1/(\alpha_A + a_B - \beta_A^2 q_1 - b_B^2\Delta_2 + 2\beta_A b_B\Delta_1\Delta_2), \end{aligned}\right\} \quad (2.10)$$

and $f^* = 1/k^*$ is the compliance of the spring. If there is no crack, $f^* = 0$ and the expressions in Eq. (2.9) reduce to those of Eq. (2.6) for a uniform beam of length $l_m = l_A + l_B$. The expansions of the 4 × 4 stiffness matrix elements in the case of one crack, obtained using the MATLAB (MathWorks 2012) symbolic math toolbox, are given by:

$$\begin{aligned} a_m = &-\frac{4EI\lambda^3}{D_m}(\cos\lambda l_m \sinh\lambda l_m + \cosh\lambda l_m \sin\lambda l_m) \\ &-\frac{EI\mu\omega^2 f^*}{D_m}[2\cosh\lambda l_m \cos\lambda l_m \\ &+ \cosh\lambda l_m \cos\lambda(l_A - l_B) + \cos\lambda l_m \cosh\lambda(l_A - l_B) \\ &+ \sinh\lambda l_m \sin\lambda(l_A - l_B) - \sin\lambda l_m \sinh\lambda(l_A - l_B) \\ &+ 4\cos\lambda l_A \cosh\lambda l_A], \end{aligned} \quad (2.11)$$

$$\begin{aligned} b_m = &-\frac{4EI\lambda^2}{D_m}\sin\lambda l_m \sinh\lambda l_m \\ &-\frac{E^2I^2 f^*\lambda^3}{D_m}[\cos\lambda l_m \sinh\lambda l_m + \cosh\lambda l_m \sin\lambda l_m \\ &+ \cosh\lambda l_m \sin\lambda(l_A - l_B) + \cos\lambda l_m \sinh\lambda(l_A - l_B) \\ &+ 2\cos\lambda l_A \sinh\lambda l_A + 2\cosh\lambda l_A \sin\lambda l_A], \end{aligned} \quad (2.12)$$

$$\begin{aligned} -d_m = &\frac{4EI\lambda^3}{D_m}(\sinh\lambda l_m + \sin\lambda l_m) \\ &+\frac{EI\mu\omega^2 f^*}{D_m}[\cosh\lambda l_m + \cos\lambda l_m + \cos\lambda(l_A - l_B) \\ &+ \cosh\lambda(l_A - l_B) + 2\cos\lambda l_A \cosh\lambda l_B \\ &+ 2\cosh\lambda l_A \cos\lambda l_B], \end{aligned} \quad (2.13)$$

$$e_m = -\frac{4EI\lambda^2}{D_m}(\cosh\lambda l_m - \cos\lambda l_m) - \frac{E^2I^2f^*\lambda^3}{D_m}[\sinh\lambda l_m + \sin\lambda l_m - \sin\lambda(l_A - l_B) - \sinh\lambda(l_A - l_B) + 2\cos\lambda l_A \sinh\lambda l_B + 2\cosh\lambda l_A \sin\lambda l_B], \quad (2.14)$$

$$c_m = -\frac{4EI\lambda}{D_m}(\cosh\lambda l_m \sin\lambda l_m - \cos\lambda l_m \sinh\lambda l_m) - \frac{E^2I^2f^*\lambda^2}{D_m}[2\sin\lambda l_m \sinh\lambda l_m - \cosh\lambda l_m \cos\lambda(l_A - l_B) + \cos\lambda l_m \cosh\lambda(l_A - l_B) + \sinh\lambda l_m \sin\lambda(l_A - l_B) + \sin\lambda l_m \sinh\lambda(l_A - l_B) + 4\sin\lambda l_A \sinh\lambda l_A], \quad (2.15)$$

$$-\varepsilon_m = \frac{4EI\lambda}{D_m}(\cosh\lambda L_m - \cos\lambda L_m) + \frac{E^2I^2f^*\lambda^3}{D_m}[\sinh\lambda L_m + \sin\lambda L_m + \sin\lambda(L_A - L_B) + \sinh\lambda(L_A - L_B) + 2\cos\lambda L_B \sinh\lambda L_A + 2\cosh\lambda L_B \sin\lambda L_A], \quad (2.16)$$

$$f_m = -\frac{4EI\lambda}{D_m}(\sinh\lambda l_m - \sin\lambda l_m) - \frac{E^2I^2f^*\lambda^2}{D_m}[-\cos\lambda l_m + \cosh\lambda l_m + \cos\lambda(l_A - l_B) - \cosh\lambda(l_A - l_B) + 2\sin\lambda l_A \sinh\lambda l_B + 2\sinh\lambda l_A \sin\lambda l_B], \quad (2.17)$$

$$\alpha_m = -\frac{4EI\lambda^3}{D_m}(\cos\lambda l_m \sinh\lambda l_m + \cosh\lambda l_m \sin\lambda l_m) - \frac{EI\mu\omega^2f^*}{D_m}[\cosh\lambda l_m \cos\lambda(l_A - l_B) + \cos\lambda l_m \cosh\lambda(l_A - l_B) - \sinh\lambda l_m \sin\lambda(l_A - l_B) + \sin\lambda l_m \sinh\lambda(l_A - l_B) + 4\cos\lambda l_B \cosh\lambda l_B + 2\cosh\lambda l_m \cos\lambda l_m], \quad (2.18)$$

$$
\begin{aligned}
-\beta_m = {} & \frac{4EI\lambda^2}{D_m}\sin\lambda l_m \sinh\lambda l_m \\
& + \frac{E^2I^2f^*\lambda^3}{D_m}[\cos\lambda l_m \sinh\lambda l_m + \cosh\lambda l_m \sin\lambda l_m \\
& - \cosh\lambda l_m \sin\lambda(l_A - l_B) - \cos\lambda l_m \sinh\lambda(l_A - l_B) \\
& + 2\cos\lambda l_B \sinh\lambda l_B + 2\cosh\lambda l_B \sin\lambda l_B],
\end{aligned} \tag{2.19}
$$

$$
\begin{aligned}
\gamma_m = {} & \frac{4EI\lambda}{D_m}(\cos\lambda l_m \sinh\lambda l_m - \cosh\lambda l_m \sin\lambda l_m) \\
& + \frac{E^2I^2f^*\lambda^2}{D_m}[-2\sin\lambda l_m \sinh\lambda l_m \\
& + \cosh\lambda l_m \cos\lambda(l_A - l_B) - \cos\lambda l_m \cosh\lambda(l_A - l_B) \\
& + \sinh\lambda l_m \sin\lambda(l_A - l_B) + \sin\lambda l_m \sinh\lambda(l_A - l_B) \\
& - 4\sin\lambda l_B \sinh\lambda l_B],
\end{aligned} \tag{2.20}
$$

where

$$
\begin{aligned}
D_m = {} & 4(\cosh\lambda l_m \cos\lambda l_m - 1) \\
& + EIf^*\lambda[\cos\lambda l_m \sinh\lambda l_m - \cosh\lambda l_m \sin\lambda l_m \\
& + \sinh\lambda l_m \cos\lambda(l_A - l_B) - \sin\lambda l_m \cosh\lambda(l_A - l_B) \\
& + 2\cos\lambda l_A \sinh\lambda l_A - 2\cosh\lambda l_A \sin\lambda l_A \\
& + 2\cos\lambda l_B \sinh\lambda l_B - 2\cosh\lambda l_B \sin\lambda l_B].
\end{aligned} \tag{2.21}
$$

These expansions match those of the matrix elements formulated by Caddemi and Caliò (2013) using Dirac's delta distribution functions.

Multiple cracks connecting elements A, B, C,…, whether having the same or different severities, are modelled by recursively applying the above procedure to derive element AB from elements A and B, element ABC from AB and C, and so on, until a 4 × 4 dynamic stiffness matrix **K** is obtained for the whole beam. The decoupled axial stiffness terms are then inserted, giving the stiffness matrix of the whole beam in its final 6 × 6 form, similar to that utilised by Howson (1979) but with the incorporation of the rotational spring stiffness:

$$
\mathbf{K}(\omega) = \begin{bmatrix}
z_m & 0 & 0 & \overline{z}_m & 0 & 0 \\
0 & a_m & b_m & 0 & -d_m & e_m \\
0 & b_m & c_m & 0 & -\varepsilon_m & f_m \\
\overline{z}_m & 0 & 0 & z_m & 0 & 0 \\
0 & -d_m & -\varepsilon_m & 0 & \alpha_m & -\beta_m \\
0 & e_m & f_m & 0 & -\beta_m & \gamma_m
\end{bmatrix}, \tag{2.22}
$$

where

$$z_m = EA\eta \cot \eta l_m\,, \qquad \overline{z}_m = -EA\eta \operatorname{cosec} \eta l_m, \tag{2.23}$$

in which

$$\eta = \omega\sqrt{\frac{\mu}{EA}}. \tag{2.24}$$

Thus, a cracked beam can easily be assembled into a larger frame structure.

If the loss of axial stiffness through the crack is to be taken into account, then an axial spring with stiffness $\bar{k}^*$ can be added at Node 1, resulting in separate axial forces and displacements at either side of the crack. Working with the decoupled axial stiffness, the stiffness equations can be written as:

$$\begin{Bmatrix} P_{1A} \\ P_{1B} \\ P_2 \\ P_3 \end{Bmatrix} = \begin{bmatrix} z_A + \bar{k}^* & -\bar{k}^* & \overline{z}_A & 0 \\ -\bar{k}^* & z_B + \bar{k}^* & 0 & \overline{z}_B \\ \overline{z}_A & 0 & z_A & 0 \\ 0 & \overline{z}_B & 0 & z_B \end{bmatrix} \begin{Bmatrix} u_{1A} \\ u_{1B} \\ u_2 \\ u_3 \end{Bmatrix}, \tag{2.25}$$

where P and u are the axial forces and displacements, respectively. A 4 × 4 axial stiffness matrix is obtained, contrary to the 2 × 2 matrix in the uncracked case given by:

$$\mathbf{K}_{\text{Axial}} = \begin{bmatrix} z_m & \overline{z}_m \\ \overline{z}_m & z_m \end{bmatrix}. \tag{2.26}$$

Similar to the case of the rotational spring, partial Gaussian elimination is applied, but to the first two rows and columns of the 4 × 4 axial stiffness matrix in Eq. (2.25), giving the stiffness equations of the combined element (AB) in the form:

$$\begin{Bmatrix} P_2 \\ P_3 \end{Bmatrix} = \begin{bmatrix} z_A - \overline{z}_A{}^2 \bar{f}^* \Delta_4 - \overline{z}_A{}^2 \Delta_4{}^2 \Delta_5 & -\overline{z}_A \overline{z}_B \Delta_4 \Delta_5 \\ -\overline{z}_A \overline{z}_B \Delta_4 \Delta_5 & z_B - \overline{z}_B{}^2 \Delta_5 \end{bmatrix} \begin{Bmatrix} u_2 \\ u_3 \end{Bmatrix}, \tag{2.27}$$

in which

$$\Delta_4 = 1/\left(1 + z_A \bar{f}^*\right), \qquad \Delta_5 = 1/(z_B + z_A \Delta_4), \tag{2.28}$$

and $\bar{f}^* = 1/\bar{k}^*$ is the compliance of the axial spring. If there is no crack, $\bar{f}^* = 0$ and the expressions in Eq. (2.27) reduce to those of Eq. (2.26) for a uniform beam of length $l_m = l_A + l_B$. The stiffness matrix terms in Eq. (2.27) can replace

the axial stiffness terms, z_m and $\overline{z}_m$, in Eq. (2.22) if the loss of axial stiffness through the crack is to be taken into account. However, throughout this thesis, as stated in the introduction of this chapter, the axial stiffness is assumed to be intact.

2.2.3. Calculation of the natural frequencies and extracting the mode shapes

Referring to Eqs. (2.5) and (2.22), the external force vector vanishes for a beam vibrating at any of its natural frequencies ω_i, where i is the mode number. The following condition must then be satisfied:

$$\det.\{\mathbf{K}(\omega_i)\} = 0, \tag{2.29}$$

Due to the irregular behaviour of the determinant function, the roots of Eq. (2.29), i.e. the natural frequencies, can be calculated to any required accuracy using the highly efficient Wittrick–Williams algorithm (Wittrick and Williams 1971). The number of natural frequencies lying below a trial frequency ω^* is given by:

$$J = \left[s\{\mathbf{K}\} + \sum_m J_m + \sum_c s_c \right]_{\omega=\omega^*}. \tag{2.30}$$

The terms $s\{\mathbf{K}\}$ and J_m are defined according to Wittrick and Williams (1971) for intact elements, where $s\{\mathbf{K}\}$ is the sign count of $\mathbf{K}$, which is the number of negative leading diagonal elements of the upper triangular matrix obtained from $\mathbf{K}$ by standard Gaussian elimination without row interchange; and for each element $m = \mathrm{A}, \mathrm{B}, \mathrm{C}, \ldots$, J_m is the number of fixed end natural frequencies lying below ω^*. J_m is calculated using the equation implemented by Williams and Wittrick (1970):

$$J_m = \mathrm{int}\left(\frac{\eta l_m}{\pi}\right) + \mathrm{int}\left(\frac{\lambda l_m}{\pi}\right) - 0.5\left\{1 - (-1)^{\mathrm{int}\left(\frac{\lambda l_m}{\pi}\right)}\mathrm{sn}(\sigma_m)\right\}, \tag{2.31}$$

where int is the integer portion of the value in between the brackets and $\mathrm{sn}(\sigma_m) = 1$ if $\sigma_m > 0$, and $= -1$ if $\sigma_m < 0$. The application of the partial Gaussian elimination to the first three rows and columns of the 7 × 7 matrix in Eq. (2.8) requires additional sign counts s_c to be taken into account for each crack c. s_c is given by:

$$s_c = \mathrm{sg}\{\Delta_1\} + \mathrm{sg}\{\Delta_2\} + \mathrm{sg}\{\Delta_3\}, \tag{2.32}$$

where Δ_1, Δ_2 and Δ_3 are derived from the first three leading diagonal elements after performing the partial Gaussian elimination, and are defined in Eq. (2.10). The function $\mathrm{sg}\{\Delta_j\} = 1$ if $\Delta_j < 0$, and $= 0$ otherwise, for $j = 1, 2, 3$.

The calculation of the required natural frequencies begins with arranging them in ascending order of the modes. For the lowest required mode, r, a near zero trial value ω^* is assumed and J is calculated. If $J \geq r$, then the natural frequency value is zero, as in the case of the first three natural frequencies of a beam with free ends. Otherwise, ω^* is taken as a lower bound and doubled successively until $J \geq r$ (Howson 1979). An upper bound is thus established. Bisection is then used iteratively to converge on the required frequency. In each iteration, J is calculated for new values of ω^* equal to the mean of the bounds. New upper or lower bounds are established when $J \geq r$ or $J < r$, respectively. The iterations are stopped when the difference between the bounds decreases to a specified tolerance. The last bisected value of ω^* is taken as the required natural frequency. Further natural frequencies are calculated in a similar manner, taking the previously calculated frequency as the first lower bound. Another more time efficient convergence method has been formulated by Williams and Kennedy (1988), namely the multiple determinant parabolic interpolation method. However, the bisection method is used throughout this thesis due to its simplicity and the power of today's computers which outweigh the extra programming effort. The above procedure has been programmed into MATLAB (MathWorks 2012). The tolerance between the natural frequency bounds is generally specified at 10^{-11} rad s^{-1}. In some cases, this value causes MATLAB to get stuck in an infinite loop, so the tolerance in these cases is increased to 10^{-9} rad s^{-1}. Calculating the first ten natural frequencies of the two bay, two storey frame described in Section 2.3.2.2 takes 0.55 seconds, while calculating the first one hundred takes 4.90 seconds.

The mode shapes are plotted by dividing the beam into a large number of small elements in such a way that the crack falls between the two nodes of an element. The bending and shear stiffness matrix terms for such an element are given by Eq. (2.9), while those for the uncracked elements are given by

Eq. (2.6). The axial stiffness terms, given by Eq. (2.23), are the same for all elements. The calculated natural frequencies corresponding to the required mode are used as input data. With N degrees of freedom, a new $N \times N$ dynamic stiffness matrix is assembled for the divided beam. The stiffness equations at any natural frequency take the form:

$$\begin{bmatrix} k_{1,1} & \cdots & k_{1,N-1} & k_{1,N} \\ \vdots & \ddots & \vdots & \vdots \\ k_{N-1,1} & \cdots & k_{N-1,N-1} & k_{N-1,N} \\ k_{N,1} & \cdots & k_{N,N-1} & k_{N,N} \end{bmatrix} \begin{Bmatrix} \psi_1 \\ \vdots \\ \psi_{N-1} \\ \psi_N \end{Bmatrix} = \underline{\mathbf{0}}, \tag{2.33}$$

where ψ_j is the displacement (or rotation) corresponding to degree of freedom j. ψ_N is assumed to be -1.0. The rest of the displacements (and rotations) are then calculated by rewriting Eq. (2.33) in the form:

$$\begin{Bmatrix} \psi_1 \\ \vdots \\ \psi_{N-1} \end{Bmatrix} = \begin{bmatrix} k_{1,1} & \cdots & k_{1,N-1} \\ \vdots & \ddots & \vdots \\ k_{N-1,1} & \cdots & k_{N-1,N-1} \end{bmatrix}^{-1} \begin{Bmatrix} k_{1,N} \\ \vdots \\ k_{N-1,N} \end{Bmatrix}. \tag{2.34}$$

The mode shapes can thus be plotted. A different calculation procedure was followed by Howson (1979), based on the assumption of a random force vector. Blevins (1979) reported explicit equations describing the mode shapes for different cases of beam boundary conditions. For cracked beams, explicit equations can be deduced by enforcing the displacements (and rotations) calculated at the beam boundaries and at each crack location, including the two rotations to the left and right of each crack (Fig. 2.1). A different and higher order matrix than that of Eq. (2.22) must then be used. Explicit closed-form expressions have been formulated by Caddemi and Caliò (2009) using Dirac's delta distribution functions. For consistency, the numerical procedure described by Eqs. (2.33) and (2.34) has been implemented in this thesis and programmed into MATLAB. Appropriate scaling may be required to display the mode shapes properly. The MATLAB code takes just a few seconds to run. Calculating the first ten natural frequencies and plotting the corresponding mode shapes of the two bay, two storey frame described in Section 2.3.2.2 takes 2.80 seconds.

2.2.4. Numerical examples

2.2.4.1. Beam with free ends

Fig. 2.3 shows a beam with free ends having two open cracks represented by two rotational springs of stiffness k_1^* and k_2^*. The mass per unit length of the HE100B steel beam μ is 20.775 kg m^{-1}, the bending stiffness EI is 961421 N m^2 and the axial stiffness EA is 5.57 × 10^8 N. Different cases for the rotational spring stiffnesses, considered previously by Caddemi and Morassi (2013), are shown in Table 2.2. The infinite stiffness denotes no crack. For each case, the first four natural frequencies (disregarding the rigid body modes) obtained using the present theory and those reported by Caddemi and Morassi (2013) are presented in Table 2.3. The mode shapes corresponding to Case 5 are shown in Fig. 2.4.

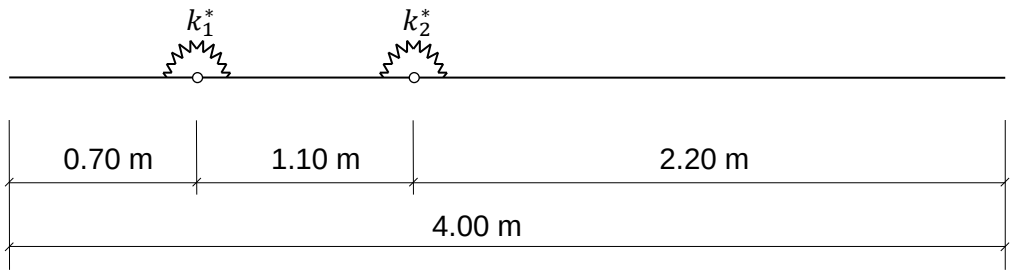

Fig. 2.3. Multiple cracks in a beam with free ends.

Table 2.2. Different cases for k_1^* and k_2^*.

Case no.	1	2	3	4	5
k_1^* (kN m rad^{-1})	∞	1936.4	439.0	439.0	439.0
k_2^* (kN m rad^{-1})	∞	∞	∞	1915.6	426.2

Table 2.3. First four natural frequencies of the free-free beam.

Case no.	ω_1 (Hz)		ω_2 (Hz)		ω_3 (Hz)		ω_4 (Hz)	
	Present	Previous*	Present	Previous*	Present	Previous*	Present	Previous*
1	47.87	47.9	131.97	132.0	258.71	258.7	427.66	427.7
2	47.12	47.1	123.37	123.4	232.67	232.7	392.87	392.9
3	44.50	44.5	101.81	101.8	201.08	201.1	368.46	368.5
4	39.62	39.6	101.52	101.5	182.64	182.6	367.57	367.6
5	30.00	30.0	101.02	101.0	161.66	161.7	366.54	366.6

* Caddemi and Morassi (2013)

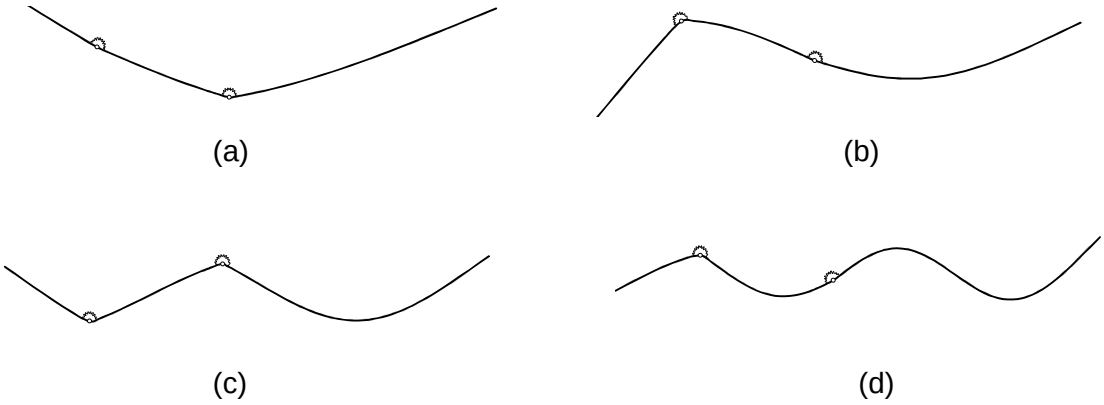

Fig. 2.4. First four mode shapes of cracked beam with free ends. (a) $\omega_1 = 30.00$ Hz; (b) $\omega_2 = 101.02$ Hz; (c) $\omega_3 = 161.66$ Hz; (d) $\omega_4 = 366.54$ Hz.

2.2.4.2. Cantilever beam

The cantilever beam shown in Fig. 2.5 has length 0.20 m, cross-sectional depth $h = 0.0078$ m, mass per unit length $\mu = 1.5308$ kg m^{-1} and bending stiffness $EI = 231.548$ N m^2 (Banerjee and Guo 2009). A single open crack is introduced, where different cases for its location and severity were considered previously by Banerjee and Guo (2009) and are illustrated in Table 2.4. Eq. (2.3d) from Table 2.1 is used to obtain the equivalent spring stiffness. For each case, the first three natural frequencies of the beam obtained using the present theory and those reported by Banerjee and Guo (2009) are presented in Table 2.5. The mode shapes corresponding to Case 4 are shown in Fig. 2.6.

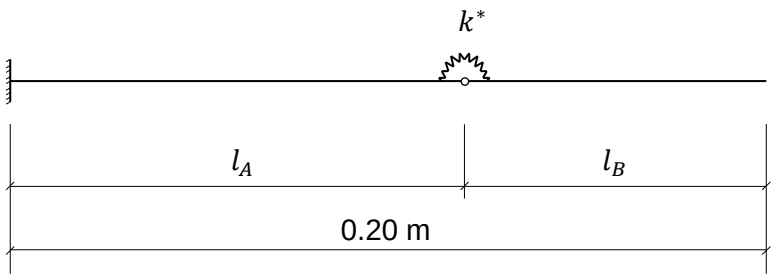

Fig. 2.5. Cantilever beam with a single crack.

Table 2.4. Different cases for k^*, l_A and l_B.

Case no.	1	2	3	4	5	6	7
l_A (m)	-	0.08	0.08	0.08	0.12	0.12	0.12
l_B (m)	-	0.12	0.12	0.12	0.08	0.08	0.08
d/h	Intact	0.20	0.40	0.60	0.20	0.40	0.60
k^* (kN m rad^{-1})	∞	130.00	28.80	8.39	130.00	28.80	8.39

Table 2.5. First three natural frequencies of the cantilever beam.

Case no.	ω_1 (rad s^{-1})		ω_2 (rad s^{-1})		ω_3 (rad s^{-1})	
	Present	Previous*	Present	Previous*	Present	Previous*
1	1038.2	1038.2	6506.3	6506.4	18218	18218
2	1034.6	1031.8	6469.6	6441.3	18152	18098
3	1022.2	1010.1	6348.9	6237.0	17942	17740
4	985.98	949.82	6036.0	5768.5	17447	17015
5	1037.3	1036.6	6456.8	6419.0	18137	18070
6	1034.2	1030.9	6292.3	6139.9	17879	17633
7	1024.4	1013.7	5852.0	5468.2	17276	16761

* Banerjee and Guo (2009)

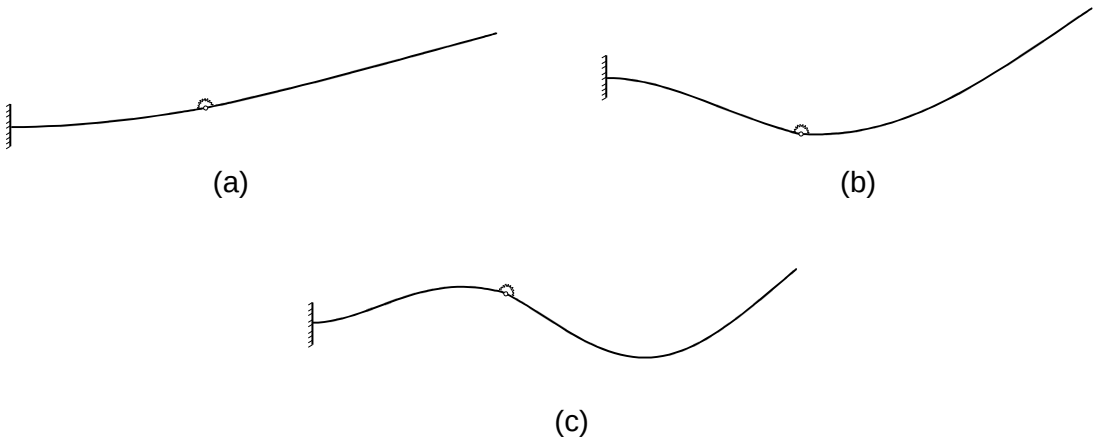

Fig. 2.6. First three mode shapes of cracked cantilever beam. (a) $\omega_1 = 985.98$ rad s^{-1}; (b) $\omega_2 = 6036.0$ rad s^{-1}; (c) $\omega_3 = 17447$ rad s^{-1}.

2.3. Natural frequencies of cracked frames

2.3.1. Assembling the global dynamic stiffness matrix

The global dynamic stiffness matrix of a cracked frame is assembled using those of the individual constituent cracked beams, obtained in Section 2.2.2. The stiffness matrix of each beam in the local coordinate system is transformed to that in the global coordinate system using the relation (Howson 1979):

$$\mathbf{K}_{\text{global}} = \mathbf{T}^{t}\mathbf{K}_{\text{local}}\mathbf{T}, \tag{2.35}$$

where $\mathbf{T}$ is the transformation matrix, given by:

$$\mathbf{T} = \begin{bmatrix} \mathbf{t} & \mathbf{0} \\ \mathbf{0} & \mathbf{t} \end{bmatrix}, \tag{2.36}$$

in which

$$\mathbf{t} = \begin{bmatrix} \cos\theta & \sin\theta & 0 \\ -\sin\theta & \cos\theta & 0 \\ 0 & 0 & 1 \end{bmatrix}, \tag{2.37}$$

with θ being the inclination angle of the beam's longitudinal axis from an arbitrary global axis. The degrees of freedom represented by $\mathbf{K}_{\text{local}}$ and $\mathbf{T}$ are in the same order as in Eq. (2.22). At each node of the frame, having three degrees of freedom, i.e. two translations and one rotation, the stiffness terms of the members connected at the node are added together, to form the global stiffness matrix of the frame. The natural frequencies are then calculated and the corresponding mode shapes are extracted in a similar manner to that described in Section 2.2.3 for cracked beams. The above process has been programmed using MATLAB.

2.3.2. Numerical examples

2.3.2.1. Two bay, single storey frame example

Table 2.6 shows the first eleven natural frequencies of the frame shown in Fig. 2.7, for the undamaged case and damage scenarios i and ii. The results obtained previously by Caddemi and Caliò (2013) and those obtained using the current method are presented. Both methods use the values 2.06×10^{11} N m^{-2} and 185.40 kg m^{-1} for Young's modulus and the mass per unit length, respectively. The beams and columns have the same length $l = 12.00$ m and

cross-sectional dimensions 198 mm × 122 mm. The crack depth to section height ratio d/h for the beams and columns is 0.90 in the case of damage scenario i, so that λ^* is 1.1183. For damage scenario ii, $\lambda^* = 0.20$ for columns and 0.40 for beams, so that $d/h = 0.7688$ and 0.8343, respectively. The cracks are assumed to be always open. Eq. (2.4) is used to obtain the equivalent spring stiffness. The mode shapes corresponding to the first five natural frequencies for damage scenario i are shown in Fig. 2.8. The first six natural frequencies, in the case of damage scenario iii, for different crack depth to section height ratios are presented in Table 2.7. This scenario represents cracking due to earthquake loading.

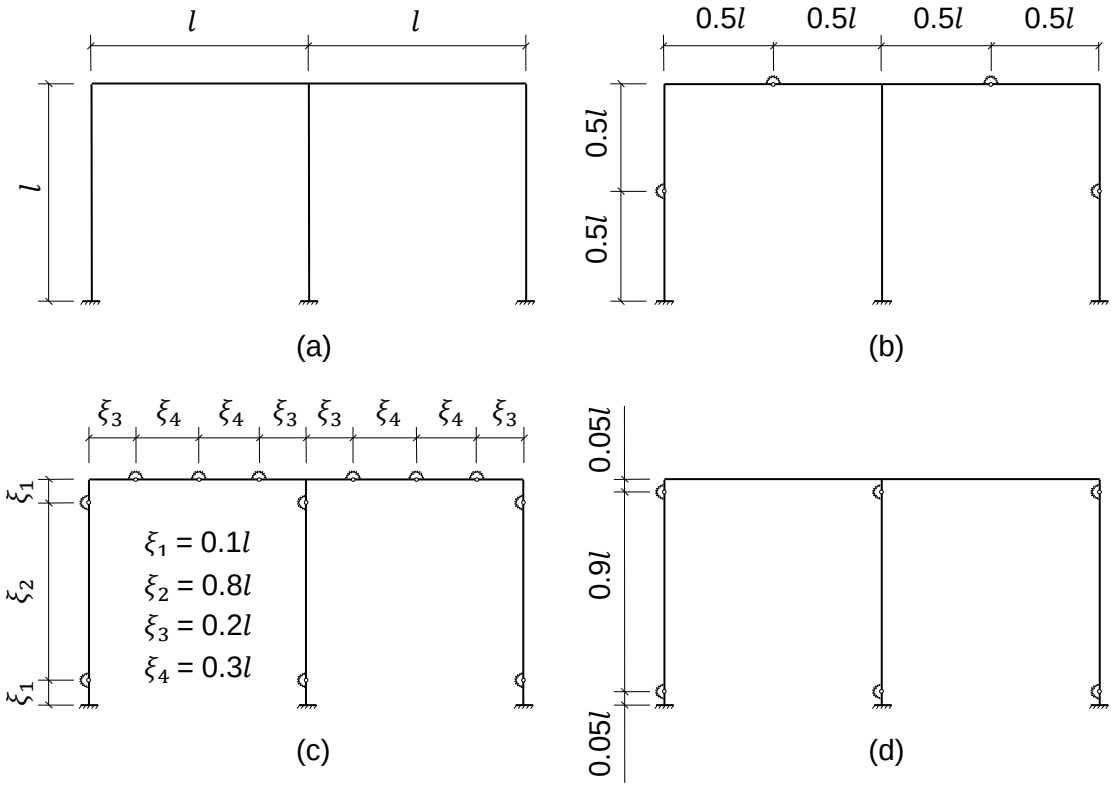

Fig. 2.7. Two bay, single storey frame damage scenarios. (a) Undamaged frame; (b) Damage scenario i; (c) Damage scenario ii; (d) Damage scenario iii.

Table 2.6. First eleven natural frequencies of the frame in Fig. 2.7 for damage scenarios i and ii.

i	ω_i (Hz)								
	Intact case			Damage scenario i			Damage scenario ii		
	Present	Previous*	%Diff.	Present	Previous*	%Diff.	Present	Previous*	%Diff.
1	0.5987	0.5987	0.00	0.5919	0.5919	0.00	0.4489	0.4489	0.00
2	2.4662	2.4667	0.02	1.7167	1.7167	0.00	1.8389	1.8389	0.00
3	3.1080	3.1095	0.05	2.2836	2.2842	0.03	2.4482	2.4486	0.02
4	4.1885	4.1894	0.02	3.2057	3.2062	0.02	3.5469	3.5474	0.01
5	4.5085	-	-	3.3609	-	-	3.7735	-	-
6	4.5110	-	-	4.2796	-	-	3.8458	-	-
7	8.9315	-	-	8.7921	-	-	6.4160	-	-
8	10.0628	-	-	9.5945	-	-	7.7875	-	-
9	11.3283	-	-	10.8836	-	-	9.5373	-	-
10	12.4102	-	-	12.4101	-	-	11.7423	-	-
11	12.7854	-	-	12.7785	-	-	12.3510	-	-

* Caddemi and Caliò (2013)

Table 2.7. Natural frequencies of the frame in Fig. 2.7, corresponding to damage scenario iii.

i	ω_i (Hz)							
	d/h = 0.2 λ^* = 0.0064		d/h = 0.4 λ^* = 0.0200		d/h = 0.6 λ^* = 0.0593		d/h = 0.8 λ^* = 0.2711	
	Present	Previous*	Present	Previous*	Present	Previous*	Present	Previous*
1	0.5916	0.5916	0.5771	0.5771	0.5410	0.5410	0.4214	0.4214
2	2.4554	-	2.4335	-	2.3814	-	2.2307	-
3	3.0952	-	3.0693	-	3.0061	-	2.8129	-
4	4.1539	-	4.0847	-	3.9200	-	3.4344	-
5	4.4617	-	4.3637	-	4.1348	-	3.5143	-
6	4.4756	-	4.4099	-	4.2547	-	3.8139	-

* Caddemi and Caliò (2013)

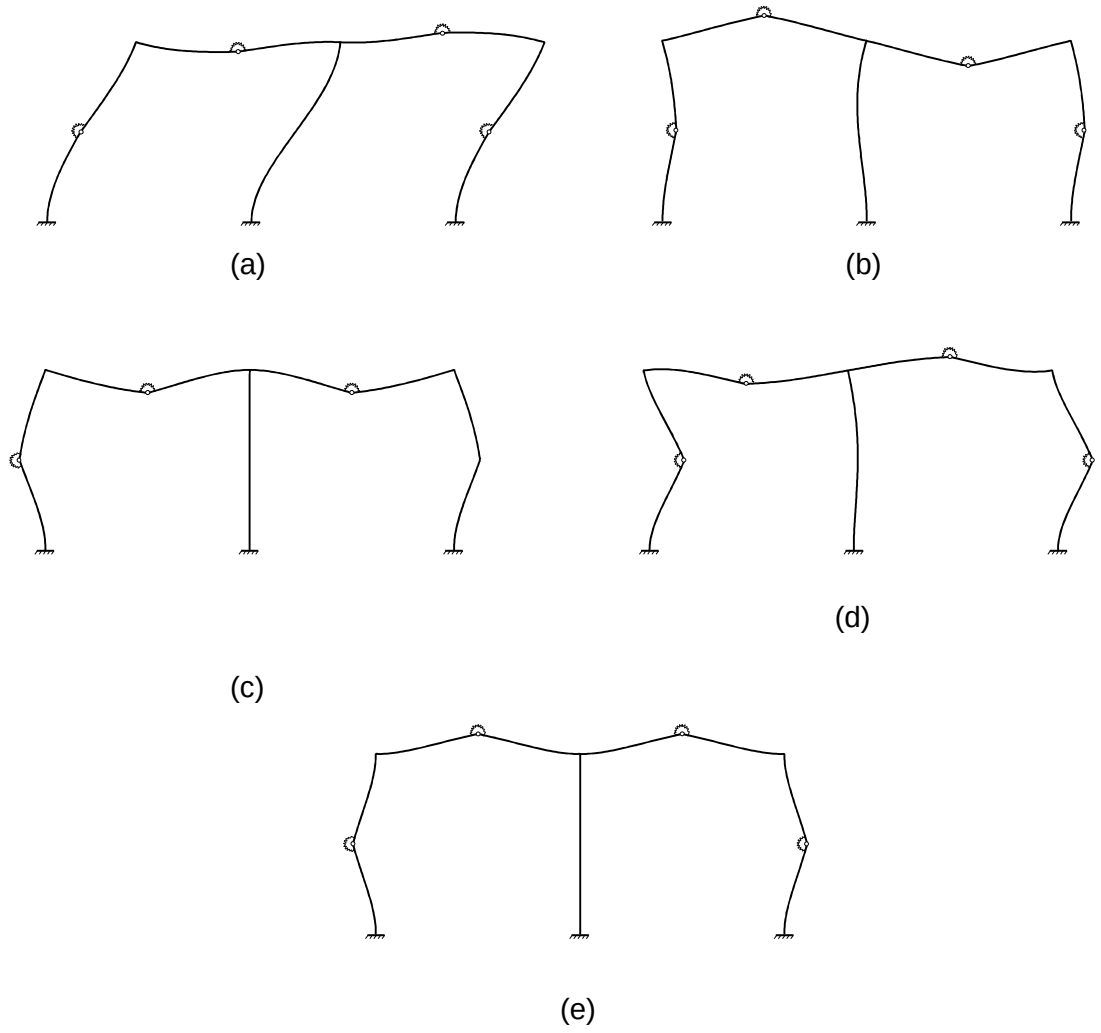

Fig. 2.8. First five mode shapes of two bay, single storey frame for damage scenario i. (a) $\omega_1 = 0.5919$ Hz; (b) $\omega_2 = 1.7167$ Hz; (c) $\omega_3 = 2.2836$ Hz; (d) $\omega_4 = 3.2057$ Hz; (e) $\omega_5 = 3.3609$ Hz.

2.3.2.2. Two bay, two storey frame example

The frame in Fig. 2.9 has the same material properties and cross-sectional dimensions as the previous example, with column lengths $l = 3.00$ m and beam lengths $2l$. The effect of changing the location of a single open crack, in any one individual member, on the natural frequencies is studied assuming a crack depth to section height ratio of 0.2. Eq. (2.4) is also used to obtain the equivalent spring stiffness. The variation of the first five natural frequencies between the uncracked and cracked cases $\Delta\omega_i$, normalised with respect to those of the uncracked case ω_{iu}, is plotted against the crack location in each member, as shown in Fig. 2.10. As the frame is symmetric, only one bay is

considered. A sample of these frequencies is given in Table 2.8, for the cases where a single crack is located at the middle of columns A, B, D, E, and at 2.5 m from the left of beams C and I. The first five mode shapes when the crack is located in Member C are shown in Fig. 2.11.

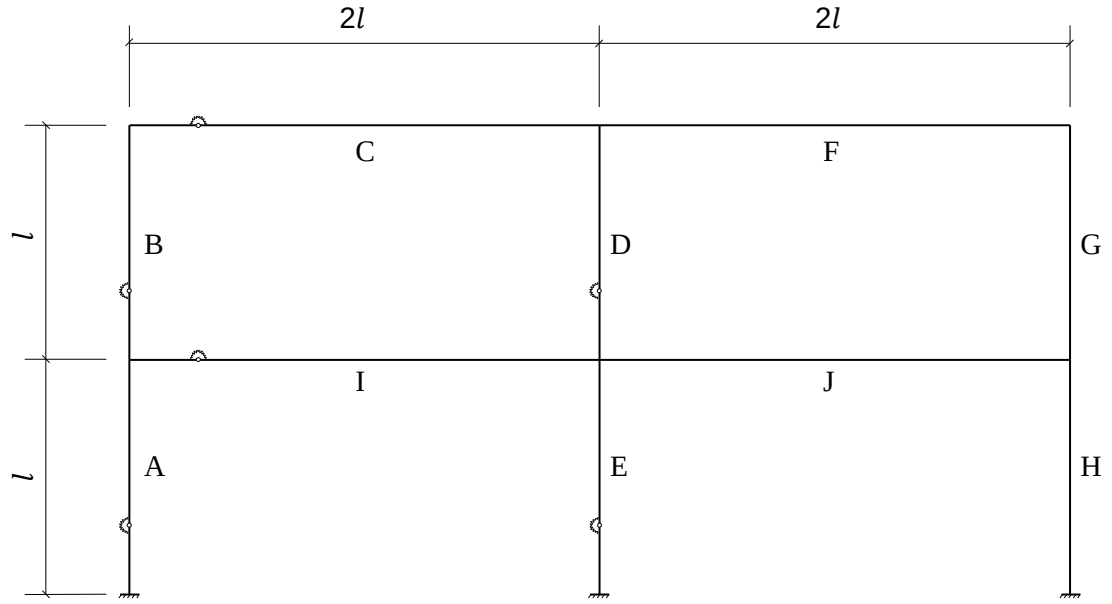

Fig. 2.9. Two bay, two storey frame.

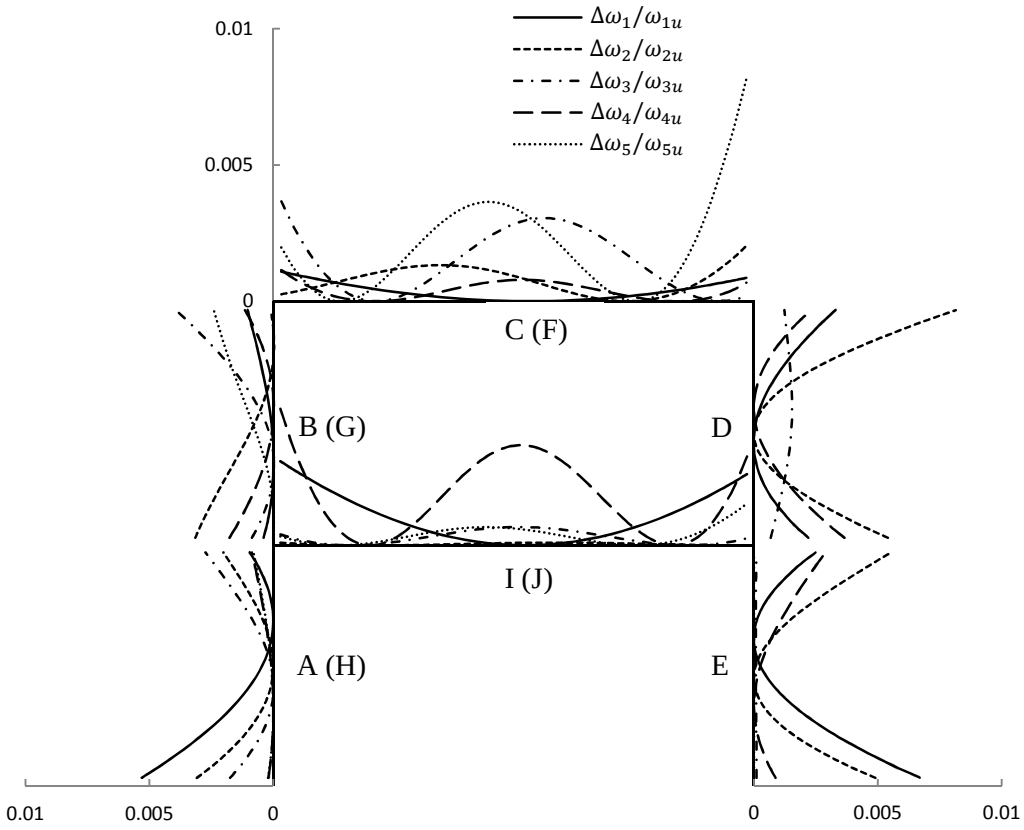

Fig. 2.10. Variation of natural frequencies $\Delta\omega_i/\omega_{iu}$ of the two bay, two storey frame with the crack location when $d/h = 0.2$.

Table 2.8. First five natural frequencies of the frame in Fig. 2.9 for different crack locations.

	ω_i (Hz)						
i	Cracked member						
	-	A	B	C	D	E	I
1	3.2675	3.2661	3.2672	3.2673	3.2673	3.2667	3.2670
2	10.8528	10.8528	10.8441	10.8393	10.8522	10.8519	10.8521
3	12.0841	12.0829	12.0802	12.0600	12.0656	12.0832	12.0772
4	14.3204	14.3191	14.3199	14.3116	14.3194	14.3166	14.2787
5	14.9931	14.9919	14.9802	14.9396	14.9931	14.9931	14.9833

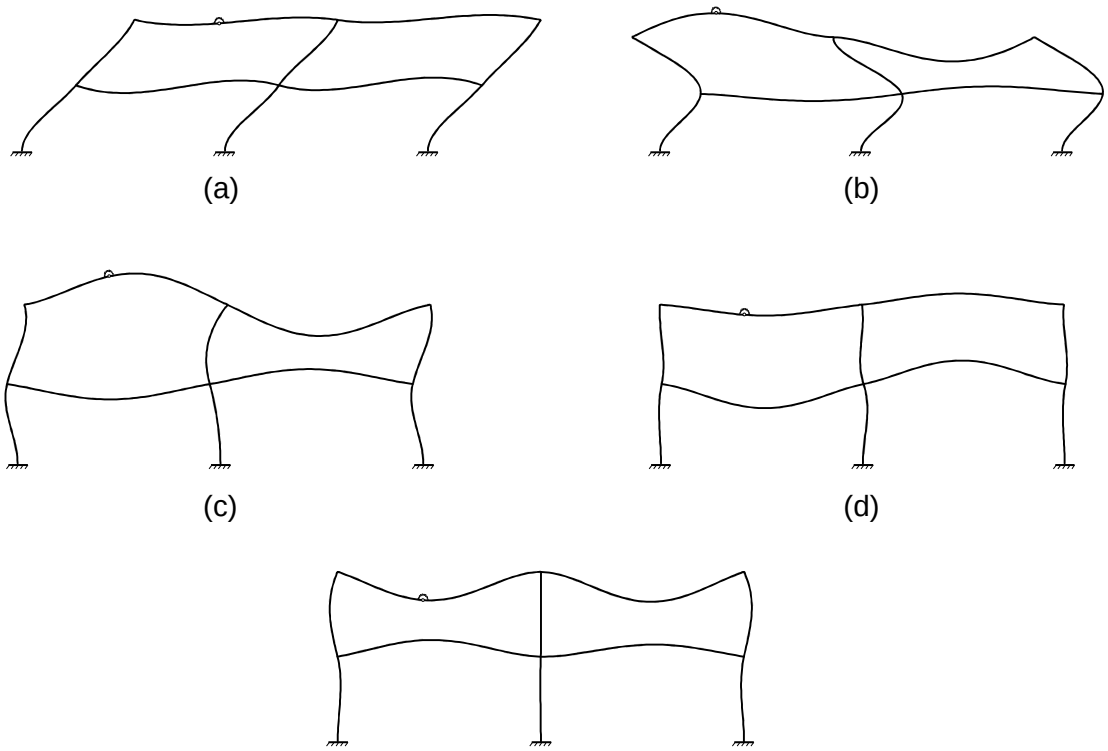

Fig. 2.11. First five mode shapes of two bay, two storey frame in the case of a crack in Member C. (a) $\omega_1 =$ 3.2673 Hz; (b) $\omega_2 =$ 10.8393 Hz; (c) $\omega_3 =$ 12.0600 Hz; (d) $\omega_4 =$ 14.3116 Hz; (e) $\omega_5 =$ 14.9396 Hz.

2.4. Discussion

The natural frequencies obtained for the cracked beam with free ends, using the theory developed here, up to two decimal places, are in close agreement with those obtained by Caddemi and Morassi (2013) up to one decimal place. It can be seen that the one decimal place is an approximation of the two decimal places. Caddemi and Morassi (2013) solved implicit formulas for the natural frequencies, obtained by applying distribution functions. The results of the cracked cantilever beam while following similar trends, however, are higher than those reported by Banerjee and Guo (2009) by a maximum of 7% (ω_2 in Case 7, where $d/h = 0.6$), as the present theory does not implement shear springs to model the crack. As the aim of crack detection methods is to identify non-severe cracks, and as the detection method demonstrated in the next chapter is generally not affected by the crack severity when locating the

crack, then the rotational spring is sufficient for crack modelling. The results of the cracked cantilever beam also show that as the crack depth to section height ratio is doubled from 0.2 to 0.4, the variation in the first three natural frequencies, between the uncracked and cracked cases, is almost quadrupled.

The dynamic stiffness matrices for the two bay single storey frame, obtained using the newly developed theory here and the distribution functions method formulated by Caddemi and Caliò (2013), produce matching results. Higher natural frequencies are obtained easily without requiring the re-insertion of additional nodes in the global stiffness matrix of the frame by taking into account the additional sign counts s_c. The effect of these is illustrated by considering damage scenarios i and ii in the example of Section 2.3.2.1. In each scenario there are eleven natural frequencies in the range 0 - 13 Hz. Using the MATLAB code, the contributions of $s\{\mathbf{K}\}$, $\sum_m J_m$, and $\sum_c s_c$ to the J count of the Wittrick–Williams algorithm (Wittrick and Williams 1971) in that frequency range are logged and shown in Figs. 2.12 and 2.13. Each increment in J represents a natural frequency. It is clear that if the additional sign counts are not taken into account above the fifth natural frequency in damage scenario i, or the fourth natural frequency in damage scenario ii, a number of natural frequencies are missed and the orders of those converged on afterwards become erroneous.

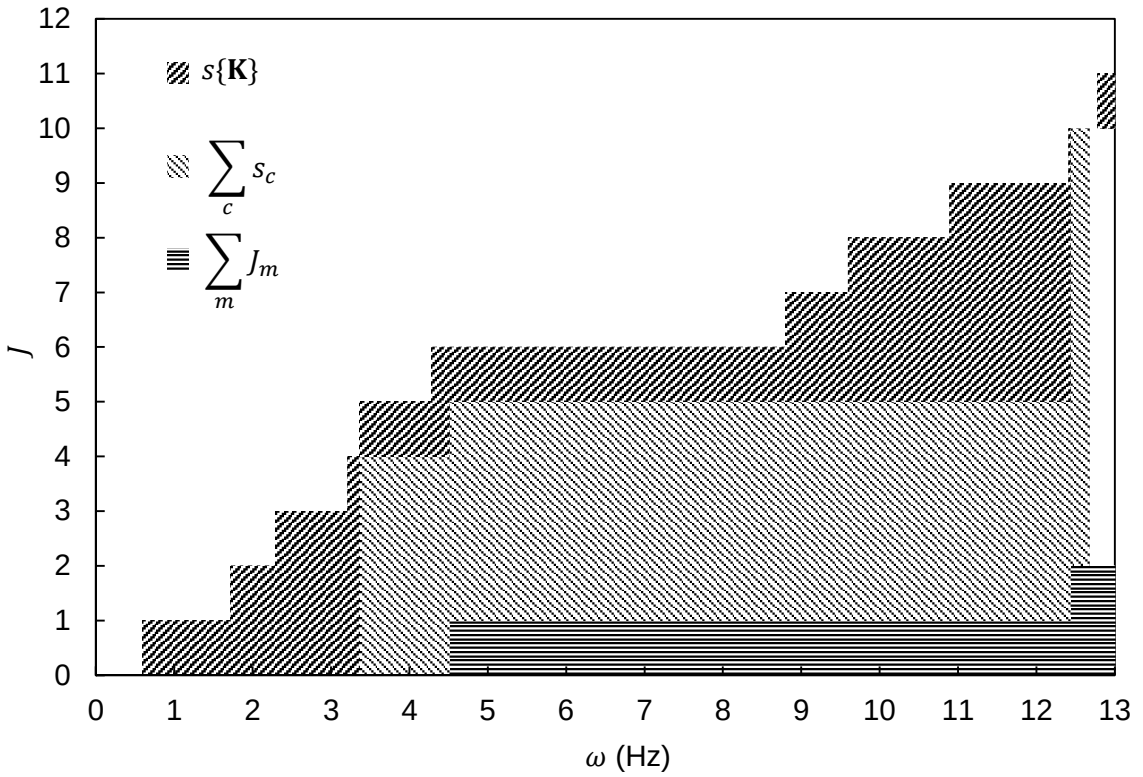

Fig. 2.12. J count and the contributions of each of its components for damage scenario i.

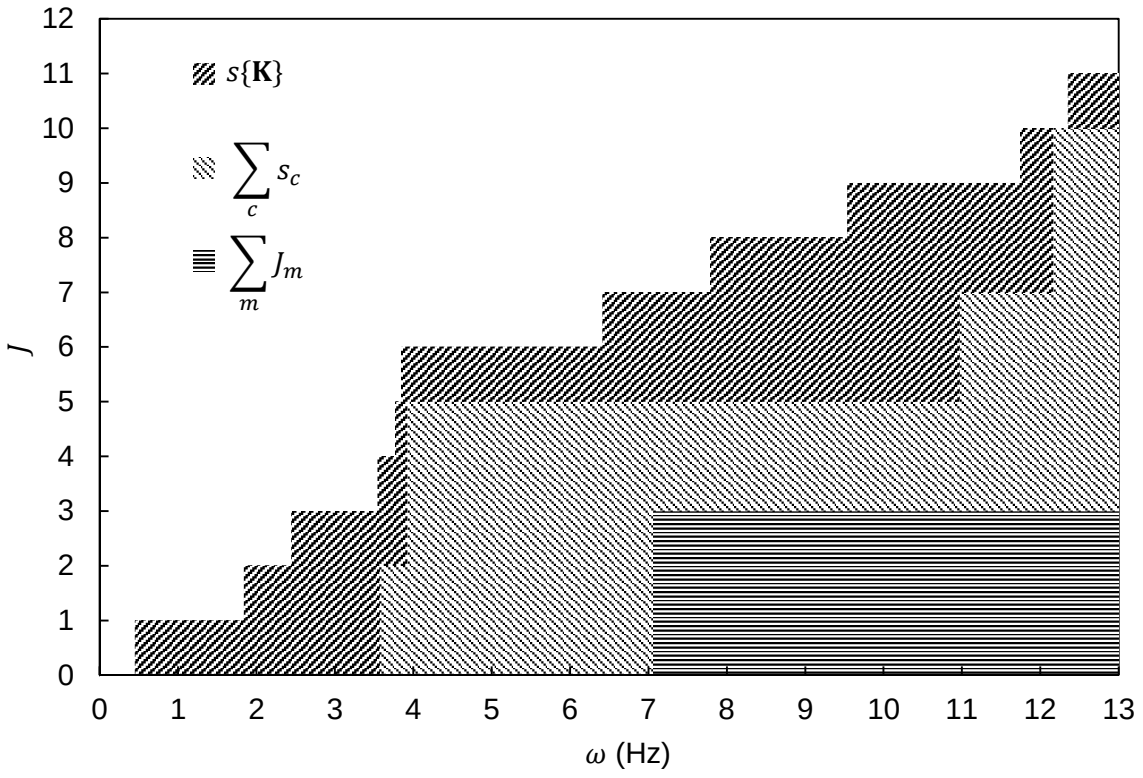

Fig. 2.13. J count and the contributions of each of its components for damage scenario ii.

The results obtained for the two bay, two storey frame show that different natural frequencies have different sensitivities to a crack according to its location in each member. A crack located close to the middle of the columns causes negligible changes to all the natural frequencies, apart from the third frequency in the upper central column, in addition to the second and fifth frequencies in the upper outer column. By observing the mode shapes in Fig. 2.11, it can be seen that at these frequencies, the crack is not coincident with an inflection point. The fifth frequency is insensitive to a crack, located anywhere in the central columns, as this frequency corresponds to a symmetric mode of vibration in which the central columns remain straight.

The relative sensitivities of the different natural frequencies to the crack location and severity can be used in devising a method for crack detection. The curves in Fig. 2.10 suggest that up to three natural frequencies, or more, may be required to accurately locate a crack, depending on the complexity of the structure. It can also be deduced that the natural frequencies have to be measured to a reasonable accuracy in the uncracked and cracked cases, which is a realistic proposition in contrast to alternative approaches based on comparisons of the vibration modes which, in practice, need a large number of measurement points.

2.5. Conclusions

This chapter presents a new method for calculating the natural frequencies of cracked beams and frames. Dynamic stiffness matrices for beams with multiple cracks are evaluated in a recursive manner according to the number of cracks, following which the global dynamic stiffness matrix of the cracked frame is assembled. The Wittrick–Williams algorithm (Wittrick and Williams 1971) is used to calculate the natural frequencies of the multiply cracked beams and frames. The method compares well with earlier approaches, as long as the spring models representing the cracks are the same. To evaluate higher order frequencies and to avoid missing any, additional sign counts removed by the partial Gaussian elimination must be accounted for. The method can be extended to incorporate shear and axial springs with the view of accurately solving the inverse problem of identifying damage location and magnitude from measured natural frequencies.

Chapter 3 – Single crack detection in frames

3.1. Introduction

Crack detection in a structural element comprises locating the crack and determining its severity. In this chapter, a new method is devised for detecting a single crack in a frame using natural frequency simulations. The assumptions outlined in Section 2.1 for beams are adopted and the rotational spring model is used. Crack localisation is based on normalising the variation between the uncracked and cracked natural frequencies. The method requires the uncracked natural frequencies to be known before any crack is introduced to the structure under consideration. Working with the frequency variations justifies neglecting structural damping (Adams et al. 1978), although its incorporation, whilst outside the scope of this thesis, can be advantageous in determining the crack severity. The crack severity is instead determined by applying the Wittrick–Williams algorithm (Wittrick and Williams 1971) to converge on the crack depth to section height ratio instead of the natural frequency.

Simulated noise free and noisy natural frequency measurements are considered. The effect of measurement noise is studied by applying the principles of interval arithmetic (Moore 1979) to the normalised simulated natural frequency variations. Empirical probability distributions are used to graphically represent the detected crack locations in the presence of measurement noise. The extracted crack severities are plotted over the detected locations.

3.2. Eliminating the crack severity variable through normalisation

As established in Chapter 2, the presence of a crack in a frame member causes degradation in the natural frequencies, according to the crack location and severity. An approximate relationship between the natural frequencies in the uncracked and cracked cases can be written as (Adams et al. 1978; Hearn and Testa 1991; Morassi 1993, 2008):

$$\omega_{ic} = \omega_{io}\left(1 - \tilde{s}.\, f_i(x/l)\right), \tag{3.1}$$

where ω_{io} and ω_{ic} are the natural frequencies in the uncracked and cracked cases, respectively, i is the mode number, $\tilde{s}$ is a function of the crack severity which does not depend on the mode number, x is the crack location measured along the longitudinal axis of the member, l is the length of the frame member, and $f_i(x/l)$ is a function of the dimensionless crack location x/l. Eq. (3.1) is originated by the evaluation of the first order variation of the natural frequencies and applicable only for the case of small intensity cracks (Morassi 2008). As mentioned in the previous chapter, it is assumed in this thesis that small intensity cracks have crack depth to section height ratios $d/h \leq 0.4$. The variation between the uncracked and cracked natural frequencies, δ_i, thus takes the form:

$$\delta_i = 1 - \frac{\omega_{ic}}{\omega_{io}} = \tilde{s}.f_i(x/l). \tag{3.2}$$

Normalising the frequency variation set has the important benefit of eliminating the dependency on the crack severity, similar to the trend previously emphasized by Adams et al. (1978), Hearn and Testa (1991), and Morassi (1993, 2008) for the ratio between the natural frequency changes of two different vibration modes. Normalisation gives the equation:

$$\overline{\delta}_i(x/l) = \frac{\delta_i}{\sqrt{\sum_i \delta_i^2}} = \frac{f_i(x/l)}{\sqrt{\sum_i \left(f_i(x/l)\right)^2}}, \tag{3.3}$$

where the summation extends over the total number of selected natural frequencies, which can be of any order. The set of $\overline{\delta}_i$ thus represents a vector of magnitude 1.0, such that $0 \leq \overline{\delta}_i \leq 1.0$.

The crack detection procedure, whether using noise free or noisy natural frequency simulations, begins with the selection of a number of discrete points randomly along the length of each individual frame member. These points represent possible crack locations. The associated natural frequencies can then be accurately calculated using the method formulated in Chapter 2, assuming an arbitrary crack depth d^* with d^*/h less than 0.4. These natural frequencies correspond to preselected vibration modes. The natural frequencies in the uncracked case are also calculated. From Eq. (3.3), the normalised frequency

variations $\{\overline{\delta}_i(x/l)\}$ which do not depend on the crack severity, i.e. crack depth to section height ratio d^*/h, are then obtained at each point for each mode i.

3.3. Detecting a single crack in a frame using noise free simulations

3.3.1. Detection procedure

For a single crack having a crack depth to section height ratio d/h, the set of normalised measured (or simulated) natural frequency variations $\overline{\delta}_{im}$, is calculated in a similar manner to Eqs. (3.2) and (3.3), assuming no measurement noise. This set is then subtracted from the normalised frequency variation set at each discrete point $\overline{\delta}_i(x/l)$, giving the function:

$$G_i(x/l) = \overline{\delta}_i(x/l) - \overline{\delta}_{im}, \tag{3.4}$$

where -1.0 ≤ G_i ≤ 1.0. G_i is then plotted against the varying crack location in the frame member. The procedure is repeated for all frame members. The crack location is the point through which all curves pass through zero, i.e. $G_i(x/l) = 0$, for all i. If the frame is symmetric, two such locations are detected.

In practice, the actual crack location is not known a priori and can fall between any two successive discrete points. As a result, the zeros of the curves, near the correct crack location, may not coincide but will be closely spaced. The zeros of each curve are obtained using the cubic spline interpolation in MATLAB (MathWorks 2012) which converts the discrete G_i values to a piecewise polynomial, as shown in Fig. 3.1. A small tolerance is imposed on the spacing between the zeros of the interpolated G_i curves to make a preliminary estimation of the crack location between two discrete points x_1/l and x_2/l as shown in Fig. 3.2a. A pin-point estimation, point a shown in Fig. 3.2b, is then made by applying the parabolic least squares fitting method described in Section 3.3.2. The fitting method has been incorporated when programming the detection procedure into MATLAB.

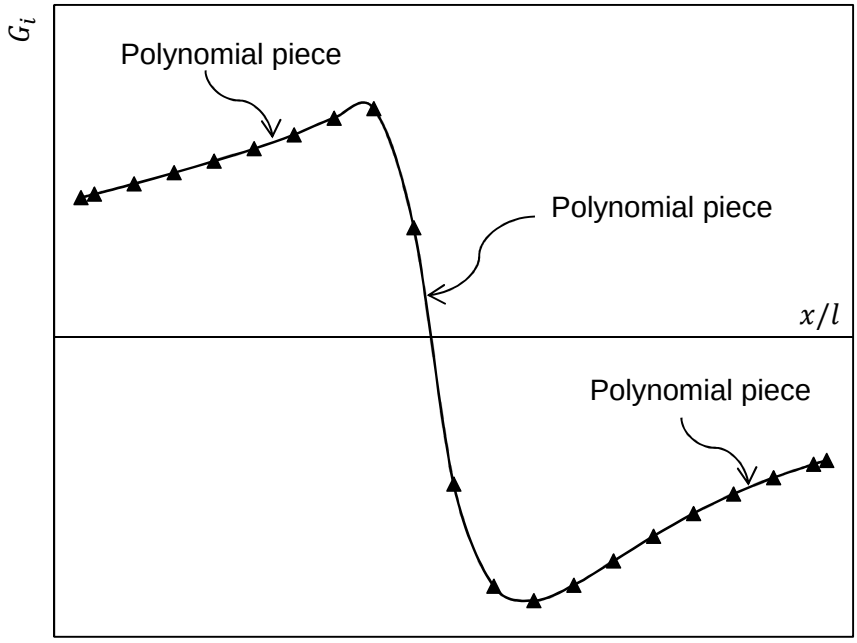

Fig. 3.1. Piecewise polynomial G_i.

(a)

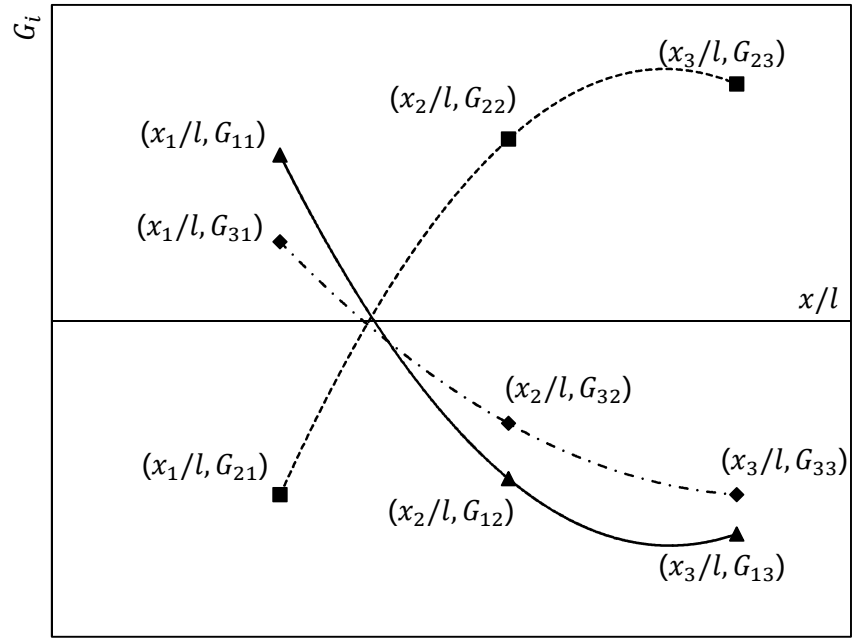

(b)

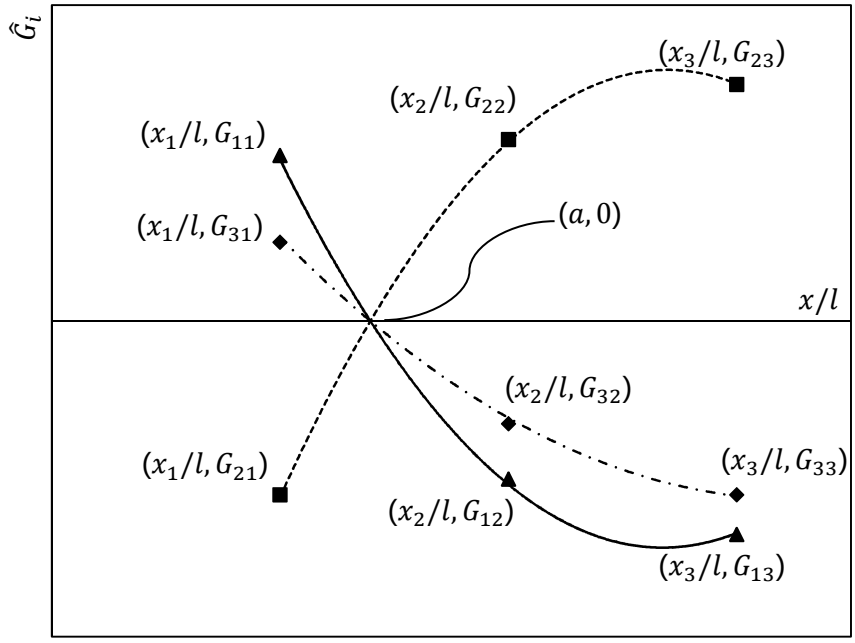

Fig. 3.2. Estimation of the crack location. (a) G_i curves with non-coincident zeros; (b) Parabolic least squares fitted curves $\hat{G}_i$ with a common zero at a.

The crack severity is recovered by applying the Wittrick–Williams algorithm (Wittrick and Williams 1971) to converge on the ratio d/h. The detected crack location and any individual simulated natural frequency in the cracked case are treated as input data. The J count of Eq. (2.30) is re-programmed into MATLAB, so that it varies with d/h, instead of the frequency ω. The initial lower and upper bounds of d/h are known to be 0.0 and 1.0, respectively. The bisection procedure is carried out in a similar manner to that used in the natural frequency calculation, such that new upper or lower bounds are established when $J \geq i$ or $J < i$, respectively. It must be noted that if the severity recovery procedure is repeated using any other simulated frequency, near-equal values of d/h are obtained.

3.3.2. Parabolic least squares fit

Referring to Fig. 3.2, to find a family of parabolic functions $\hat{G}_i(x/l)$ providing a best fit to the values

$$G_i(x_1/l) = G_{i1}, \qquad G_i(x_2/l) = G_{i2}, \qquad G_i(x_3/l) = G_{i3}, \tag{3.5}$$

for each i and which all cross the x/l axis at some point a satisfying:

$$\hat{G}_i(a) = 0, \tag{3.6}$$

let

$$\hat{G}_i(x/l) = b_i(x/l - a) + c_i(x/l - a)^2. \tag{3.7}$$

The functions $\hat{G}_i(x/l)$ are found by minimising the least squares residual

$$F(a, \{b_i, c_i\}) = \sum_i \sum_{j=1}^{3} \left[b_i\left(x_j/l - a\right) + c_i\left(x_j/l - a\right)^2 - G_{ij} \right]^2. \tag{3.8}$$

Assuming a is known, then for each i

$$\frac{\partial F}{\partial b_i} = \sum_{j=1}^{3} 2\left(x_j/l - a\right) \left[b_i\left(x_j/l - a\right) + c_i\left(x_j/l - a\right)^2 - G_{ij} \right] = 0, \tag{3.9}$$

$$\frac{\partial F}{\partial c_i} = \sum_{j=1}^{3} 2\left(x_j/l - a\right)^2 \left[b_i\left(x_j/l - a\right) + c_i\left(x_j/l - a\right)^2 - G_{ij} \right] = 0. \tag{3.10}$$

Writing

$$S_2 = \sum_{j=1}^{3} \left(x_j/l - a\right)^2, \qquad S_3 = \sum_{j=1}^{3} \left(x_j/l - a\right)^3, \qquad S_4 = \sum_{j=1}^{3} \left(x_j/l - a\right)^4, \tag{3.11}$$

$$T_{i1} = \sum_{j=1}^{3} \left(x_j/l - a\right) G_{ij}\,, \qquad T_{i2} = \sum_{j=1}^{3} \left(x_j/l - a\right)^2 G_{ij}, \tag{3.12}$$

Eqs. (3.9) and (3.10) take the form:

$$\begin{pmatrix} S_2 & S_3 \\ S_3 & S_4 \end{pmatrix} \begin{pmatrix} b_i \\ c_i \end{pmatrix} = \begin{pmatrix} T_{i1} \\ T_{i2} \end{pmatrix}, \tag{3.13}$$

giving

$$b_i = \frac{S_4 T_{i1} - S_3 T_{i2}}{S_2 S_4 - S_3^2}, \qquad c_i = \frac{-S_3 T_{i1} + S_2 T_{i2}}{S_2 S_4 - S_3^2}. \tag{3.14}$$

Eq. (3.8) can be evaluated to give the least squares residual $F(a)$ as a function of a, which can be minimised by repeating the above calculations at successive trial values of a. These calculations do not involve evaluation of the underlying functions $\hat{G}_i(x/l)$.

3.3.3. Numerical example

The crack detection procedure is applied to the two-bay, two-storey frame shown in Fig. 3.3. The geometric and material properties are described in Section 2.3.2.2. A single crack is introduced in the frame.

It is generally reported that the minimum number of required natural frequencies for crack detection is three (Greco and Pau 2012). The first three natural frequencies are selected in the analysis. Table 3.1 shows different cases for the crack location and the ratio of the crack depth to section height d/h, along with the corresponding first four natural frequencies, calculated accurately up to the eleventh decimal place, but reported to the fourth decimal place. The fourth frequency will be used later when simulated noise is introduced. The natural frequencies are calculated using the method described in Chapter 2.

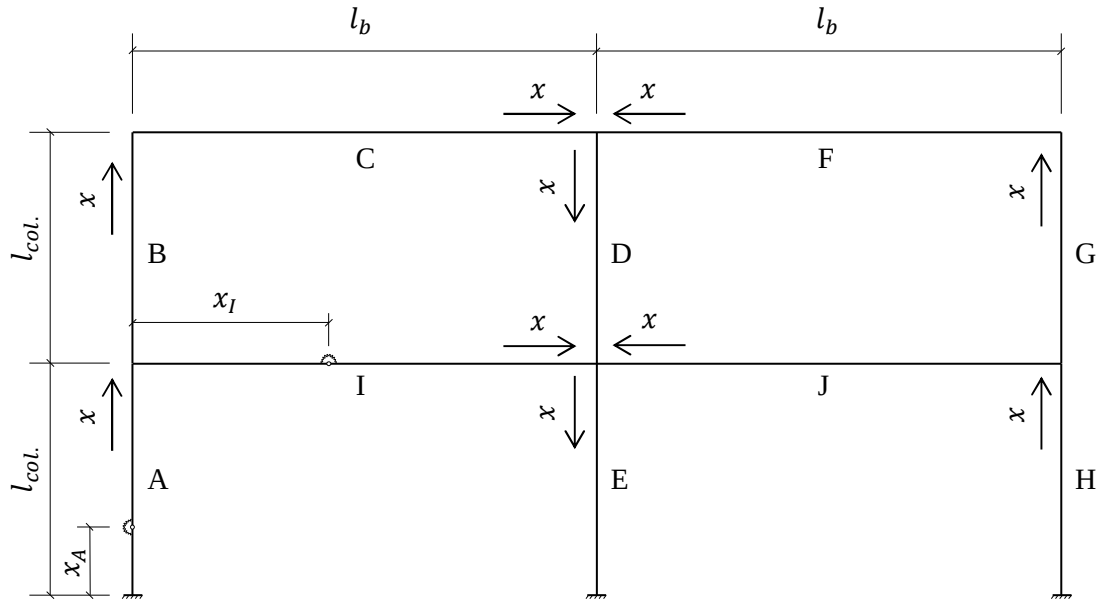

Fig. 3.3. Two bay, two storey frame.

Table 3.1. First four natural frequencies of the two-bay, two-storey frame.

Case no.	Crack location			d/h	ω_1 (Hz)	ω_2 (Hz)	ω_3 (Hz)	ω_4 (Hz)
	Member	x/l	x (m)					
0	Uncracked case				3.2675	10.8528	12.0840	14.3203
1	A	0.240	0.720	0.300	3.2527	10.8346	12.0762	14.3200
2	I	0.485	2.910	0.300	3.2674	10.8509	12.0690	14.2236
3	I	0.485	2.910	0.005	3.2675	10.8527	12.0839	14.3194
4	I	0.485	2.910	0.900	3.2634	10.0462	10.9830	12.5105

The columns are discretised such that the crack is assumed to be located in turn at each of the 21 points distanced at {0.033, 0.050, 0.100, 0.150…0.850, 0.900, 0.950, 0.967} $l_{col.}$ from the ends, while the beams are discretised into 41 points distanced at {0.017, 0.025, 0.050, 0.075…0.925, 0.950, 0.975, 0.983} l_b. Thus, the columns and the beams are discretised at {0.10, 0.15, 0.30, 0.45…2.55, 2.70, 2.85, 2.90} m and {0.10, 0.15, 0.30, 0.45…5.55, 5.70, 5.85, 5.90} m, respectively, from the ends. The first and last points are chosen to be conveniently close to the joints. Assuming $d^*/h = 0.3$, the natural frequencies are calculated accurately as the crack is located in turn

at each discretisation point, then logged internally during the execution of the MATLAB code.

The first three natural frequencies shown in Table 3.1 are calculated accurately up to a tolerance of 10^{-11} rad s^{-1}. Applying Eq. (3.4), Fig. 3.4 shows the behaviour of the G_i curves obtained for all frame members when the actual crack location is in Member A. It can be seen that the only point satisfying the condition $G_i(x/l) = 0$ falls in Member A (H). The MATLAB code correctly identifies that point at 0.24 $l_{col.}$. The results for different crack cases, along with the simulated frequency variations, are shown in Table 3.2.

Table 3.2. Detected crack locations and severities.

Case no.		1	2	3	4
δ_1		0.00452	0.00004	0.004E-4	0.00125
δ_2		0.00167	0.00017	0.016E-4	0.07432
δ_3		0.00064	0.00125	0.117E-4	0.09112
$\overline{\delta}_1$		0.92936	0.02902	0.03047	0.01066
$\overline{\delta}_2$		0.34455	0.13505	0.13624	0.63201
$\overline{\delta}_3$		0.13256	0.99041	0.99021	0.77489
	Member	A (H)	I (J)	I (J)	-
Detected crack	x/l	0.2400	0.4851	0.4844	-
	d/h	0.300	0.300	0.005	-

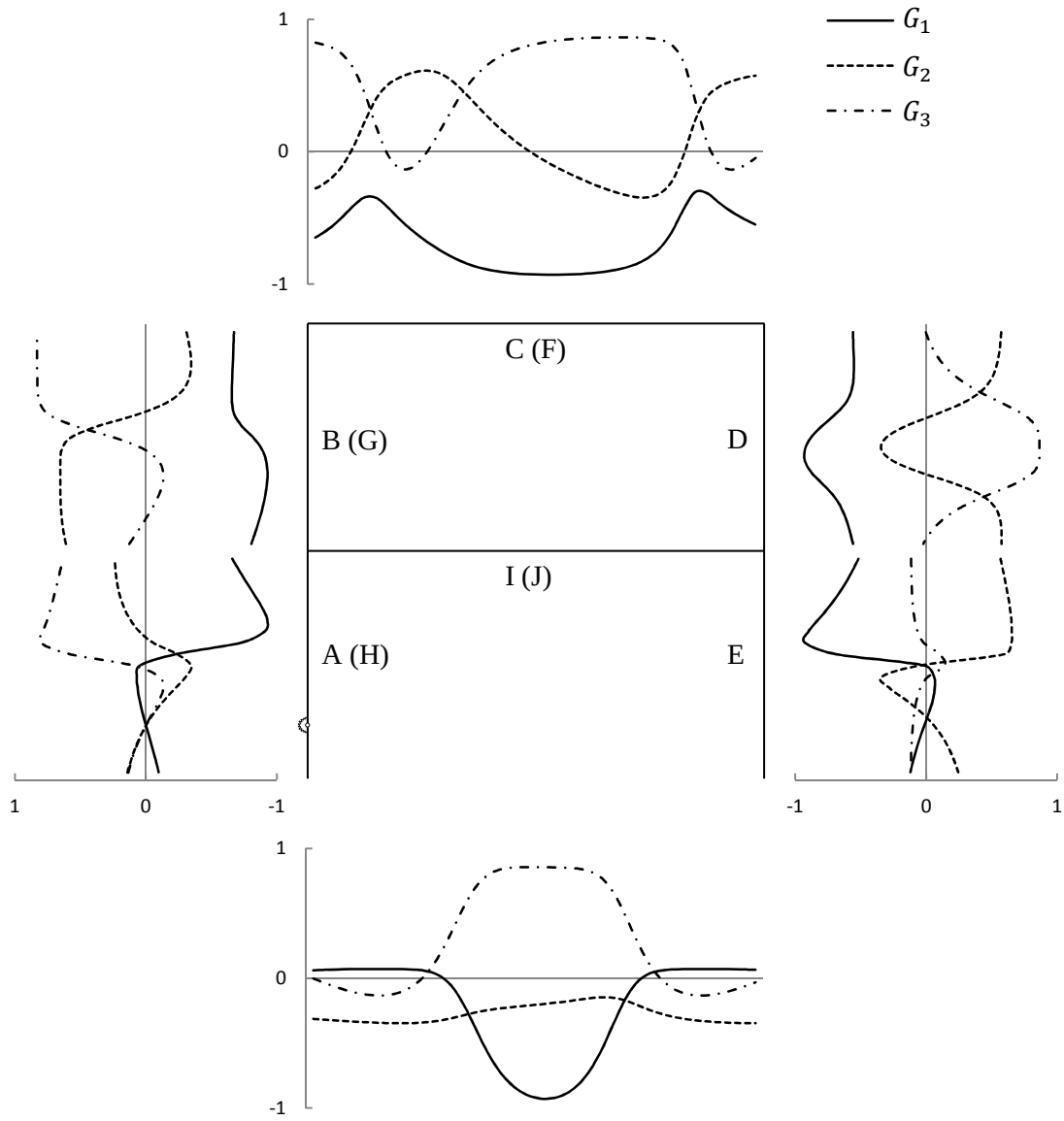

Fig. 3.4. Variation of G_i with the assumed crack location in all frame members when the actual crack location is in Member A.

Changing the assumed d^*/h to 0.5, while using the same values of the simulated frequencies, the identified crack locations are 0.2382 $l_{col.}$ and 0.4837 l_b in Members A (H) and I (J), respectively, when the actual $d/h = 0.3$. In all cases considered, the recovered values of d/h closely match the actual ones.

It must be noted that due to symmetry, the detected crack locations in Members A and I have symmetrical equivalents in Members H and J, respectively.

3.4. Detecting a single crack in a frame using simulated noisy measurements

3.4.1. Basic operations of interval arithmetic

Assuming two ranges of positive real numbers X and Y, which can be written in interval form as (Moore 1979):

$$X = [X_{LL},\, X_{UL}], \qquad Y = [Y_{LL},\, Y_{UL}], \tag{3.15}$$

where X_{LL} and Y_{LL} are the lower limits of X and Y, while X_{UL} and Y_{UL} are the upper limits, then:

$$X + Y = [X_{LL} + Y_{LL},\, X_{UL} + Y_{UL}], \tag{3.16}$$

$$X - Y = [X_{LL} - Y_{UL},\, X_{UL} - Y_{LL}], \tag{3.17}$$

$$\frac{1}{Y} = \left[\frac{1}{Y_{UL}}, \frac{1}{Y_{LL}}\right], \tag{3.18}$$

$$\frac{X}{Y} = \left[\frac{X_{LL}}{Y_{UL}}, \frac{X_{UL}}{Y_{LL}}\right]. \tag{3.19}$$

The above operations yield the narrowest intervals possible, as each variable, X and Y, occurs only once in the required operations. However, when the expressions become more complex and the variables are repeated, simplifications must first be attempted to eliminate the repetitions. Otherwise, special convergence techniques, some of which are described by Moore (1979), must be used.

3.4.2. Effect of noise and frequency variation intervals

The effect of noise in the simulated uncracked and cracked natural frequencies is studied with the aid of interval arithmetic operations. The simulated frequencies, ω_{iom} and ω_{icm}, in the uncracked and cracked cases, respectively, are assumed to lie within narrow intervals $[\omega_{iom}^{L}, \omega_{iom}^{U}]$ and $[\omega_{icm}^{L}, \omega_{icm}^{U}]$, where superscript L denotes the lower limit and U denotes the upper limit. Interval arithmetic operations are then applied to Eq. (3.2), giving

$$\delta_{im}^{L} = 1 - \frac{\omega_{icm}^{U}}{\omega_{iom}^{L}}, \qquad \delta_{im}^{U} = 1 - \frac{\omega_{icm}^{L}}{\omega_{iom}^{U}}. \tag{3.20}$$

It can be seen from Eq. (3.20) that if the simulated uncracked and cracked natural frequencies are closely spaced, their intervals can yield a negative value for δ_{im}^{L}. In this case, it can be practically assumed that the lower limit for δ_{im} is zero. The interval for each normalised frequency variation component $\overline{\delta}_{im}$, is evaluated by rewriting Eq. (3.3) in the simulated case as:

$$\overline{\delta}_{im} = \frac{1}{\sqrt{1 + \frac{\sum_{j \neq i} \delta_{jm}^{2}}{\delta_{im}^{2}}}}, \tag{3.21}$$

where each variable occurs only once, giving the narrowest possible interval $\left[\overline{\delta}_{im}^{L}, \overline{\delta}_{im}^{U}\right]$.

3.4.3. Detection procedure

As described in Section 3.2, a number of possible crack locations are assumed at discrete points along each member of the frame. The selected natural frequencies are calculated for each assumed crack location using the method described in Chapter 2. Eq. (3.3) is then applied, giving the exact normalised natural frequency variation components $\overline{\delta}_{i}(x/l)$ ranging from 0.0 to 1.0. Each $\overline{\delta}_{i}(x/l)$ is plotted against the varying crack location in all frame members. The calculated intervals $\left[\overline{\delta}_{im}^{L}, \overline{\delta}_{im}^{U}\right]$ obtained by applying interval arithmetic operations on Eq. (3.21) are then represented by horizontal lines which intersect the plotted curves, as illustrated in Fig. 3.5, giving a number of possible crack location ranges corresponding to each chosen natural frequency. Use is made of the cubic spline interpolation on $\overline{\delta}_{i}(x/l)$ in MATLAB to accurately detect the intersections. The ranges corresponding to all the utilised natural frequencies are then combined to extract the common ranges. This step is integrated in the plotting of the empirical probability distributions described in the following section.

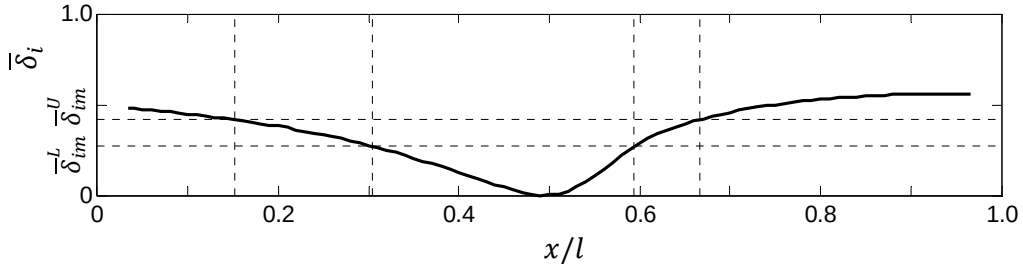

Fig. 3.5. Variation of $\overline{\delta}_i$ with the crack location.

The crack severity, represented by d/h, is detected in a similar manner to that described in Section 3.3.1, but in the form of varying lower and upper limits, at selected points within the combined crack location ranges. The limits of the detected crack location intervals are used as input data, together with the simulated natural frequencies ω^L_{icm} and ω^U_{icm}. It must be noted that if $\omega^U_{icm} > \omega^L_{iom}$, the lower limit of d/h is set to zero in the MATLAB code. The MATLAB codes for detecting the crack locations and severities in the presence of noise are given in the appendix.

3.4.4. Empirical probability distributions for crack location ranges

Empirical probability distributions can be plotted by combining the detected crack location ranges. Referring to Fig. 3.6, and working with x instead of x/l, a triangular probability distribution is assumed for each detected range, such that the total area for all ranges detected in the whole frame, corresponding to a single frequency is 1.0. The common triangle height corresponding to this frequency is given by:

$$\tilde{h}_i = \frac{1}{\sum_{j=1}^{r_i} m_{ij}}, \tag{3.22}$$

where j is the range number, r_i is the total number of ranges corresponding to frequency i, and m_{ij} is half the range length, $(U_{ij} - L_{ij})/2$. L_{ij} is the lower limit and U_{ij} is the upper limit. The gradient of each distribution can be written as:

$$g_{ij} = \pm\frac{\tilde{h}_i}{m_{ij}} = \pm\frac{1}{m_{ij}\sum_{j=1}^{r_i} m_{ij}}, \tag{3.23}$$

where g_{ij} is positive for the left triangle leg and negative for the right leg. The empirical probability distribution function $P(x)$ corresponding to all frequencies combined thus takes the form:

$$P(x) = \prod_{i=1}^{n} p_i(x) \tag{3.24}$$

where n is the total number of frequencies used and $p_i(x)$ is the probability distribution function for frequency i, given by:

$$p_i(x) = \begin{cases} |g_{ij}|.\min\left((x) - L_{ij},\ U_{ij} - (x)\right), & L_{ij} < x < U_{ij} \\ 0, & \text{otherwise} \end{cases}. \tag{3.25}$$

Plotting $P(x)$ gives the combined ranges $[L_{c1}, U_{c1}]$, $[L_{c2}, U_{c2}]$,…, in which $P(x) > 0$.

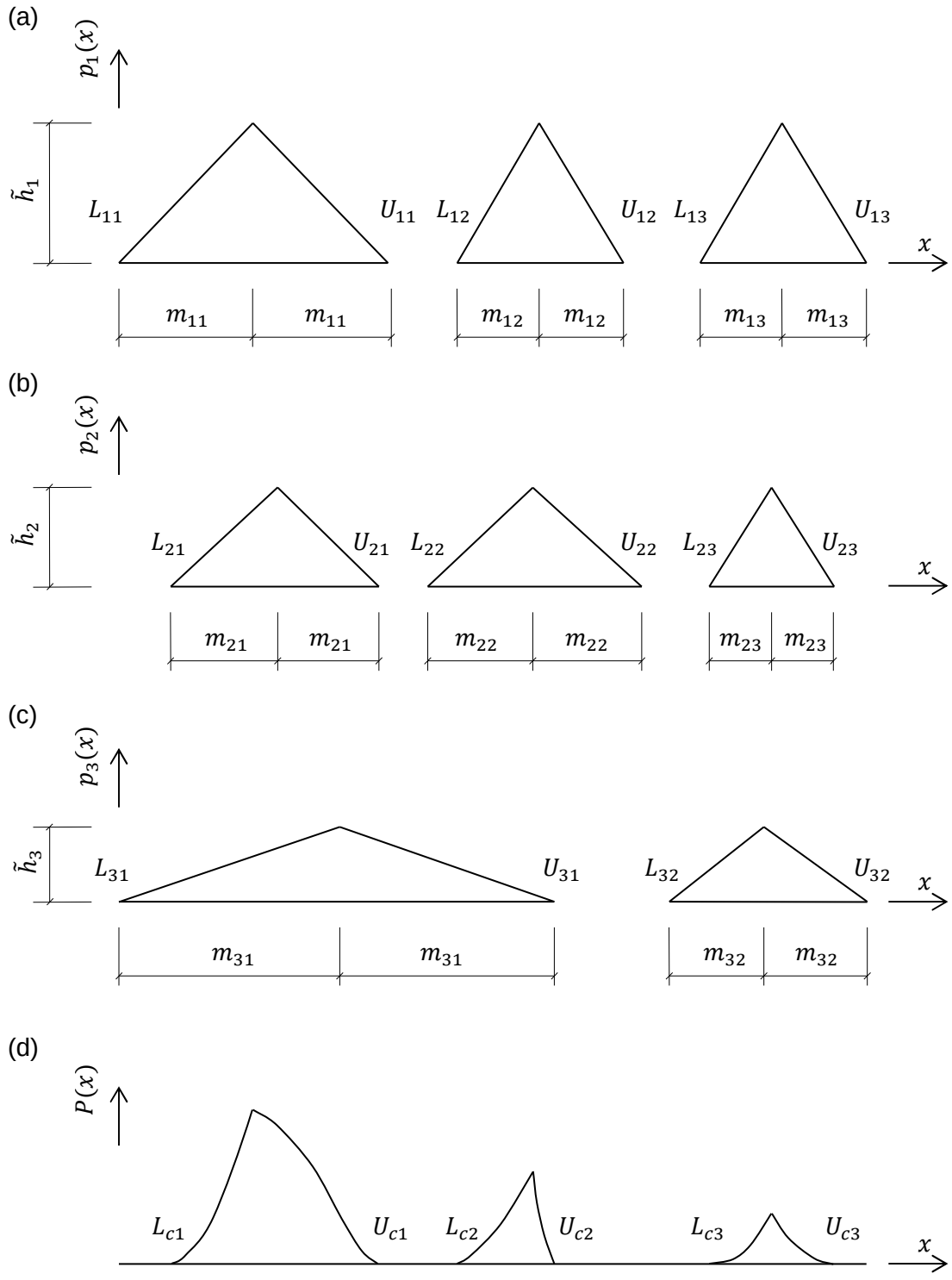

Fig. 3.6. Multiple detected crack location ranges and their distributions in a frame member when three natural frequencies are used. (a) Three ranges detected corresponding to the first frequency; (b) Three ranges detected corresponding to the second frequency; (c) Two ranges detected corresponding to the third frequency; (d) Combined ranges.

3.4.5. Numerical example

Working with the same example as that used in Section 3.3.3 and introducing some noise into the simulated natural frequencies for the uncracked and cracked cases, the method explained in Section 3.4.3 for the detection of crack location ranges is applied using a MATLAB code. The natural frequencies in Table 3.1 are considered up to the third decimal place only and the crack depth to section height ratio d^*/h is taken as 0.1. Considering the case when the actual crack location is in Member A, Figs. 3.7 and 3.8 show the detected ranges in Members A (H) and E, respectively, when the first three natural frequencies are used along with a randomly assumed error of ±0.001 Hz. The lightly shaded areas represent the detected ranges corresponding to each frequency, while the hatched darkly shaded areas represent the combined ranges, if any, for all frequencies used.

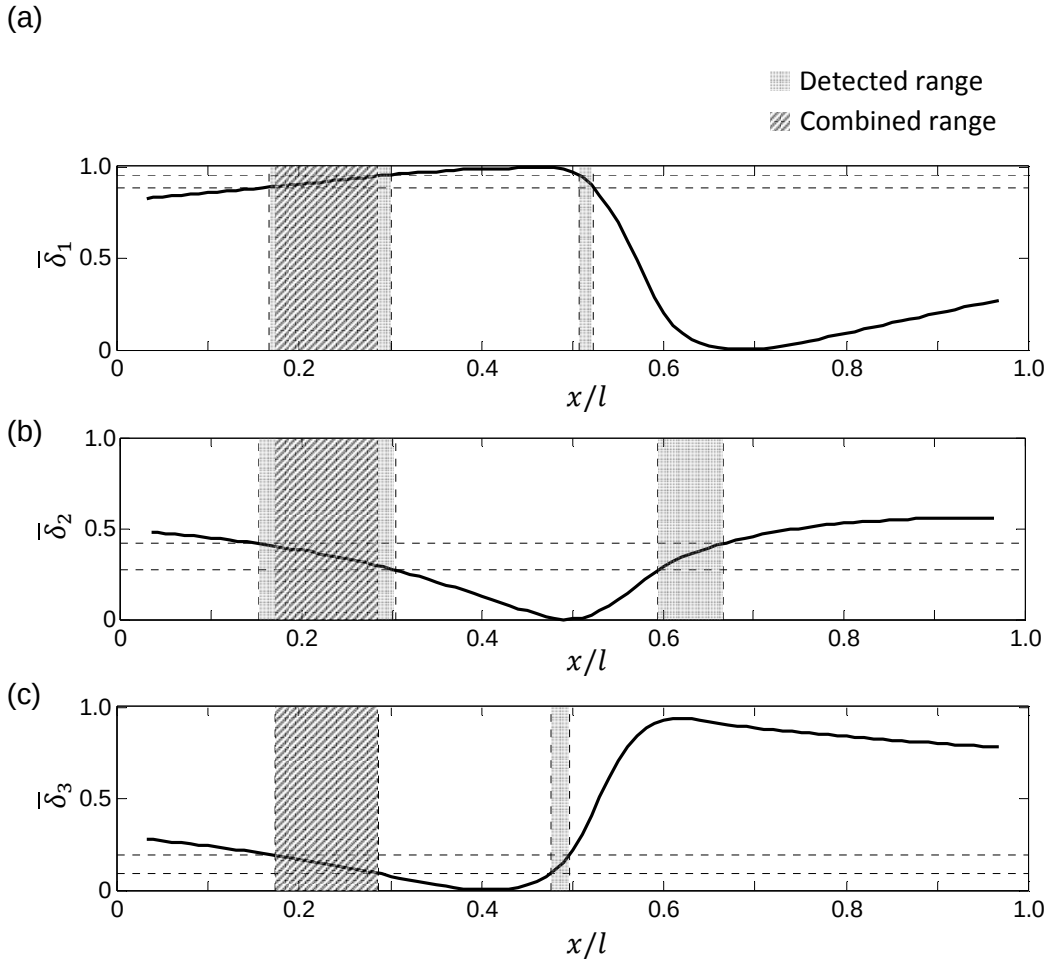

Fig. 3.7. Variation of $\overline{\delta}_i$ with the crack location in Member A (H) and the detected crack location ranges assuming a simulated error of ±0.001 Hz and the actual crack location in Member A, with $d/h = 0.3$. (a) $i = 1$; (b) $i = 2$; (c) $i = 3$.

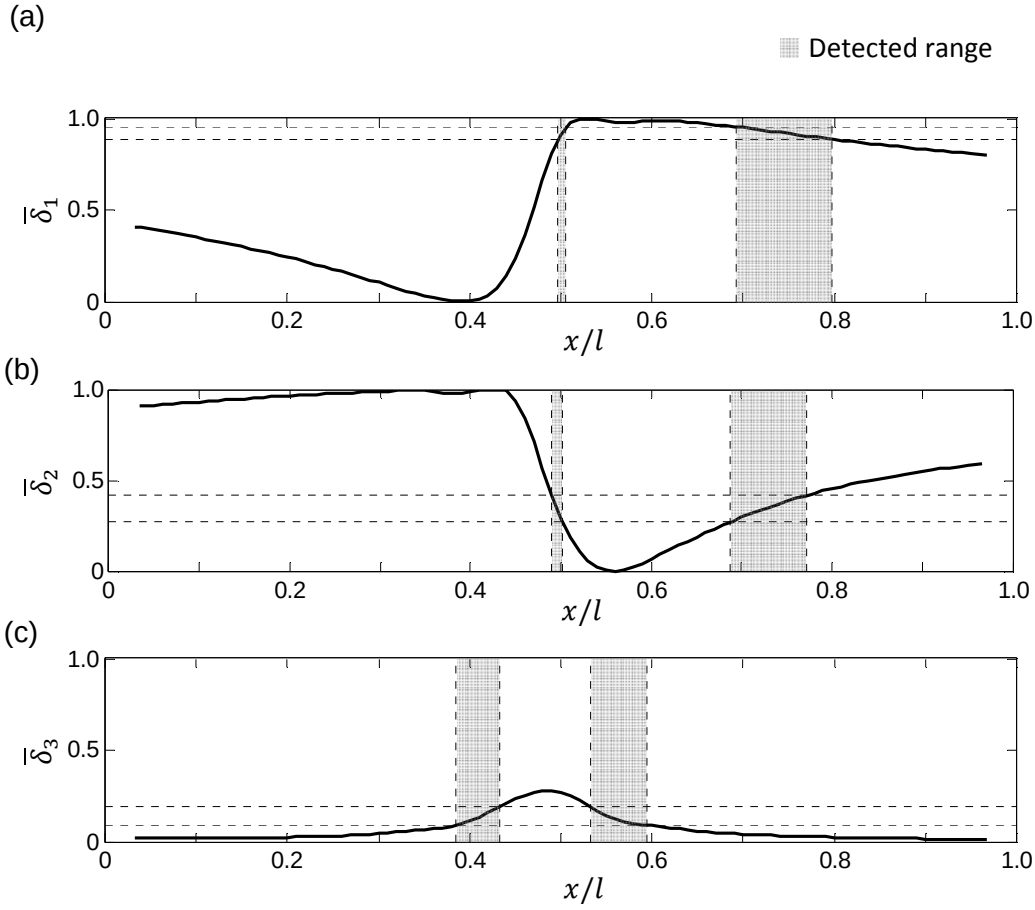

Fig. 3.8. Variation of $\overline{\delta}_i$ with the crack location in Member E and the detected crack location ranges assuming a simulated error of ±0.001 Hz and the actual crack location in Member A, with $d/h = 0.3$. (a) $i = 1$; (b) $i = 2$; (c) $i = 3$.

The empirical probability distributions and the relative areas under the distributions for each of the combined ranges in the frame are shown in Fig. 3.9. It can be seen that using the first three natural frequencies yields only two symmetrical combined ranges, [0.174, 0.287], in Members A and H with the peak value at 0.231. No combined ranges are detected in the other members. The relative area 0.5 implies that the crack has an equal probability of being located within the combined range of Member A or H.

The detected ranges for d/h are illustrated in Fig. 3.10. At the locations of the two empirical distribution peaks, the lower and upper limits of d/h are 0.290 and 0.303, respectively.

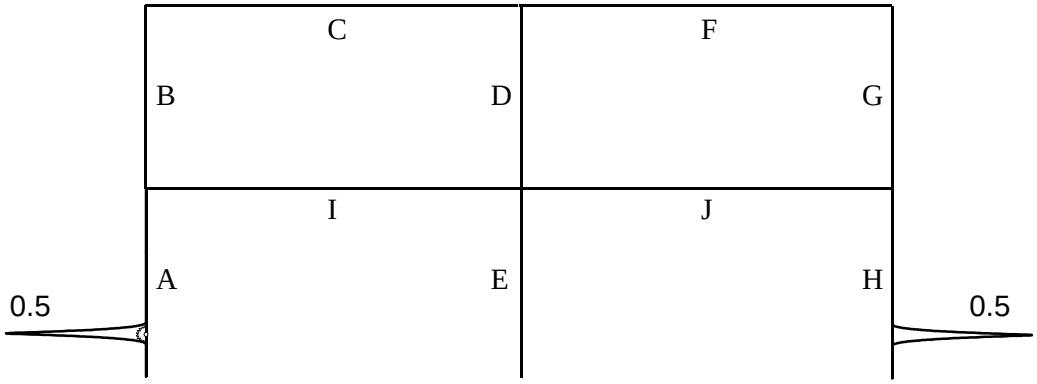

Fig. 3.9. Empirical probability distribution for the crack location in each frame member when the first three natural frequencies are used assuming a simulated error of ±0.001 Hz and the actual crack location shown in Member A.

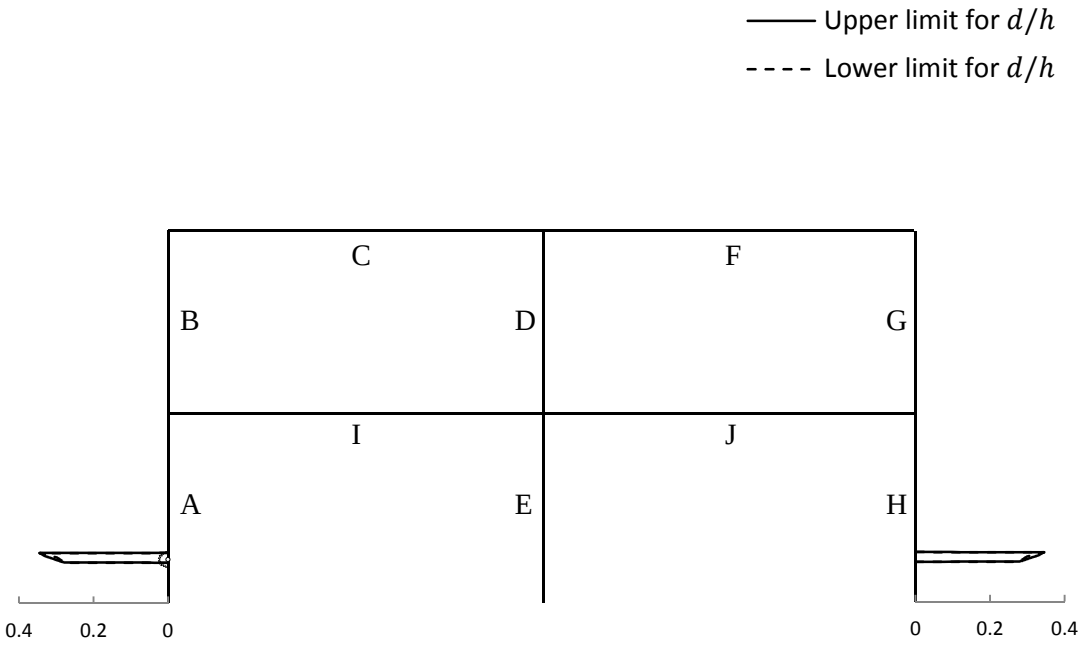

Fig. 3.10. Detected ranges for d/h in each frame member when the first three natural frequencies are used assuming a simulated error of ±0.001 Hz and the actual crack location shown in Member A.

Figs. 3.11 and 3.12 show the detected ranges in Members A (H) and E, respectively, when the simulated error is increased to ±0.005 Hz. The empirical distributions and the relative areas under the distributions are shown in Fig. 3.13.

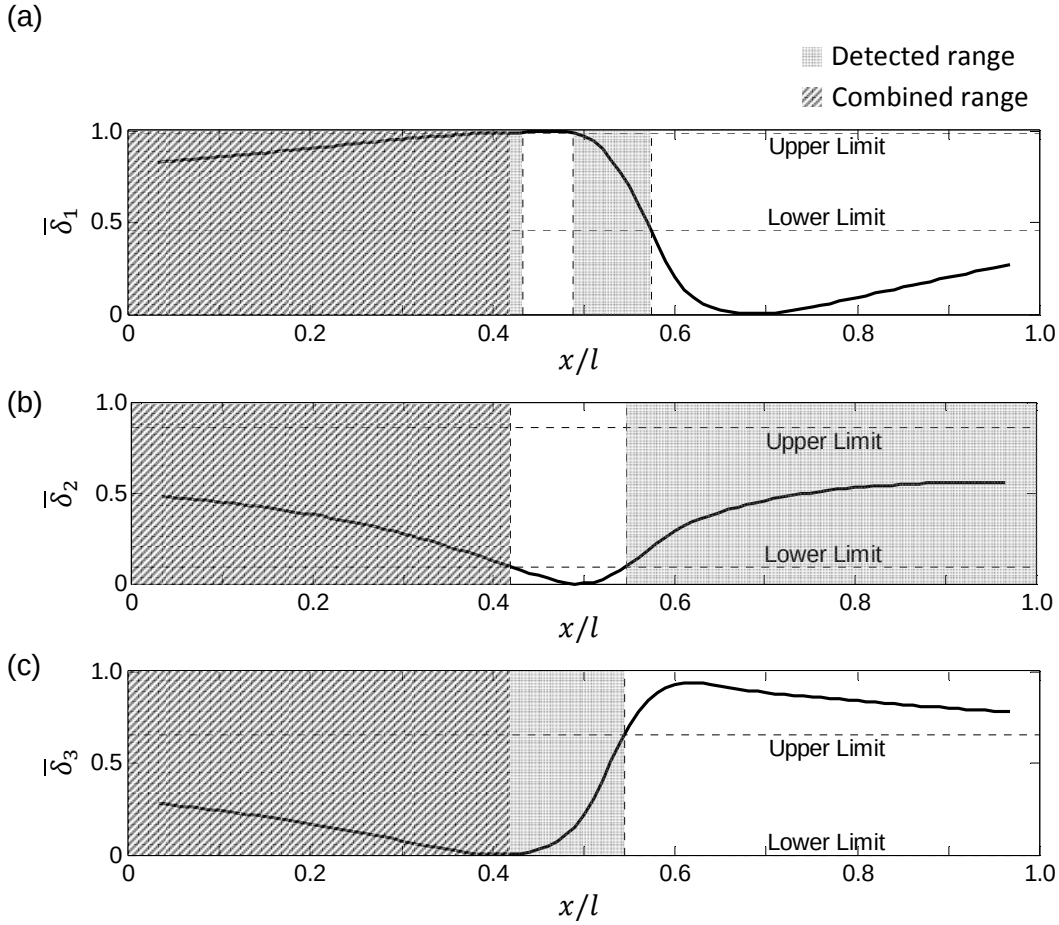

Fig. 3.11. Variation of $\overline{\delta}_i$ with the crack location in Member A (H) and the detected crack location ranges assuming a simulated error of ±0.005 Hz and the actual crack location in Member A, with $d/h = 0.3$. (a) $i = 1$; (b) $i = 2$; (c) $i = 3$.

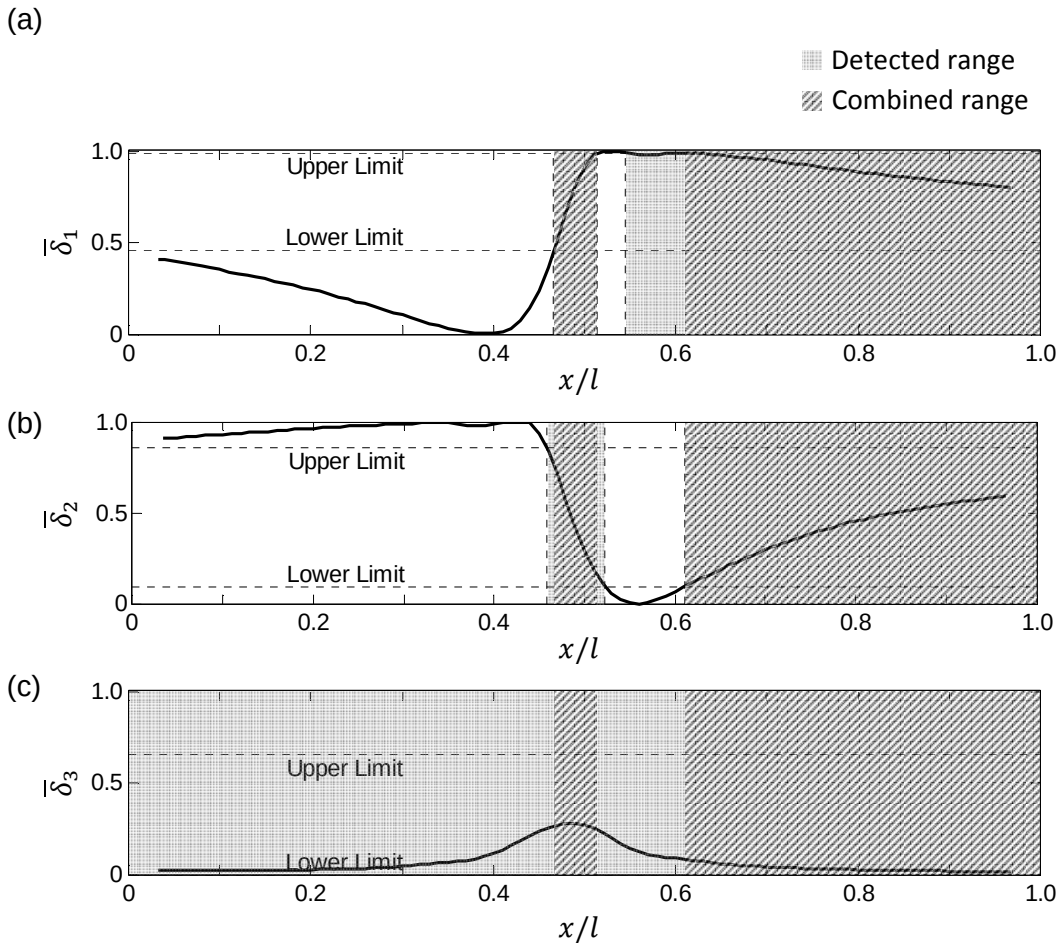

Fig. 3.12. Variation of $\overline{\delta}_i$ with the crack location in Member E and the detected crack location ranges assuming a simulated error of ±0.005 Hz and the actual crack location in Member A, with $d/h = 0.3$. (a) $i = 1$; (b) $i = 2$; (c) $i = 3$.

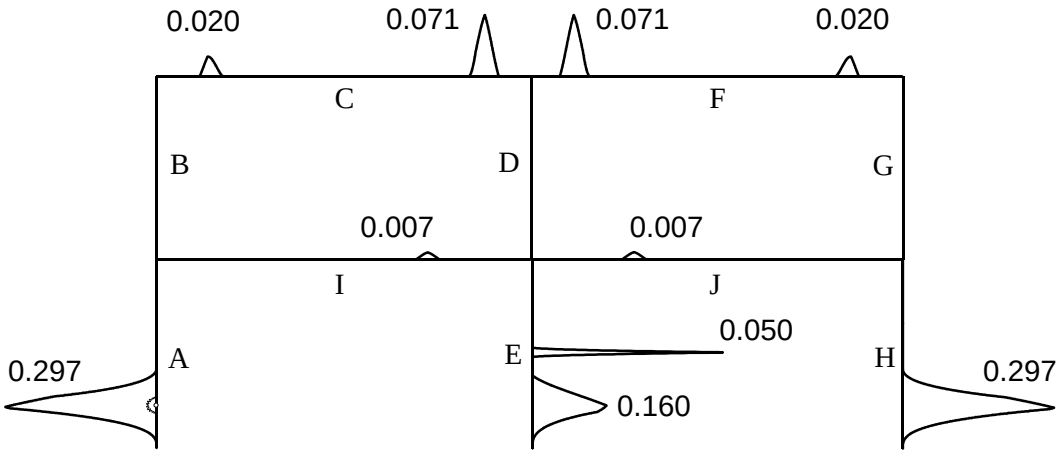

Fig. 3.13. Empirical probability distribution for the crack location in each frame member when the first three natural frequencies are used assuming a simulated error of ±0.005 Hz and the actual crack location shown in Member A.

The detected ranges for d/h are illustrated in Fig. 3.14. The effect of using the additional fourth natural frequency on the empirical distributions is shown in Fig. 3.15. The detected ranges for d/h in this case are illustrated in Fig. 3.16. The combined crack location ranges using three and four natural frequencies, and the locations of the distribution peaks are summarised in Table 3.3. The detected ranges for d/h at the distribution peaks are summarised in Table 3.4.

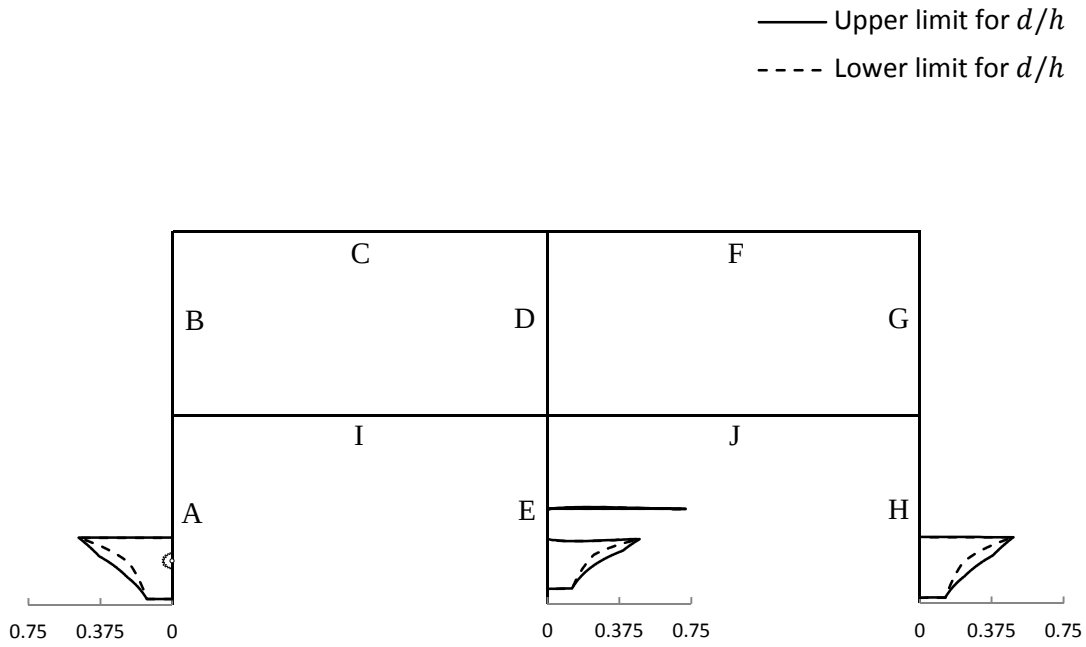

Fig. 3.14. Detected ranges for d/h in each frame member when the first three natural frequencies are used assuming a simulated error of ±0.005 Hz and the actual crack location shown in Member A.

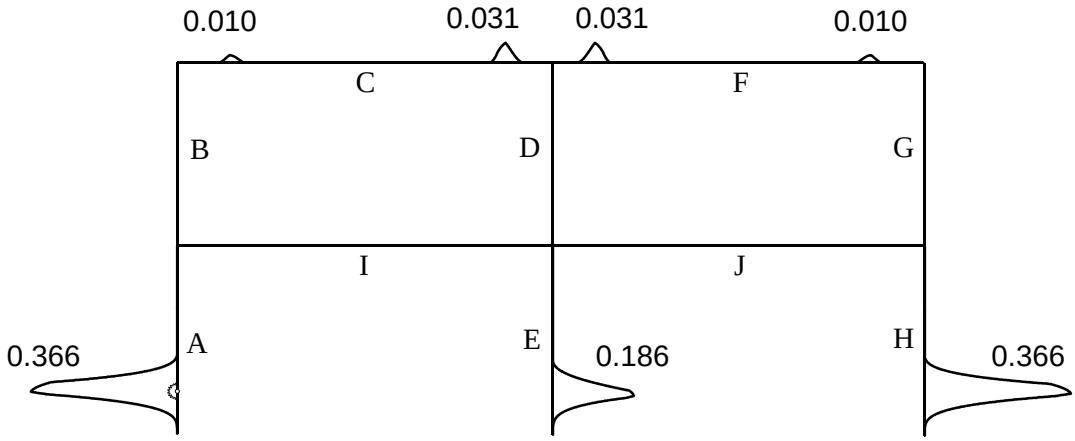

Fig. 3.15. Empirical probability distribution for the crack location in each frame member when the first four natural frequencies are used assuming a simulated error of ±0.005 Hz and the actual crack location shown in Member A.

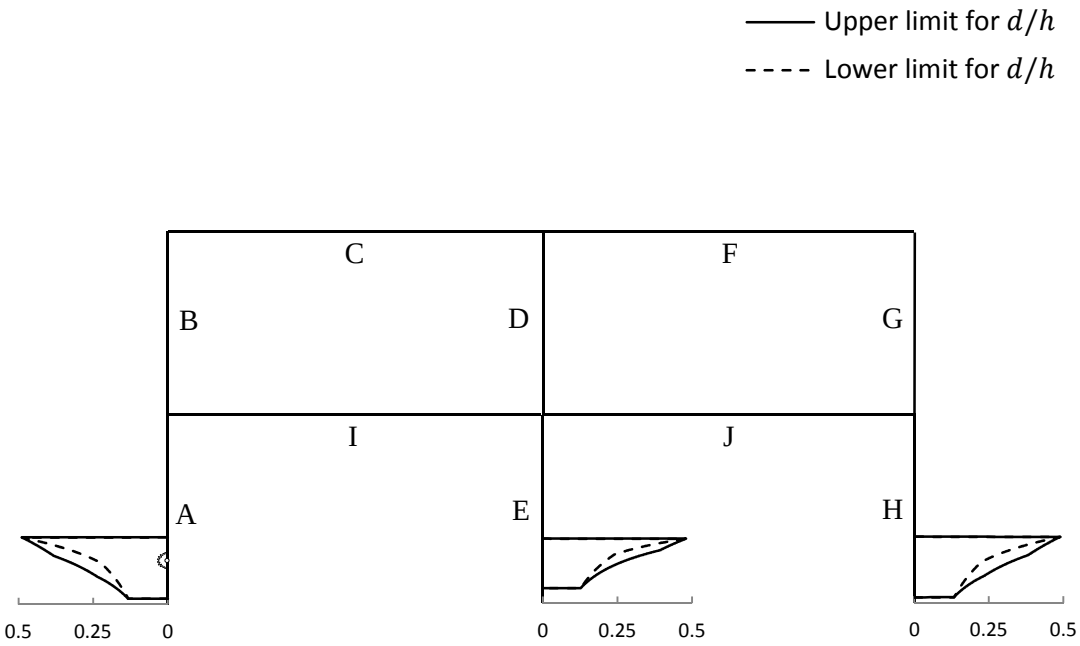

Fig. 3.16. Detected ranges for d/h in each frame member when the first four natural frequencies are used assuming a simulated error of ±0.005 Hz and the actual crack location shown in Member A.

Table 3.3. Lower and upper limits for the detected common ranges and the peak locations in each frame member when the actual crack location is in Member A at $x = 0.72$ m.

Member	x (m)							
	Three frequencies				Four frequencies			
	j	L_{cj}	U_{cj}	Peak	j	L_{cj}	U_{cj}	Peak
A (H)	**1**	**0.0**	**1.254**	**0.648**	**1**	**0.0**	**1.254**	**0.669**
B (G)	-	-	-	-	-	-	-	-
C (F)	1	0.696	1.068	0.831	1	0.684	1.068	0.843
	2	5.040	5.514	5.289	2	5.040	5.556	5.286
D	-	-	-	-	-	-	-	-
E	1	1.398	1.542	1.470	1	1.833	3.0	2.385
	2	1.836	3.0	2.319	-	-	-	-
I (J)	1	4.158	4.542	4.350	-	-	-	-

Table 3.4. Lower and upper limits for the detected d/h ranges at the distribution peaks in each frame member when the actual crack location is in Member A at $x = 0.72$ m.

Member	d/h					
	Three frequencies			Four frequencies		
	j	Lower limit	Upper limit	j	Lower limit	Upper limit
A (H)	**1**	**0.222**	**0.318**	**1**	**0.228**	**0.328**
B (G)	-	-	-	-	-	-
C (F)	1	-	-	1	-	-
	2	-	-	2	-	-
D	-	-	-	-	-	-
E	1	0.718*	0.720*	1	0.194	0.243
	2	0.210	0.277	-	-	-
I (J)	1	-	-	-	-	-

* Values detected at the closest possible location to that of the distribution peak.

Figs. 3.17 and 3.19 show the distribution plots when three and four natural frequencies, respectively, are used assuming a simulated error of ±0.005 Hz and the actual crack location is in Member I, with $d/h = 0.3$. Figs. 3.18 and 3.20 illustrate the detected d/h ranges for these two cases. The combined crack location ranges and peak locations are summarised in Table 3.5. The detected ranges for d/h at the peak locations are summarised in Table 3.6.

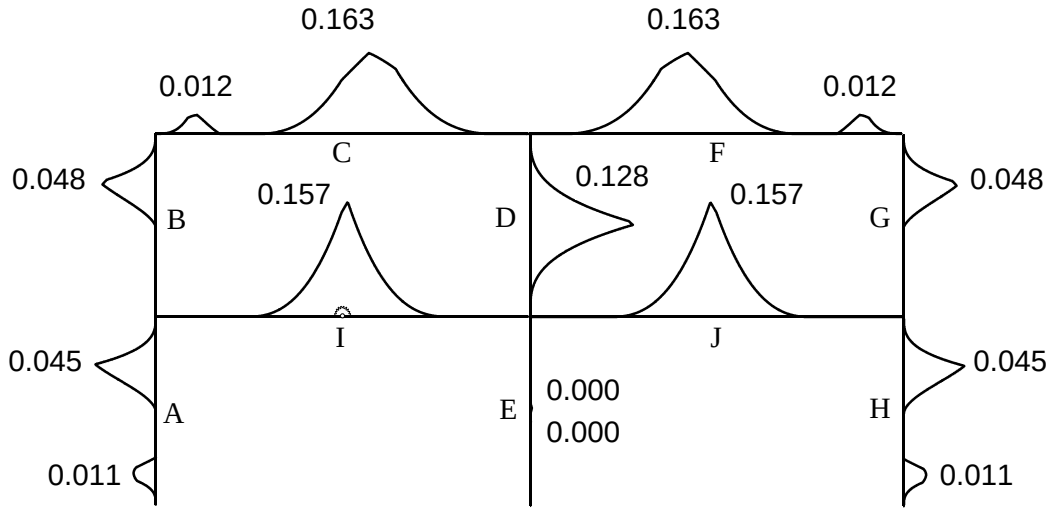

Fig. 3.17. Empirical probability distribution for the crack location in each frame member when the first three natural frequencies are used assuming a simulated error of ±0.005 Hz and the actual crack location shown in Member I, with $d/h = 0.3$.

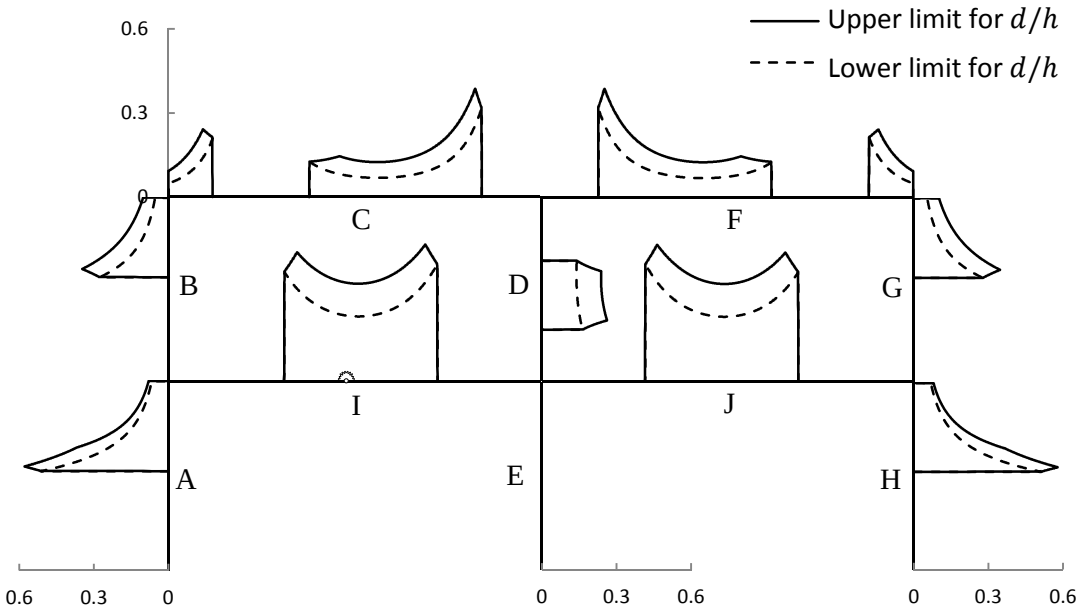

Fig. 3.18. Detected ranges for d/h in each frame member when the first three natural frequencies are used assuming a simulated error of ±0.005 Hz and the actual crack location shown in Member I.

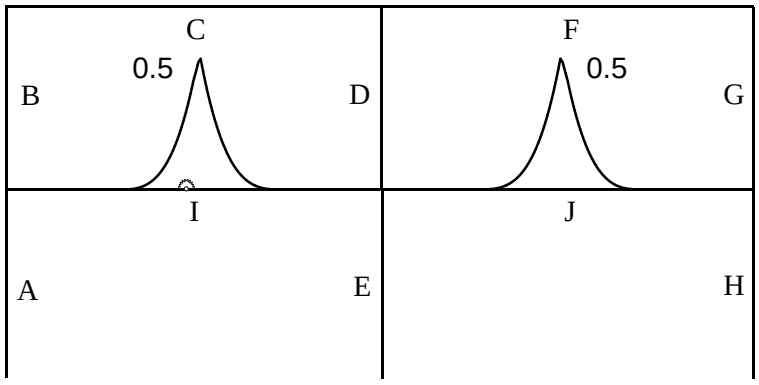

Fig. 3.19. Empirical probability distribution for the crack location in each frame member when the first four natural frequencies are used assuming a simulated error of ±0.005 Hz and the actual crack location shown in Member I, with $d/h = 0.3$.

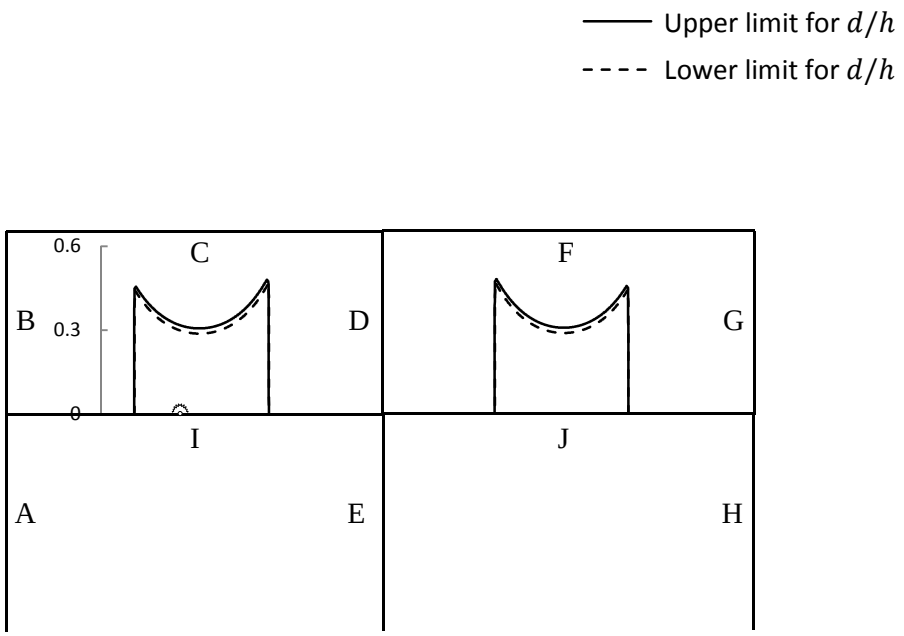

Fig. 3.20. Detected ranges for d/h in each frame member when the first four natural frequencies are used assuming a simulated error of ±0.005 Hz and the actual crack location shown in Member I.

Table 3.5. Lower and upper limits for the detected common ranges and the peak locations in each frame member when the actual crack location is in Member I at $x = 2.91$ m.

Member	x (m)							
	Three frequencies				Four frequencies			
	j	L_{cj}	U_{cj}	Peak	j	L_{cj}	U_{cj}	Peak
A (H)	1	0.0	0.747	0.498	-	-	-	-
	2	1.473	3.0	2.229				
B (G)	1	1.485	3.0	2.166	-	-	-	-
C (F)	1	0.0	1.038	0.672	-	-	-	-
	2	1.740	5.316	3.438				
D	1	0.0	2.874	1.500	-	-	-	-
E	1	1.353	1.536	1.446	-	-	-	-
	2	1.647	1.674	1.662				
I (J)	**1**	**1.530**	**4.662**	**3.090**	**1**	**1.878**	**4.356**	**3.117**

Table 3.6. Lower and upper limits for the detected d/h ranges at the distribution peaks in each frame member when the actual crack location is in Member I at $x = 2.91$ m.

Member	d/h					
	Three frequencies			Four frequencies		
	j	Lower limit	Upper limit	j	Lower limit	Upper limit
A (H)	1	-	-	-	-	-
	2	0.154	0.209			
B (G)	1	0.116	0.200	-	-	-
C (F)	1	0.188	0.222	-	-	-
	2	0.069	0.125			
D	1	0.124	0.212	-	-	-
E	1	-	-	-	-	-
	2	-	-			
I (J)	**1**	**0.232**	**0.349**	**1**	**0.289**	**0.307**

When d/h is lowered to 0.005, the changes in each of the natural frequencies are less than the noise. As a result, the distribution plots cover the whole frame, with the peaks at the mid-span of each member, as shown in Fig. 3.21.

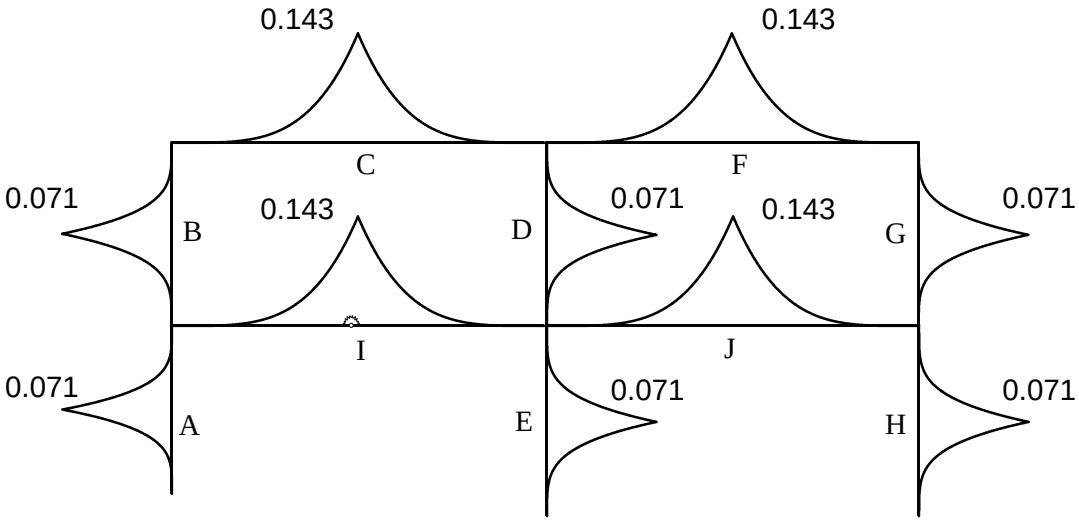

Fig. 3.21. Empirical probability distribution for the crack location in each frame member when the first four natural frequencies are used assuming a simulated error of ±0.005 Hz and the actual crack location shown in Member I, with $d/h = 0.005$.

3.5. Discussion

The crack detection method described in Section 3.3, based on noise free natural frequency simulations yields predictions for the crack locations

close to the actual ones. The predictions may vary slightly according to the crack depth to section height ratio d^*/h used in calculating the natural frequencies when the crack location is varied along the discretisation points. In some cases, no crack is detected due to a certain G_i curve barely touching zero at the correct location, as shown in Fig. 3.22. The cubic spline interpolation used by MATLAB also has an effect, however slight, on the ability to find a solution. These issues can be overcome by utilising an additional natural frequency, using more discretisation points, or trying a different value for d^*/h.

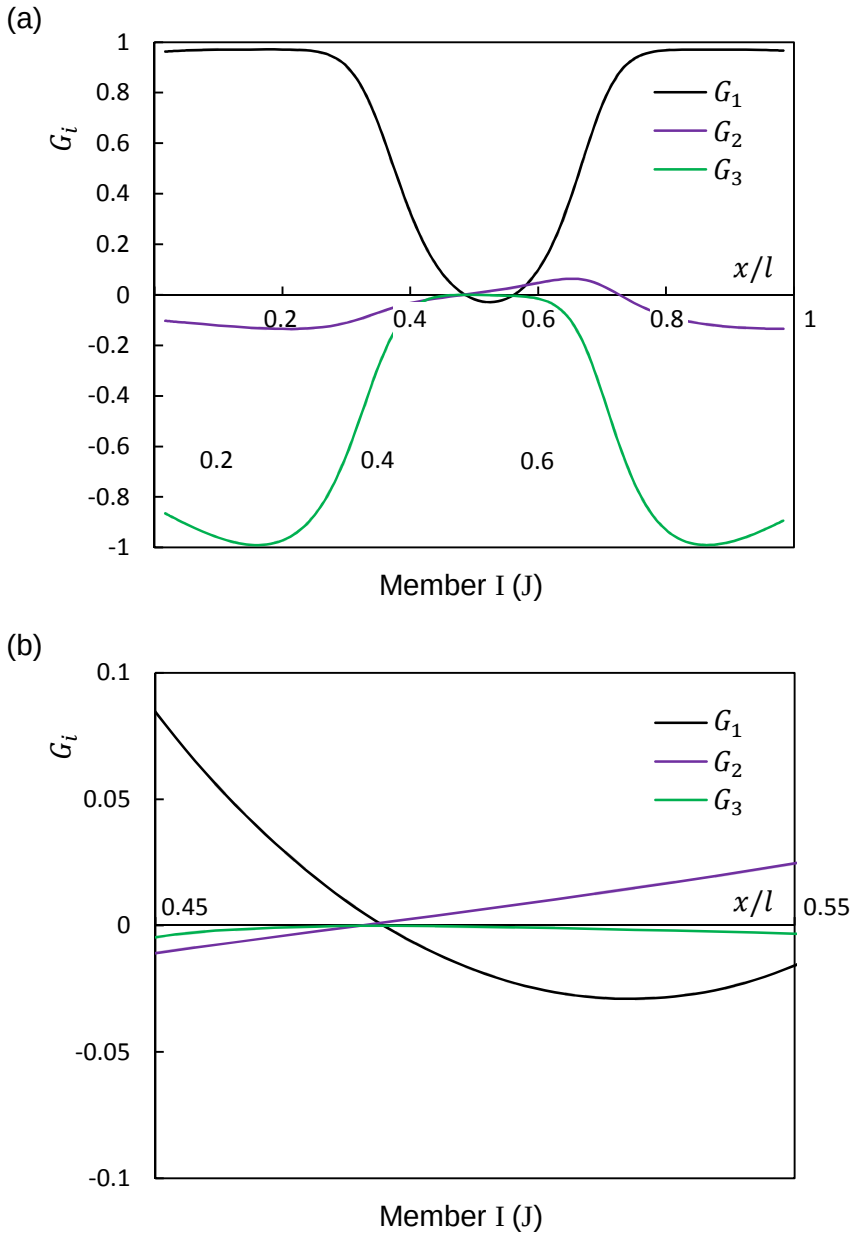

Fig. 3.22. Variation of G_i with the assumed crack location in Member I (J) when the actual crack location is in Member I, $d/h = 0.3$ and $d^*/h = 0.1$. (a) Whole member length; (b) Zoom on location interval [0.4, 0.6].

The method is applicable for very small values of d/h in case of noise free data as the simulated natural frequencies, and consequently $\overline{\delta}_{im}$, are calculated accurately in MATLAB up to a large number of decimal places using the Wittrick–Williams algorithm (Wittrick and Williams 1971), similar to $\overline{\delta}_i$ at the discretisation points. The method is, however, not applicable in the case of severe cracks in some locations, at which $\overline{\delta}_{im}$ becomes severely dependent on d/h, as discussed later. The method is also unable to distinguish between symmetric locations, so when the whole frame is considered, two symmetric locations are predicted. However, this still significantly reduces the level of follow on inspection, which would have to be done to confirm the findings, thus reducing cost and potential downtime.

Introducing some noise to the simulated natural frequencies in the uncracked and cracked cases, the crack location is estimated within ranges in two or more symmetric members of the frame. When the actual crack location is in Member A, small errors of the order ±0.001 Hz yield two symmetric ranges, one of them around the correct crack location. Increasing the error to ±0.005 Hz, multiple combined ranges are detected in more than two frame members. Using an additional natural frequency can narrow down and eliminate some of the false combined ranges. Comparing Figs. 3.13 and 3.15, it can be seen that using the fourth natural frequency eliminates one false range in Member E and two symmetric false ranges in Members I and J. All the false combined ranges, except for the symmetric counterpart of the correct range, are eliminated in the case when the actual crack location is in Member I, with $d/h = 0.3$, and the fourth natural frequency is used. When $d/h = 0.005$, the detected ranges cover the whole frame, as shown in Fig. 3.21, rendering the procedure impractical in that case.

The effects of increasing the error and using the fourth natural frequency on the detected ranges, while varying d/h, can be explained with the aid of Figs. 3.23 and 3.24, respectively. For a small error of ±0.001 Hz, when the actual crack is located in Member A, Fig. 3.23 shows that when d/h increases beyond approximately 0.1, the intervals $\left[\overline{\delta}_{im}^{L}, \overline{\delta}_{im}^{U}\right]$ narrow down from [0, 1.0] towards the corresponding noise free $\overline{\delta}_{im}$. When the error is increased to

±0.005 Hz, the intervals narrow down from [0, 1.0] when d/h increases beyond approximately 0.2. For any specific value of d/h, the narrowing intervals are wider in the case of increased error, causing the detected crack location ranges to cover greater lengths of the frame. The two values for d/h, 0.1 and 0.2, represent the lower limits for the practical applicability of the detection procedure assuming the error values ±0.001 Hz and ±0.005 Hz, respectively. Any values of d/h lower than these limits results in the detected crack location ranges covering the whole frame. Working with an increased level of error, Fig. 3.24 illustrates the advantage of using the first four natural frequencies rather than just the first three, when the actual crack location is in Member I. The lower limit for d/h decreases and for any specific value of d/h greater than this lower limit, the intervals $\left[\overline{\delta}_{im}^{L}, \overline{\delta}_{im}^{U}\right]$ are narrowed down. This is attributed to the relatively large difference in the fourth natural frequency between the uncracked and cracked cases, compared with the assumed error of ±0.005 Hz, contrary to the first three natural frequencies. It can also be seen from Fig. 3.24 that when d/h is very large, greater than 0.6, the noise free $\overline{\delta}_{im}$ behaves in an obviously irregular manner, becoming a function of d/h, thus rendering the detection method inapplicable in the case of severe cracks. It must be noted that the curves in Figs. 3.23 and 3.24 are not smooth as the corresponding natural frequencies are considered only up to three decimal places, except for the case of noise free data. If a large number of decimal places is considered while adding the same amount of errors indicated, smooth curves are obtained.

The above discussion illustrates the advantage of the normalisation step in combining the effect of all the utilised natural frequencies for each $\overline{\delta}_{im}$. Another advantage is the elimination of the need for randomly grouping the variations, $\{\delta_i\}$, of the selected natural frequencies in pairs and taking the ratio corresponding to each pair to eliminate the dependency on crack severity, contrary to the procedure recommended by Adams et al. (1978). However, the method falls short when d/h is very small or, depending on the crack location, when d/h is very large.

(a)

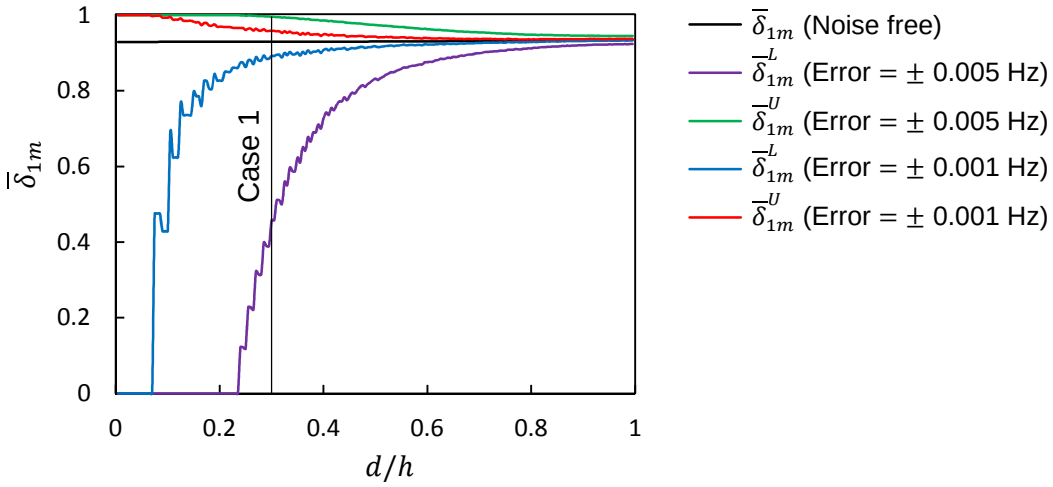

(b)

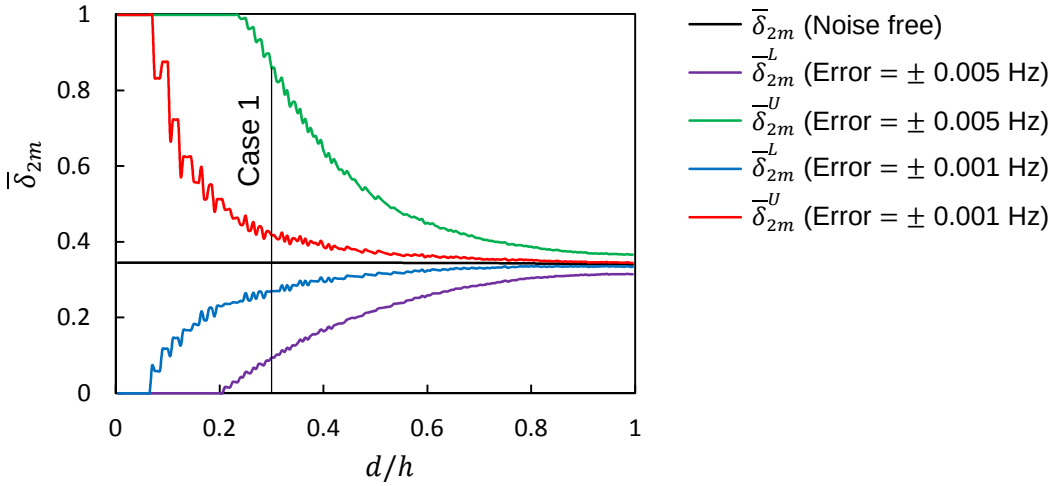

(c)

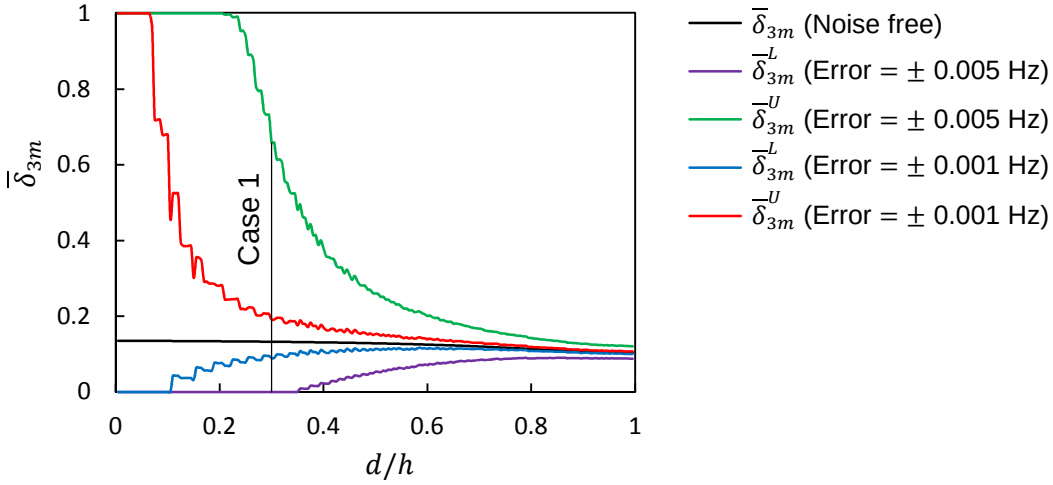

Fig. 3.23. Variation of noise free $\overline{\delta}_{im}$ and its bounds $\left[\overline{\delta}_{im}^{L}, \overline{\delta}_{im}^{U}\right]$, with d/h for Case 1 of Table 3.1 when the actual crack location is in Member A and the first three natural frequencies are used. (a) $i = 1$; (b) $i = 2$; (c) $i = 3$.

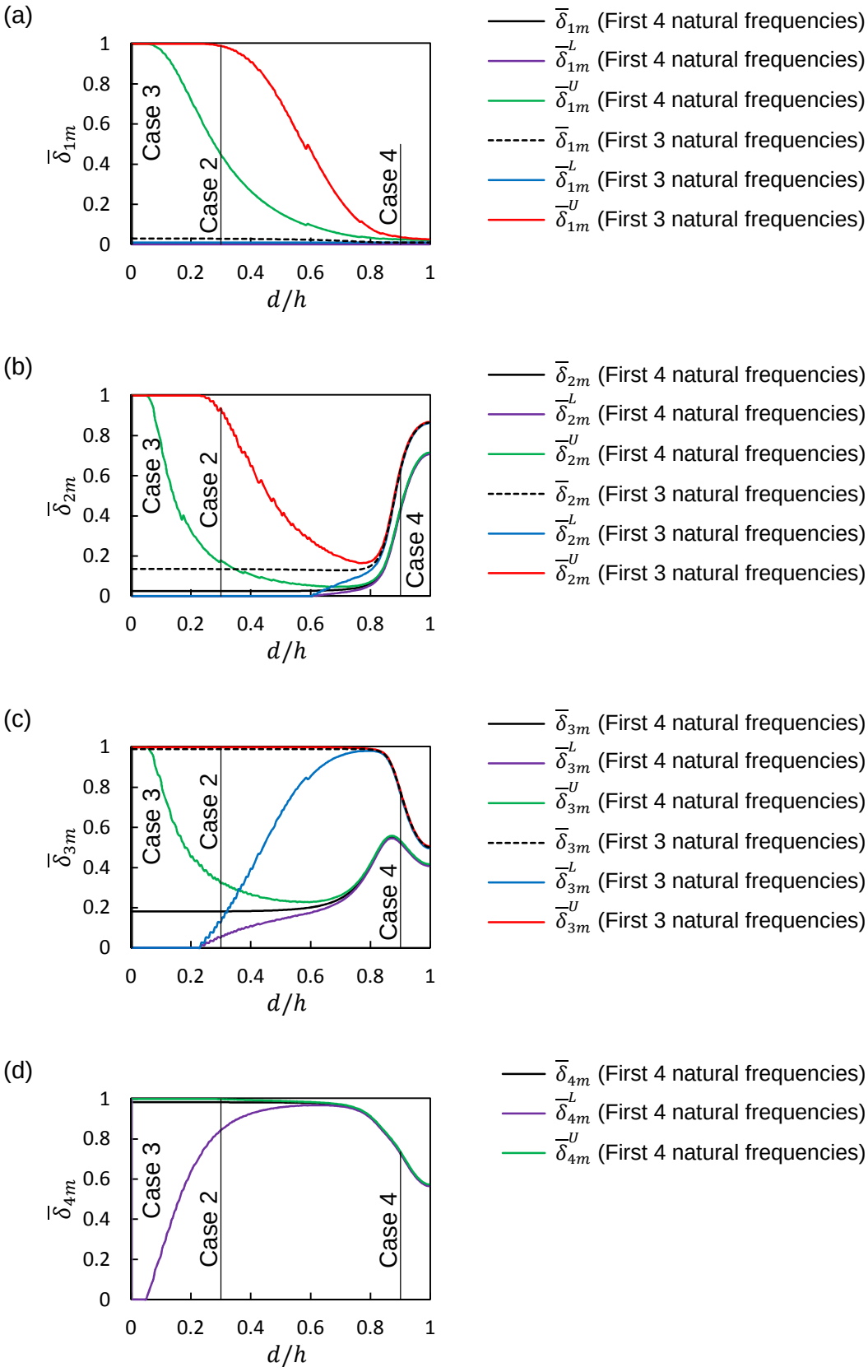

Fig. 3.24. Variation of noise free $\overline{\delta}_{im}$ and its bounds $\left[\overline{\delta}^{L}_{im}, \overline{\delta}^{U}_{im}\right]$ for a simulated error of ±0.005 Hz, with d/h for Cases 2, 3 and 4 of Table 3.1 when the actual crack location is in Member I. (a) $i = 1$; (b) $i = 2$; (c) $i = 3$; (d) $i = 4$.

The empirical probability distribution can be used as a practical means of applying the range detection method for the crack location. The correct combined range containing the actual crack location may not have the highest area under its distribution when the detected ranges cover substantial lengths of the frame, as shown in Fig. 3.17. However, the correct range will be among the high priority sites to be inspected. The peaks slightly deviate from the actual crack location, as the detected ranges corresponding to each frequency and containing the actual crack location are unlikely to be centred on that location, as can be seen in Figs. 3.7 and 3.11.

The recovered ranges for d/h are useful in narrowing down or eliminating some of the false crack location intervals. A range covering the correct value for d/h is always recovered.

The above analysis is based on neglecting the effect of the loss of axial stiffness through the crack. This assumption has negligible effect on the analysis carried out on the frame shown in Fig. 3.3, where there are no inclined members. However, frames with inclined members show a different behaviour. A one bay frame with a 45° inclined member is considered, as shown in Fig. 3.25. The frame has the same material properties and cross-sectional dimensions mentioned in Section 2.3.2.1. Working with the first three natural frequencies and utilising the rotational and translational spring models incorporated by Banerjee and Guo (2009) with $d^*/h = 0.3$, the $\overline{\delta}_i$ plots for the left hand column corresponding to the two cases when the loss of axial stiffness is taken into account and when it is neglected are shown in Fig. 3.26. It can be seen that the plots are very similar, except that for $i = 1$ and 3, $\overline{\delta}_i$ varies greatly between the two cases in small regions around $x/l = 0.25$.

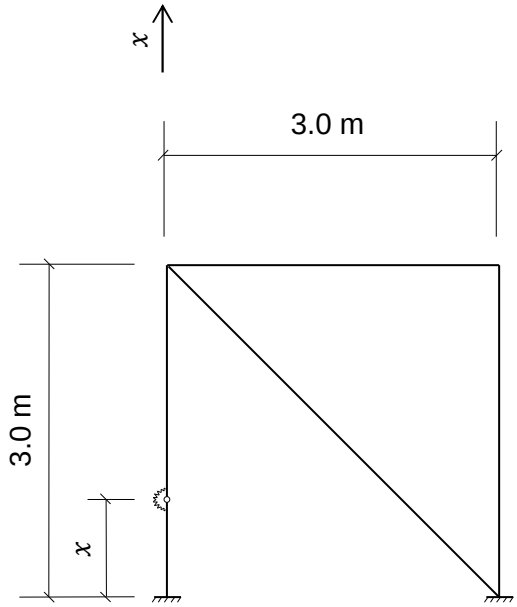

Fig. 3.25. One bay frame with 45º inclined member.

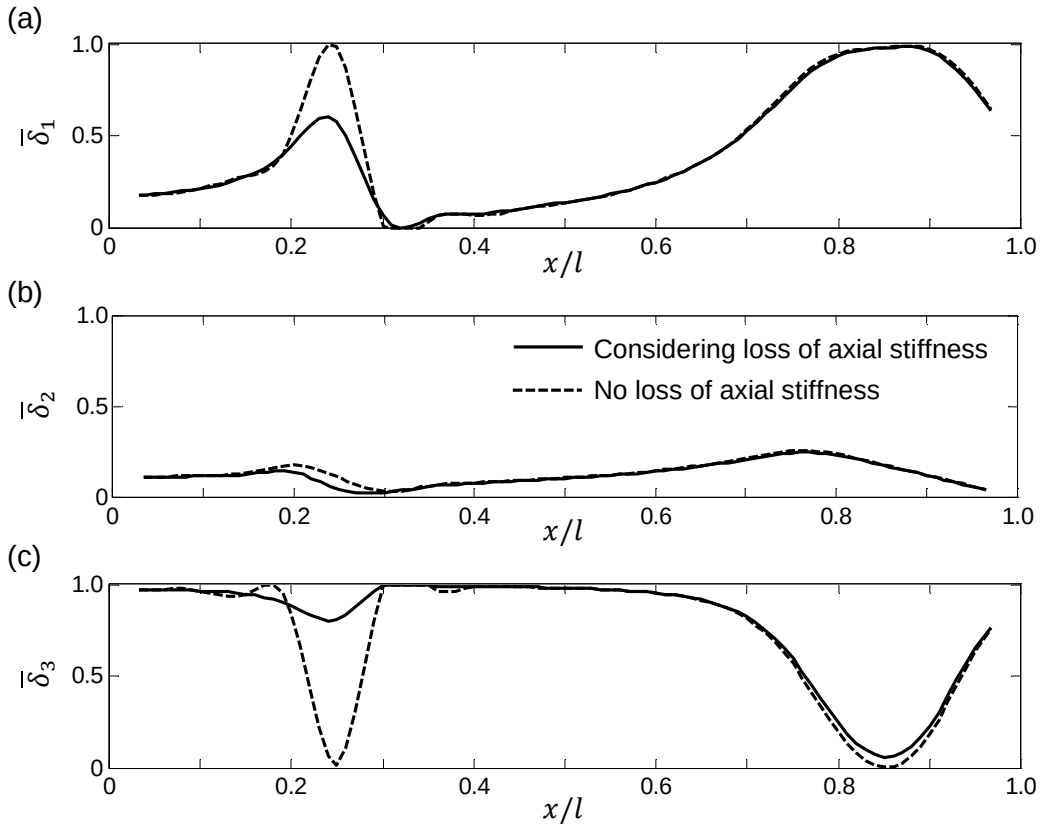

Fig. 3.26. Effect of the loss of axial stiffness on the variation of $\overline{\delta}_i$ with the crack location in the left hand column of the frame in Fig. 3.25 taking into account the loss of axial stiffness through the crack. (a) $i = 1$; (b) $i = 2$; (c) $i = 3$.

3.6. Conclusions

This study presents a new method for predicting single crack locations in frames, using natural frequency measurements. The Wittrick–Williams algorithm (Wittrick and Williams 1971) is utilised to calculate selected natural frequencies when the crack is placed at discretisation points in the frame members. Noise free measurements yield point crack predictions close to their actual locations. Introducing measurement errors produces crack location predictions in the form of ranges. Using additional natural frequencies eliminates some of the false ranges when the measurement error is greater than the frequency variation between the uncracked and cracked cases. Empirical probability distributions can then be plotted for each range and practically used to set up an inspection procedure by prioritising inspection locations. The method is efficient when the measurement noise is lower than the variations in at least one of the selected natural frequencies. For frames with inclined members, the loss of axial stiffness through the crack should be taken into account.

Chapter 4 – Experimental validation

4.1. Introduction

In order to validate the crack detection method devised in the previous chapter, it was applied experimentally to a two bay, two storey welded frame excited using a hammer and monitored using an accelerometer. Four natural frequencies in each of the uncracked and cracked cases were extracted using software supplied with the data logger attached to the accelerometer, with the aid of a simple MATLAB (MathWorks 2012) code for pinpointing the natural frequencies.

The data logger software uses Fast Fourier Transform (FFT) to plot the amplitude of vibration versus the frequency. This chapter begins, therefore, by giving a brief explanation for this type of transform, summarising the works of Ewins (1984), Brigham (1988) and Wolberg (1988).

As in the previous chapter, the crack detection calculations are carried out using three natural frequencies, followed by an additional fourth. For both sets of calculations, the empirical probability distributions for the detected crack location ranges are plotted, in addition to the crack severity ranges. For practical considerations, the natural frequencies corresponding to the first two vibration modes are excluded from the analysis. However, it will be seen that the applicability of the crack detection method is demonstrated.

4.2. Fourier transforms

The Fourier transform of a continuous function in time $h(t)$ is defined by the complex integral (Ewins 1984; Brigham 1988):

$$H(\omega) = \int_{-\infty}^{\infty} h(t) e^{-j2\pi\omega t}\, dt, \tag{4.1}$$

where $j = \sqrt{-1}$. In practice, $h(t)$ is a measured function, sampled at discrete time intervals. Denoting the number of samples as N_s, the discrete form of $H(\omega)$ is given by the equation (Ewins 1984; Brigham 1988; Wolberg 1988):

$$H_n = \sum_{k=0}^{N_s-1} h_k e^{-j2\pi nk/N_s}, \tag{4.2}$$

where $n = 0, 1, \ldots, N_s - 1$. For mathematical considerations, N_s is usually taken as a power of 2, i.e. $N_s = 2^r$, where r is an integer. Thus, H_n represents amplitude as a function of frequency. As H_n is in the frequency domain, the maximum frequency $\omega_{\max}$ (termed the Nyquist frequency) and the frequency resolution $\Delta\omega$ are given in Hz by the equations (Ewins 1984):

$$\omega_{\max} = \frac{\omega_s}{2} = \frac{N_s}{2T}, \tag{4.3}$$

$$\Delta\omega = \frac{\omega_s}{N_s} = \frac{1}{T} \tag{4.4}$$

where ω_s is the sampling frequency, i.e. the number of samples per second, and T is the total sampling period. It is essential to have the lowest possible frequency resolution $\Delta\omega$. In practice, the total sampling period T determines $\Delta\omega$ (Brigham 1988). However, zooming techniques have been formulated, one of the latest by Gillich et al. (2015), in order to decrease $\Delta\omega$ without requiring an increase in the total sampling period T. These techniques require the analysis of the raw measured data outside the acquisition software mentioned later. For simplicity, and as the aim of the experimental work described in this thesis is to validate the crack detection method devised in the previous chapter, the zooming techniques are not applied. Instead, the total sampling period T is increased appropriately.

The application of Eq. (4.2) implies a computational effort of the order $O(N_s^2)$. Using the fast Fourier transform (FFT), the computational effort can be greatly reduced to $O(N_s \log_2 N_s)$. A number of FFT algorithms have been formulated; among the most widely used is the Cooley–Tukey algorithm, which is a modification of the Danielson–Lanczos lemma (Wolberg 1988).

Some important features of the discrete Fourier transform, and consequently FFT, must be considered. These are the aliasing, leakage and windowing. Aliasing can be described as the appearance of high frequency components, greater than $\omega_{\max}$, below this value. This feature is the result of discretising the original vibration signal. Choosing a low sampling rate ω_s further

contributes to this undesirable feature. Although anti-aliasing filters are built into the measuring devices, it is advisable to reject any frequency components appearing in the range of $\omega_{\max}/2$ to $\omega_{\max}$. Another consequence of discretising the original vibration signal, along with the incorrect assumption of a perfectly periodic signal within the sampling period T, is leakage. Ideally, the amplitude at a frequency component, i.e. a natural frequency ω_i, should be distinguishably high, with the amplitudes at $\omega_i \pm \Delta\omega$ having near zero values. In practice, the FFT gives high amplitudes around ω_i. In order to correct this, windowing is used, where the measured signal in the time domain is multiplied by a chosen function to impose a certain profile on that signal, depending on the type of vibration measurement (free, forced…etc.) to minimise the leakage. The FFT is then applied on the modified signal (Ewins 1984). A commonly used window is the Hanning window, recommended for use with any type of vibration measurement. For free vibrations, the rectangular and exponential windows can also be used (Wickramarachi 2003). A comparison between the Hanning and rectangular windows, among others, can be found in the works of Ewins (1984), Brigham (1988), and Wickramarachi (2003).

4.3. Experimental setup

The free vibration experiment was carried out on a two bay, two storey welded steel frame with clamped bases. The frame model is shown in Fig. 4.1. The experimental setup is illustrated in Fig. 4.2. The natural frequencies are determined in the uncracked and cracked cases. The cracked cases correspond to a single crack having $d/h = 0.2$, which is then increased to 0.3. A saw cut is introduced in Member J, as shown in Figs. 4.1 and 4.2b, to simulate an open crack. It must be noted that as only in-plane vibrations are of interest, the frame has been fabricated such that the in-plane bending moments in the beams and columns are about the out-of-plane axis z, as illustrated in Fig. 4.1. The cross-section has the lowest moment of inertia about this axis. Consequently, the out-of-plane movement is restricted to a great extent when the frame is excited in-plane.

An accelerometer, a Honeywell Sensotec 060-F482-03, was taped on one of the members. According to the manufacturer specifications, the

accelerometer has a measurement range of ±10 g, a usable frequency range of 0-400 Hz, and weighs 0.03 Kg. It is assumed that the accelerometer does not affect the dynamic behaviour of the frame. The location of the accelerometer is shown in Fig. 4.1. The accelerometer is connected to a data logger, Vishay Micro-Measurements model 7000-128-SM. The data logger is, in turn, connected to a PC running the Vishay StrainSmart V4.7 software, which controls the measurement parameters and performs FFT.

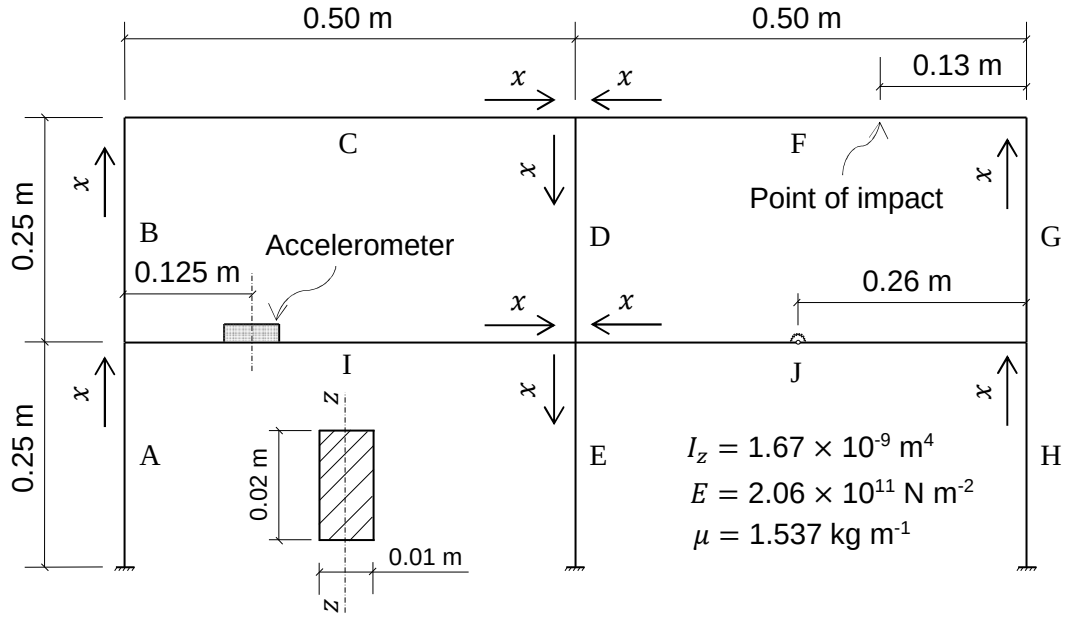

Fig. 4.1. Two bay, two storey frame.

(a) (b)

(c) (d)

Fig. 4.2. Experimental setup. (a) Two bay, two storey frame with clamped bases; (b) Crack in Member J; (c) Accelerometer; (d) Data logger.

An impulse hammer, Dytran Instruments model 5805A, was used to excite the frame into free vibration. The hammer is provided with four changeable tips; soft; medium; tough; hard. Each tip excites the frame or structure under consideration at a different frequency range, the upper limit of which equals $\sqrt{\text{contact stiffness/impactor mass}}$ (Ewins 1984). As only the first few natural frequencies are of interest, the use of the hard tip is avoided. The natural frequencies reported in the following section correspond to the use of the tough tip. However, the use of the soft or medium tip does not alter the frequencies in a significant manner. An approximate location for the point(s) of impact on the frame is shown in Fig. 4.1.

In this experiment, the measurement parameters are: total sampling period $T =$ 17 seconds, sampling frequency $\omega_s =$ 1000 Hz (samples per

second), and filters used: automatic anti-aliasing. The anti-aliasing filter is termed a Finite Impulse Response (FIR) filter by the manufacturer. When the FFT is performed by the StrainSmart software, the maximum possible number of samples N_s, strictly calculated by the software to the nearest power of 2, is selected in order to have the lowest possible frequency resolution $\Delta\omega$, according to Eq. (4.4). The maximum possible value of N_s in this experiment is 16384 $(= 2^{14})$. The resulting $\Delta\omega$ is just above 0.06 Hz. $\omega_{\max}$ in this experiment is 500 Hz. According to the analytical natural frequency calculations, the first six natural frequencies are contained in the range of 0-200 Hz, i.e. less than 0.5 $\omega_{\max}$. The aliasing effects are thus avoided if any natural frequency within that range is required to be extracted.

The natural frequencies in the range of 0-200 Hz were then extracted to enable the application of the crack detection method devised in the previous chapter. For each of the uncracked and cracked cases, the frame was excited ten consecutive times, with the accelerometer readings logged. A FFT was then performed, in turn, ten consecutive times using the Hanning window. Each time, the resulting amplitude versus frequency data was exported to a MATLAB code to extract the natural frequencies, which correspond to amplitude spikes. A FFT was repeated on the previously logged accelerometer readings, but instead, using the rectangular window to determine whether the resulting natural frequencies would differ significantly. It must be noted that the exponential window is not included in the StrainSmart software. However, according to Wickramarachi (2003), the rectangular window is an appropriate choice, as long as the total sampling period T is large enough for the vibration signal to have sufficiently decayed, as illustrated in Fig. 4.3.

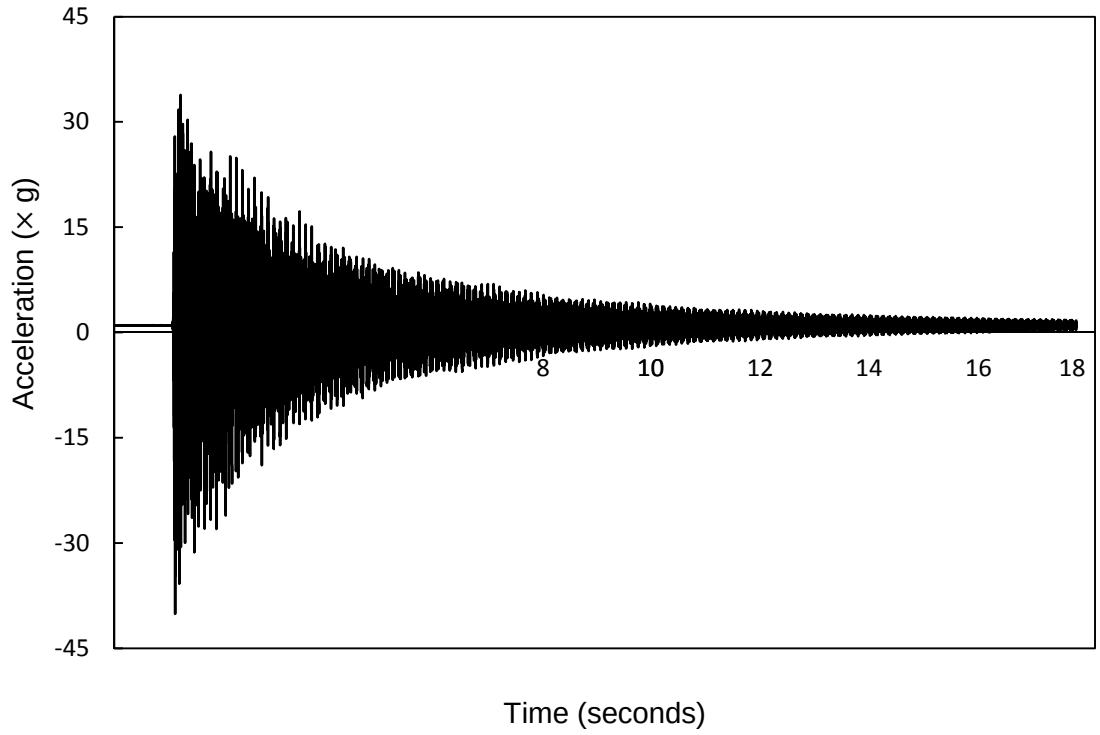

Fig. 4.3. Recorded vibration signal corresponding to Reading 1 in Tables 4.1 and 4.2.

4.4. Results and analysis

4.4.1. Natural frequency extraction

According to the analytical natural frequency calculations, the first six natural frequencies are 38.54, 128.01, 142.54, 168.92, 176.86, and 193.83 Hz. A typical amplitude versus frequency curve is shown in Fig. 4.4. Tables 4.1, 4.3, and 4.5 show the experimentally extracted natural frequencies in the uncracked and two cracked cases, respectively, when the Hanning window is used. The natural frequencies extracted using the rectangular window are given in Tables 4.2, 4.4 and 4.6.

Frequency degradations can be observed when the crack is introduced and also when the severity is increased, regardless of which window is used. For each extracted natural frequency, no variation between the readings exist when the Hanning window is used. On the contrary, some variations exist when the rectangular window is used, but they are quite small, either $+\Delta\omega$ or $-\Delta\omega$. However, the frequency values are very close to those of the Hanning window. For this reason, and in addition to being an appropriate choice for this type of

vibration testing, the frequencies obtained using the rectangular window are used.

The first two natural frequencies were not extractable, as these are sway modes, as shown in Fig. 2.11. These modes were not induced as the frame has been impacted vertically. To demonstrate the flexibility of the devised crack detection method regarding the choice of natural frequencies, the method is applied using the extractable third, fourth and fifth natural frequencies. The sixth natural frequency is used in a second iteration.

4.4.2. Application of the crack detection method

The natural frequencies are taken as an average of the ten readings in each of Tables 4.2, 4.4, and 4.6. An error (noise) value of ±0.06 Hz (i.e. ± $\Delta\omega$) is applied to each average natural frequency when the crack detection method is applied. In case there is no variation between the readings corresponding to any frequency, an error of the same value is also assumed.

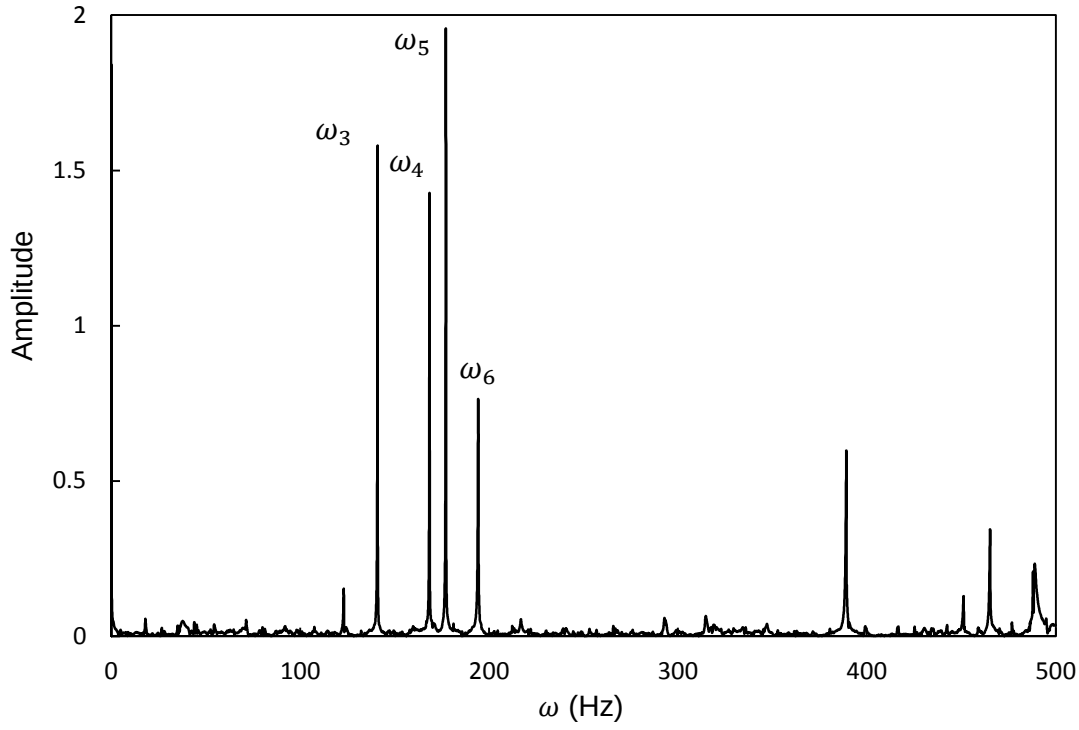

Fig. 4.4. Amplitude versus frequency curve corresponding to Reading 1 in Table 4.2.

Table 4.1. Natural frequencies of the two-bay, two-storey frame ($d/h =$ 0.0, $\Delta\omega = 0.06$ Hz, Hanning window).

Reading No.	ω_3 (Hz)	ω_4 (Hz)	ω_5 (Hz)	ω_6 (Hz)
1	140.93	168.46	177.12	194.21
2	140.93	168.46	177.12	194.21
3	140.93	168.46	177.12	194.21
4	140.93	168.46	177.12	194.21
5	140.93	168.46	177.12	194.21
6	140.93	168.46	177.12	194.21
7	140.93	168.46	177.12	194.21
8	140.93	168.46	177.12	194.21
9	140.93	168.46	177.12	194.21
10	140.93	168.46	177.12	194.21

Table 4.2. Natural frequencies of the two-bay, two-storey frame ($d/h =$ 0.0, $\Delta\omega = 0.06$ Hz, Rectangular window).

Reading No.	ω_3 (Hz)	ω_4 (Hz)	ω_5 (Hz)	ω_6 (Hz)
1	140.93	168.46	177.12	194.21
2	140.93	168.46	177.12	194.15
3	140.93	168.46	177.12	194.21
4	140.93	168.46	177.12	194.15
5	140.93	168.46	177.12	194.21
6	140.93	168.46	177.12	194.21
7	140.93	168.46	177.12	194.21
8	140.93	168.46	177.12	194.21
9	140.93	168.46	177.12	194.21
10	140.93	168.46	177.12	194.21

Table 4.3. Natural frequencies of the two-bay, two-storey frame ($d/h =$ 0.2, $\Delta\omega =$ 0.06 Hz, Hanning window).

Reading No.	ω_3 (Hz)	ω_4 (Hz)	ω_5 (Hz)	ω_6 (Hz)
1	140.87	168.03	177.06	193.73
2	140.87	168.03	177.06	193.73
3	140.87	168.03	177.06	193.73
4	140.87	168.03	177.06	193.73
5	140.87	168.03	177.06	193.73
6	140.87	168.03	177.06	193.73
7	140.87	168.03	177.06	193.73
8	140.87	168.03	177.06	193.73
9	140.87	168.03	177.06	193.73
10	140.87	168.03	177.06	193.73

Table 4.4. Natural frequencies of the two-bay, two-storey frame ($d/h =$ 0.2, $\Delta\omega =$ 0.06 Hz, Rectangular window).

Reading No.	ω_3 (Hz)	ω_4 (Hz)	ω_5 (Hz)	ω_6 (Hz)
1	140.87	168.03	177.06	193.73
2	140.81	168.03	177.06	193.66
3	140.81	168.03	177.06	193.73
4	140.81	168.03	177.06	193.73
5	140.81	168.03	177.00	193.66
6	140.81	168.03	177.06	193.66
7	140.81	168.03	177.00	193.66
8	140.81	168.03	177.00	193.66
9	140.81	168.03	177.00	193.66
10	140.81	168.03	177.00	193.66

Table 4.5. Natural frequencies of the two-bay, two-storey frame ($d/h =$ 0.3, $\Delta\omega =$ 0.06 Hz, Hanning window).

Reading No.	ω_3 (Hz)	ω_4 (Hz)	ω_5 (Hz)	ω_6 (Hz)
1	140.69	167.24	176.94	192.81
2	140.69	167.24	176.94	192.81
3	140.69	167.24	176.94	192.81
4	140.69	167.24	176.94	192.81
5	140.69	167.24	176.94	192.81
6	140.69	167.24	176.94	192.81
7	140.69	167.24	176.94	192.81
8	140.69	167.24	176.94	192.81
9	140.69	167.24	176.94	192.81
10	140.69	167.24	176.94	192.81

Table 4.6. Natural frequencies of the two-bay, two-storey frame ($d/h =$ 0.3, $\Delta\omega =$ 0.06 Hz, Rectangular window).

Reading No.	ω_3 (Hz)	ω_4 (Hz)	ω_5 (Hz)	ω_6 (Hz)
1	140.69	167.24	176.94	192.81
2	140.69	167.24	176.88	192.75
3	140.69	167.24	176.88	192.81
4	140.69	167.24	176.88	192.75
5	140.69	167.24	176.88	192.75
6	140.63	167.24	176.88	192.75
7	140.69	167.24	176.88	192.81
8	140.69	167.24	176.88	192.75
9	140.69	167.24	176.88	192.75
10	140.63	167.24	176.88	192.75

The crack location ranges are obtained assuming Young's modulus $E = 2.06 \times 10^{11}$ N m^{-2} and $d^*/h = 0.1$. Fig. 4.5 shows the empirical probability distributions for the detected crack location ranges corresponding to a crack severity $d/h = 0.2$, when the third, fourth and fifth natural frequencies are used. A number of false ranges are detected in members A (H), B (G), D, and E, along with a number of false ranges in Member I (J). When the additional sixth natural frequency is used, the probability distributions take the form shown in Fig. 4.6, where the false ranges in members D, and E are eliminated.

Increasing the crack severity d/h to 0.3, Figs. 4.7 and 4.8 show the probability distributions using the same three and four natural frequencies, respectively. No false ranges are detected in Members A (H), D, and E. Two narrow false ranges are detected, one in Member B (G), and another in Member I (J) which is eliminated when four natural frequencies are used. It is observed that using four natural frequencies narrows down the true range around the actual crack location, while maintaining the highest empirical probability. Table 4.7 lists the crack location ranges corresponding to each crack case, along with the locations of the distribution peaks.

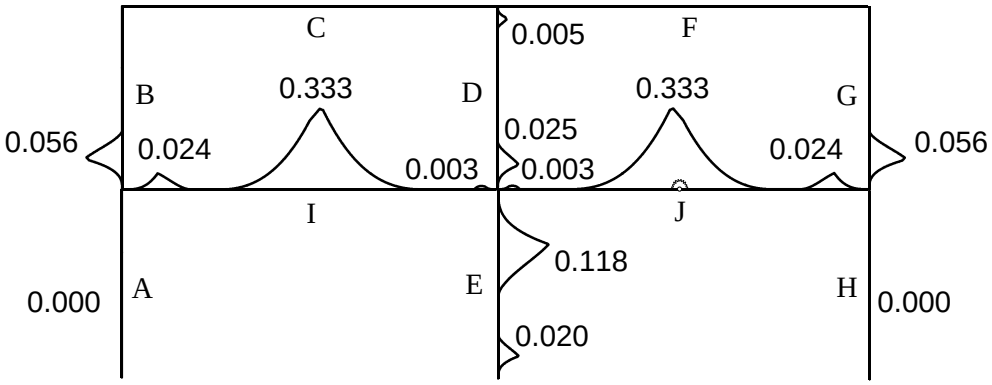

Fig. 4.5. Empirical probability distribution for the crack location in each frame member when the third, fourth, and fifth natural frequencies are used assuming an error of ±0.06 Hz and the actual crack location shown in Member J with $d/h = 0.2$.

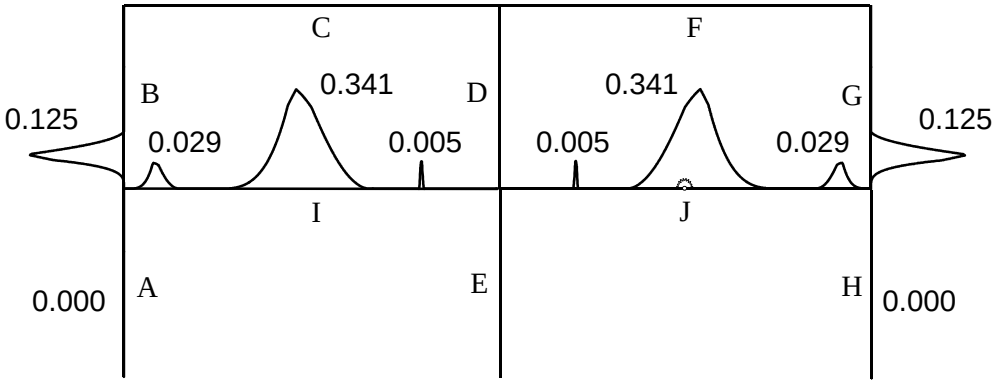

Fig. 4.6. Empirical probability distribution for the crack location in each frame member when the third, fourth, fifth, and sixth natural frequencies are used assuming an error of ±0.06 Hz and the actual crack location shown in Member J with $d/h = 0.2$.

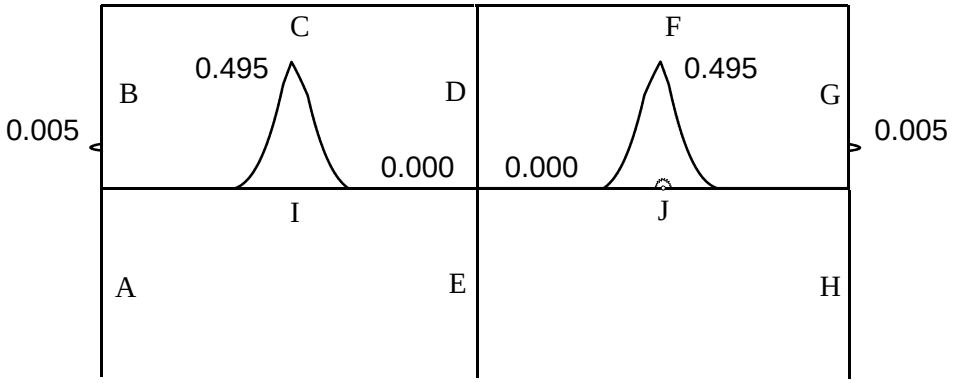

Fig. 4.7. Empirical probability distribution for the crack location in each frame member when the third, fourth, and fifth natural frequencies are used assuming an error of ±0.06 Hz and the actual crack location shown in Member J with $d/h = 0.3$.

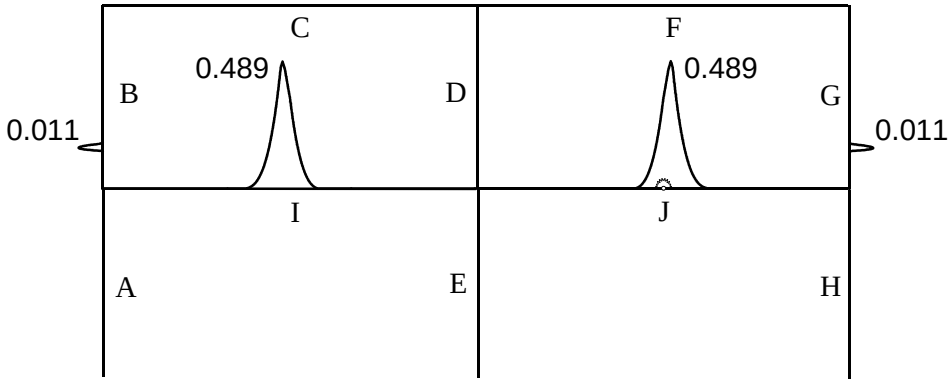

Fig. 4.8. Empirical probability distribution for the crack location in each frame member when the third, fourth, fifth, and sixth natural frequencies are used assuming an error of ±0.06 Hz and the actual crack location shown in Member J with $d/h = 0.3$.

Table 4.7. Lower and upper limits for the detected common ranges and the peak locations in each frame member when the actual crack location is in Member J at $x = 0.26$ m.

		x (m)							
d/h	Member	Three frequencies				Four frequencies			
		j	L_{cj}	U_{cj}	Peak	j	L_{cj}	U_{cj}	Peak
0.2	A (H)	1	0.09725	0.09800	0.09775	1	0.09600	0.09750	0.09700
	B (G)	1	0.0	0.07950	0.04375	1	0.0	0.07825	0.04600
	D	1	0.0	0.02900	0.01800	-	-	-	-
		2	0.18575	0.25000	0.21475				
	E	1	0.0	0.14275	0.07250	-	-	-	-
		2	0.19250	0.25000	0.22000				
	I (J)	1	0.0	0.09150	0.04600	1	0.0	0.07300	0.03750
		2	**0.13300**	**0.40250**	**0.26350**	**2**	**0.13150**	**0.32700**	**0.22925**
		3	0.47050	0.50000	0.48025	3	0.39450	0.40100	0.39775
0.3	B (G)	1	0.05200	0.06150	0.05625	1	0.05175	0.06225	0.05600
	I (J)	**1**	**0.17600**	**0.33000**	**0.25300**	**1**	**0.18600**	**0.28900**	**0.24000**
		2	0.39050	0.39150	0.39100				

Detecting the crack severity ranges using experimental data is not a straightforward task. The mathematical model has to be calibrated such that the natural frequencies calculated from the model in the uncracked case closely match those extracted from the experiment. A simple method of achieving this is the zero-setting procedure, based on iteratively changing the value of

Young's modulus in the model separately for each uncracked natural frequency utilised in the detection procedure (Xiang et al. 2014). The procedure results in a set of values for Young's modulus, each corresponding to a specific natural frequency. For this experiment, the values are {201.365, 204.870, 206.600, 206.780} $\times 10^9$ N m^{-2}, corresponding to the third, fourth, fifth, and sixth natural frequencies, respectively. For each cracked case, reliable crack severity ranges are obtained at the actual crack location, as shown in Figs. 4.9–4.12. The detected crack severity ranges at the locations of the empirical distribution peaks are summarised in Table 4.8. It is observed that plotting the crack severity ranges further eliminates some of the falsely detected crack location ranges.

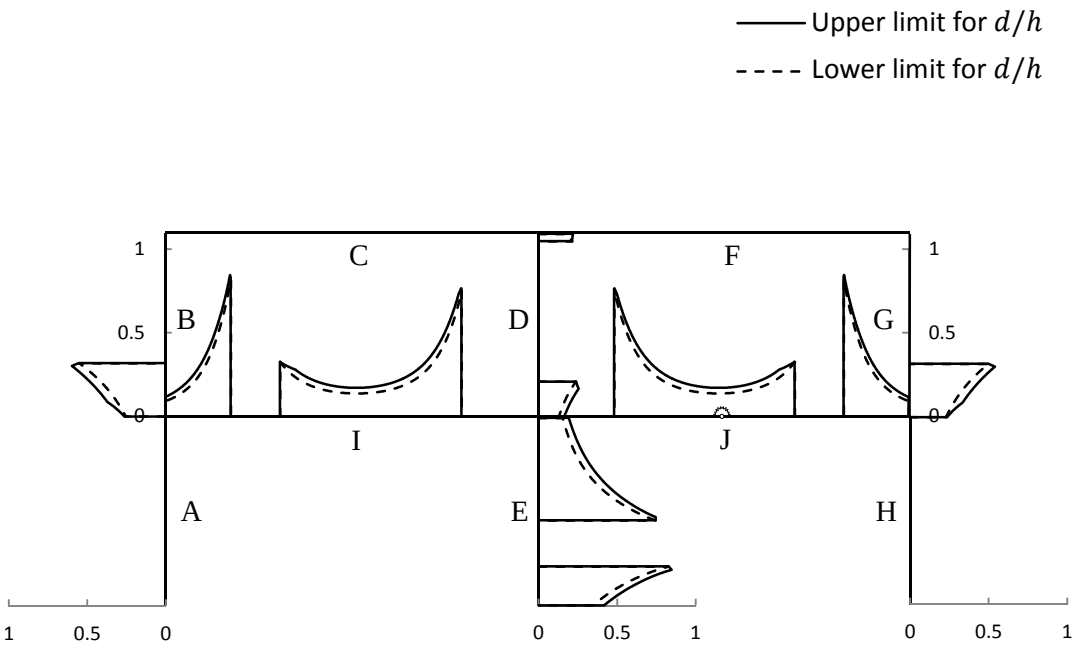

Fig. 4.9. Detected ranges for d/h in each frame member when the third, fourth, and fifth natural frequencies are used assuming an error of ±0.06 Hz and the actual crack location shown in Member J with $d/h = 0.2$.

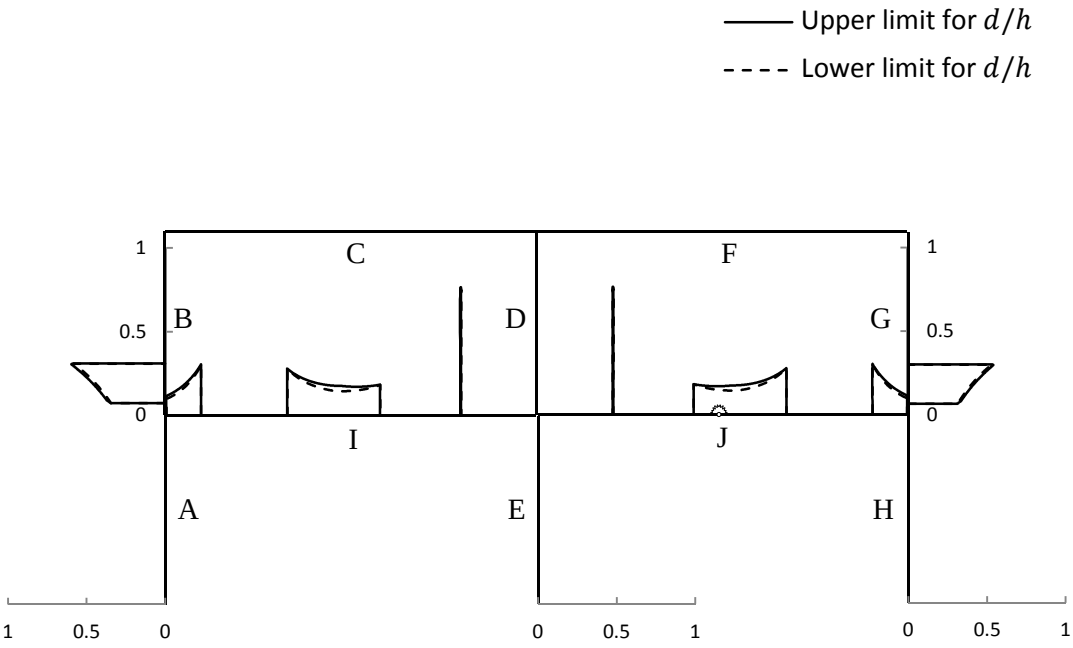

Fig. 4.10. Detected ranges for d/h in each frame member when the third, fourth, fifth, and sixth natural frequencies are used assuming an error of ±0.06 Hz and the actual crack location shown in Member J with $d/h = 0.2$.

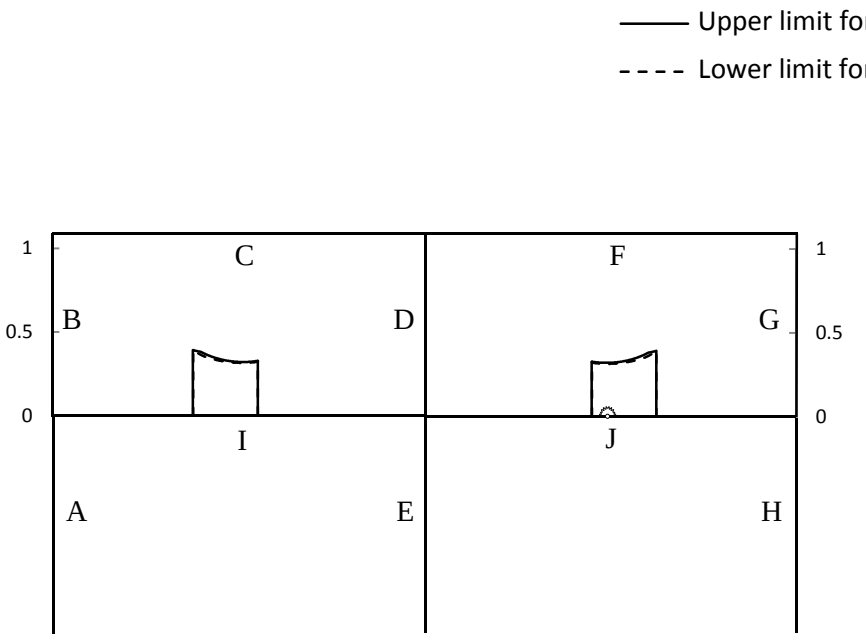

Fig. 4.11. Detected ranges for d/h in each frame member when the third, fourth and fifth natural frequencies are used assuming an error of ±0.06 Hz and the actual crack location shown in Member J with $d/h = 0.3$.

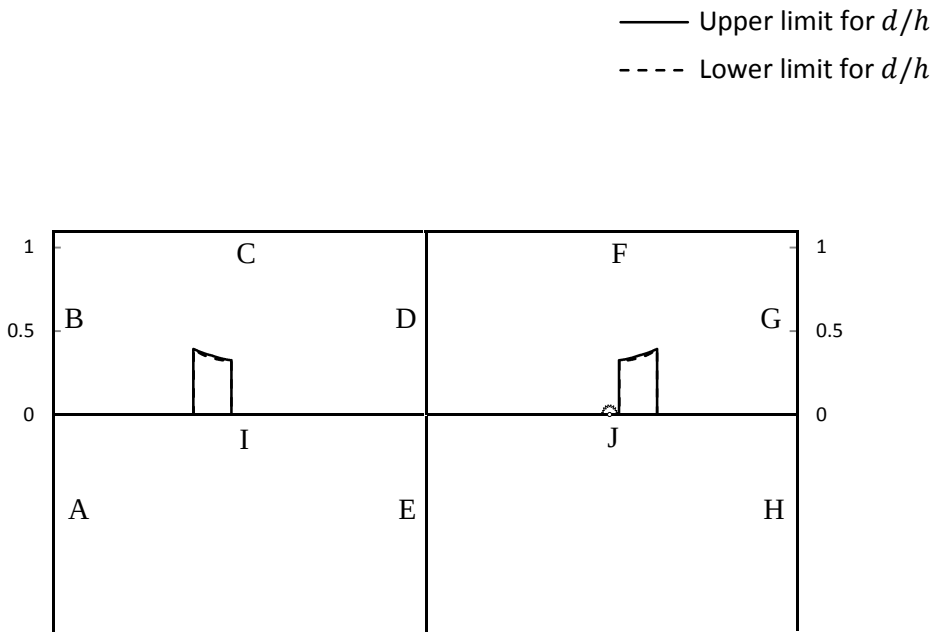

Fig. 4.12. Detected ranges for d/h in each frame member when the third, fourth, fifth, and sixth natural frequencies are used assuming an error of ±0.06 Hz and the actual crack location shown in Member J with $d/h = 0.3$.

Table 4.8. Lower and upper limits for the detected d/h ranges at the distribution peaks in each frame member when the actual crack location is in Member J at $x = 0.26$ m.

Actual d/h	Member	Detected d/h					
		Three frequencies			Four frequencies		
		j	Lower limit	Upper limit	j	Lower limit	Upper limit
0.2	A (H)	1	-	-	1	-	-
	B (G)	1	0.336	0.395	1	0.388	0.403
	D	1	0.201*	0.201*	-	-	-
		2	0.188	0.232			
	E	1	0.305	0.361	-	-	-
		2	0.554	0.634			
	I (J)	1	0.245	0.295	1	0.232	0.242
		2	**0.137**	**0.171**	**2**	**0.146**	**0.176**
		3	-	-	3	0.754	0.758
0.3	B (G)	1	-	-	1	-	-
	I (J)	**1**	**0.316**	**0.321**	**1**	**0.325**	**0.325**
		2	-	-			

* Values detected at the closest possible location to that of the distribution peak.

4.5. Conclusions

The crack detection method devised in the previous chapter has been experimentally applied to a frame and validated. Minimal equipment is required;

an impact hammer and an accelerometer connected to a data logger. The natural frequencies have been extracted using the well-established fast Fourier transform without requiring any further analysis outside the equipment software. Crack location ranges containing the actual crack location have been successfully detected, using three and four natural frequencies, even when the actual crack severity was not considerably high. The crack severity was recoverable in a reliable manner. In line with the findings in the previous chapter, using additional natural frequencies eliminates some of the falsely detected crack location ranges.

Chapter 5 – Crack detection enhancement

5.1. Introduction

In Chapter 3, the location of a single crack in a frame member was detected using the first three natural frequencies in case of noise free simulations. When noise is introduced, the fourth natural frequency enhances the detection procedure as some falsely detected crack location ranges are eliminated and some members can thus be marked as uncracked. However, the selection of the fourth natural frequency was arbitrary. In this chapter, a method is formulated to mathematically select the most effective natural frequencies required to enhance the detection procedure in the presence of simulated noise. The method is based on selecting the two natural frequencies showing the two highest variations from a group of frequencies, to be used in addition to the first three, thus making use of higher order natural frequencies.

The crack detection procedure can be enhanced in another manner, but before application, by recognising that some of the higher and lower order natural frequencies have zero (or near zero) degradations when specific frame members are cracked. If a degradation is observed in these frequencies, then these members are guaranteed to be uncracked and so can be eliminated from any subsequent analysis.

5.2. Arrangement of natural frequency variations

In the technique proposed here, the first three natural frequencies are used in a first iteration of the detection procedure described in Chapter 3. A number of possible crack location ranges are thus obtained. With the aim of eliminating some of the false ranges determined, a group of natural frequencies of orders higher than those of the first three are selected. The detected crack location ranges are then discretised into a number of points. The dimensionless natural frequency variations δ_i corresponding to each higher order mode $i \neq 1$, 2, 3 are then calculated when a crack having $d/h = 0.4$ (i.e. the upper limit for small cracks) is placed individually at the discretisation points, giving the set:

$$\boldsymbol{\delta}_i = \{\delta_i(x_1/l)\ \delta_i(x_2/l) \ldots \delta_i(x_n/l)\}, \tag{5.1}$$

where n is the number of discretisation points in all ranges combined. The maximum value $\delta_{i\max}$ in this set is logged and the process is repeated for the other higher order modes. The maximum variations of all selected higher order modes are combined in the set:

$$\boldsymbol{\delta}_{\max} = \{\delta_{4\max}\ \delta_{7\max} \dots \delta_{f\max}\}, \tag{5.2}$$

where f is the highest mode number within the natural frequency group. The two natural frequencies corresponding to the two highest variations in $\boldsymbol{\delta}_{\max}$ are used in a second iteration of the detection procedure described in Chapter 3. The above procedure has been programmed into MATLAB.

Selecting the two natural frequencies having the highest variations from a group of frequencies serves a number of purposes. Referring to the frequency variation equations in the presence of noise:

$$\delta_{im}^{L} = 1 - \frac{\omega_{icm}^{U}}{\omega_{iom}^{L}}, \qquad \delta_{im}^{U} = 1 - \frac{\omega_{icm}^{L}}{\omega_{iom}^{U}}. \tag{5.3}$$

and the normalisation equation:

$$\overline{\delta}_{im}^{L} = \frac{1}{\sqrt{1 + \frac{\sum_{j\neq i} {\delta_{jm}^{U}}^2}{{\delta_{im}^{L}}^2}}}, \qquad \overline{\delta}_{im}^{U} = \frac{1}{\sqrt{1 + \frac{\sum_{j\neq i} {\delta_{jm}^{L}}^2}{{\delta_{im}^{U}}^2}}}, \tag{5.4}$$

two distinct cases are encountered. The first case occurs when the simulated variations in at least two of the first three natural frequencies are relatively small compared to the noise such that $\overline{\delta}_{1m}^{L}, \overline{\delta}_{2m}^{L}$ and $\overline{\delta}_{3m}^{L}$, calculated using the first three natural frequencies, equal 0.0 or are close to 0.0, and $\overline{\delta}_{1m}^{U}, \overline{\delta}_{2m}^{U}$ and $\overline{\delta}_{3m}^{U}$ equal 1.0 or are close to 1.0. At the same time, at least one of the two additional natural frequencies will exhibit large simulated variations. Using the five frequencies in the normalisation process leads to $\overline{\delta}_{1m}^{L}$, $\overline{\delta}_{2m}^{L}$ and $\overline{\delta}_{3m}^{L}$ remaining 0.0 or shifting towards 0.0 and $\overline{\delta}_{1m}^{U}$, $\overline{\delta}_{2m}^{U}$ and $\overline{\delta}_{3m}^{U}$ being significantly lowered, along with $\overline{\delta}_{im}^{L}$ and $\overline{\delta}_{im}^{U}$, corresponding to at least one of the two additional frequencies, being close. The overall outcome is narrower crack location ranges. The second case occurs when the simulated variations in at least two of the first three natural frequencies are relatively large compared to the noise. At

the same time, the two additional natural frequencies exhibit zero or near zero simulated variations. Using the five frequencies in the normalisation process leads to $\overline{\delta}_{1m}^{L}$, $\overline{\delta}_{2m}^{L}$ and $\overline{\delta}_{3m}^{L}$ slightly lowering; $\overline{\delta}_{1m}^{U}$, $\overline{\delta}_{2m}^{U}$ and $\overline{\delta}_{3m}^{U}$ remaining almost unchanged; along with $\overline{\delta}_{im}^{L}$ and $\overline{\delta}_{im}^{U}$, corresponding to at least one of the two additional frequencies, being close and very low. The effect of the high variations of the two additional frequencies, occurring in one of the false crack location ranges, is manifested in the corresponding discrete values of $\overline{\delta}_{i}(x/l)$ being high within one or more of the falsely detected crack location ranges, while $\overline{\delta}_{1}(x/l)$, $\overline{\delta}_{2}(x/l)$ and $\overline{\delta}_{3}(x/l)$ within the same ranges are lowered. Similar to the first case, the overall outcome is narrower crack location ranges.

5.3. Numerical example

The selection procedure for the natural frequencies is applied to the two-bay, two-storey frame, illustrated in Chapter 3 and shown in Fig. 5.1. The material properties are described in Section 2.3.2.2. A single crack is introduced in the frame. Cases 1 and 2 of Table 3.1, reproduced in Table 5.1, are applied. The natural frequencies selected for the detection procedure are considered up to three decimal places, in a similar manner to that described in Chapter 3. A randomly assumed error of ±0.005 Hz is introduced to each frequency.

Table 5.1. First three natural frequencies of the two-bay, two-storey frame.

Case no.	Crack location			d/h	ω_1 (Hz)	ω_2 (Hz)	ω_3 (Hz)
	Member	x/l	x (m)				
0	Uncracked case				3.2675	10.8528	12.0840
1	A	0.240	0.720	0.300	3.2527	10.8346	12.0762
2	I	0.485	2.910	0.300	3.2674	10.8509	12.0690

Considering Case 1, Fig. 5.2 shows the empirical probability distributions for the detected crack location ranges, as illustrated in Chapter 3, using the first three natural frequencies when the actual crack location is in Member A. With the aim of selecting two extra frequencies out of the fourth to tenth natural frequencies, to be used in a second iteration of the detection procedure, each previously detected range is discretised into 0.1 m spaced points where a crack, having $d/h = 0.4$, is placed individually. Using the MATLAB code, $\delta_{i\max}$ for

$i = 4$ …10, and the corresponding crack locations are calculated and reported in Table 5.2. It can be seen that the highest two values for $\delta_{i\max}$ are identified as corresponding to the fifth and ninth natural frequencies. In the absence of noise, the values of these two frequencies in the uncracked case are 14.993 Hz and 40.235 Hz, respectively. For crack case 1, the values are 14.992 Hz and 40.235 Hz, respectively. These are then used in a second iteration of the crack detection procedure, along with the first three natural frequencies, after introducing the noise. The resulting empirical probability distributions are shown in Fig. 5.3.

In a similar manner, Case 2 is considered. Fig. 5.4 shows the empirical probability distributions for the detected crack location ranges using the first three natural frequencies when the actual crack location is in Member I. $\delta_{i\max}$ and the corresponding crack locations are shown in Table 5.3. The highest two values for $\delta_{i\max}$ correspond to the fourth and fifth natural frequencies. In the absence of noise, the values of these two frequencies in the uncracked case are 14.320 Hz and 14.993 Hz, respectively. For crack case 2, the values are 14.223 Hz and 14.976 Hz, respectively. The resulting empirical probability distributions from the second iteration of the detection procedure are shown in Fig. 5.5.

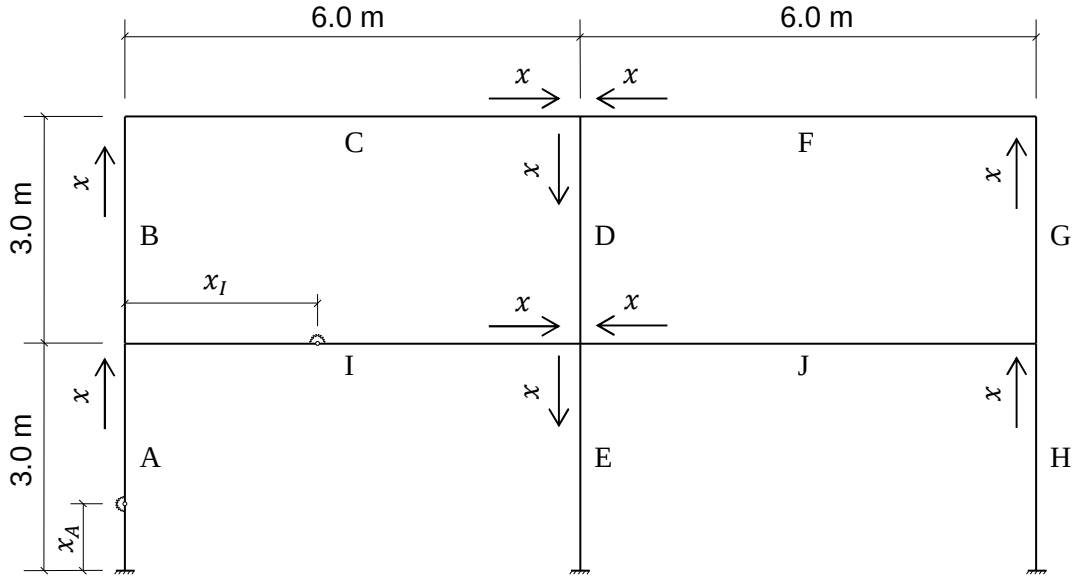

Fig. 5.1. Two bay, two storey frame.

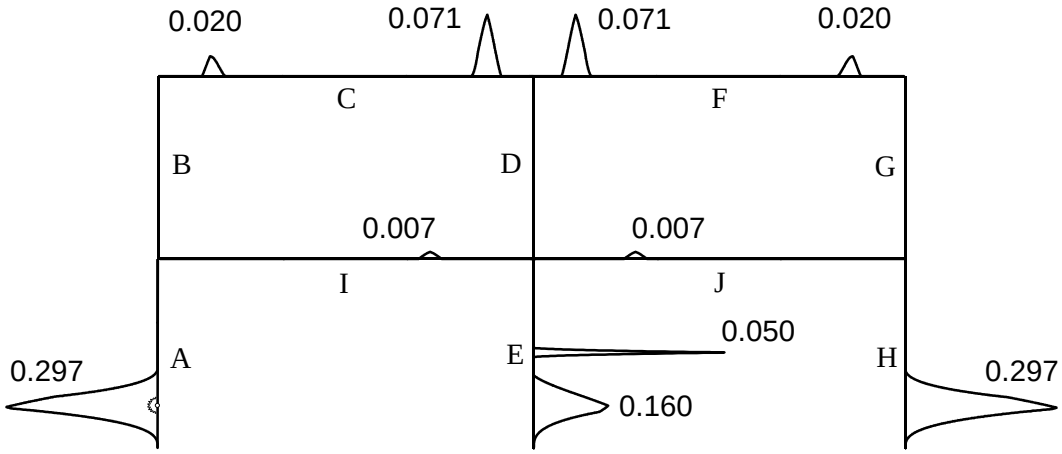

Fig. 5.2. Empirical probability distribution for the crack location in each frame member when the first three natural frequencies are used assuming a simulated error of ±0.005 Hz and the actual crack location shown in Member A, with $d/h = 0.3$.

Table 5.2. Values of $\delta_{i\max}$ for $i = 4$ …10, within the detected ranges shown in Fig. 5.2.

i		4	5	6	7	8	9	10
$\delta_{i\max}$		0.0048	0.0104	0.0019	0.0063	0.0078	0.0089	0.0075
Crack location	Member	I (J)	C (F)	I (J)	C (F)	C (F)	I (J)	I (J)
	x/l	0.693	0.907	0.693	0.840	0.166	0.726	0.693
	x (m)	4.158	5.440	4.158	5.040	0.996	4.358	4.158

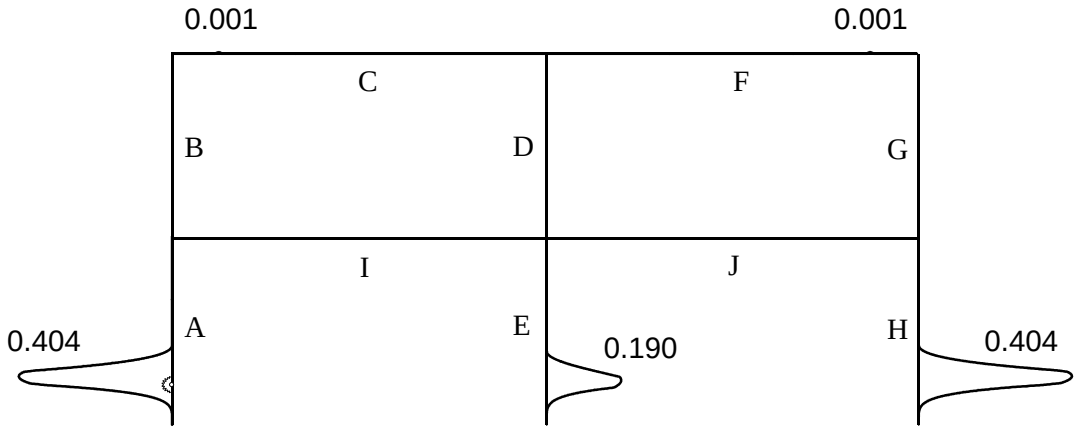

Fig. 5.3. Empirical probability distribution for the crack location in each frame member when the first, second, third, fifth and ninth natural frequencies are used assuming a simulated error of ±0.005 Hz and the actual crack location shown in Member A, with $d/h = 0.3$.

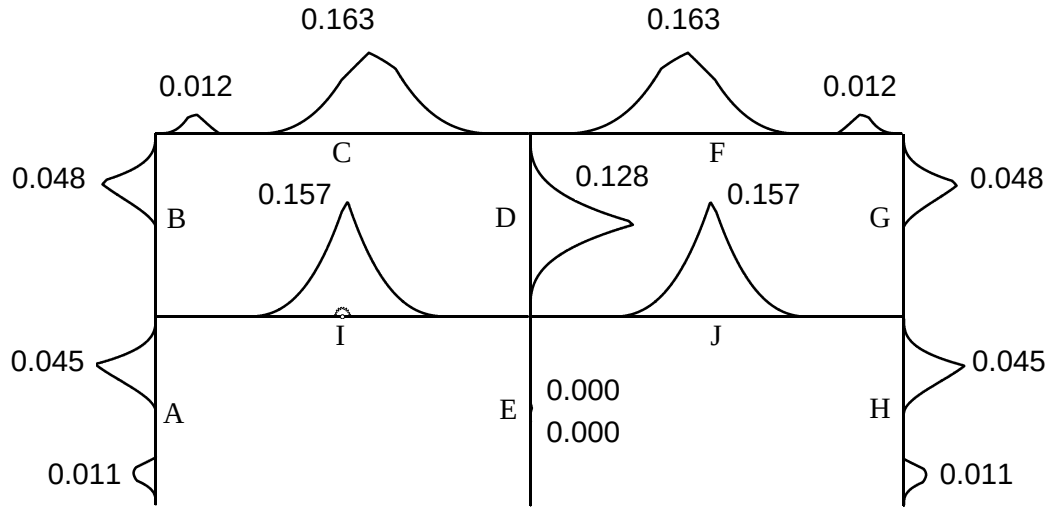

Fig. 5.4. Empirical probability distribution for the crack location in each frame member when the first three natural frequencies are used assuming a simulated error of ±0.005 Hz and the actual crack location shown in Member I, with $d/h = 0.3$.

Table 5.3. Values of $\delta_{i\max}$ for $i = 4$ …10, within the detected ranges shown in Fig. 5.4.

	i	4	5	6	7	8	9	10
	$\delta_{i\max}$	0.0119	0.0105	0.0101	0.0104	0.0096	0.0093	0.0078
Crack location	Member	I (J)	C (F)	I (J)	C (F)	B (G)	D	I (J)
	x/l	0.505	0.440	0.472	0.740	0.528	0.000	0.272
	x (m)	3.030	2.640	2.830	4.440	1.585	0.001	1.630

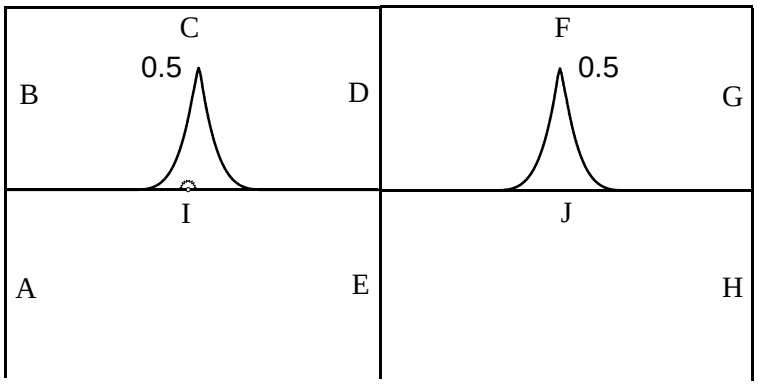

Fig. 5.5. Empirical probability distribution for the crack location in each frame member when the first, second, third, fourth and fifth natural frequencies are used assuming a simulated error of ±0.005 Hz and the actual crack location shown in Member I, with $d/h = 0.3$.

5.4. Zero change feature

The zero change feature is exhibited in natural frequencies corresponding to some of the higher order modes and also, lower order modes, depending on the complexity of the frame. When a single crack is present anywhere along specific frame members, the degradation in these natural frequencies is zero or close to zero. A specific frame member may have only one frequency exhibiting this behaviour, or several frequencies. Some frequencies may also be common among several members. It is, therefore, advantageous to search for the frequencies which are unique to one member. Two cases are encountered when one of these frequencies corresponding to a specific member is measured in the uncracked and cracked cases. If the degradation is found to be significant compared to the noise, such that the lower limit exceeds the maximum near zero value of the degradations when the crack is present in the considered member, then that member can be marked as uncracked, if only a single crack is present in the frame. However, if the degradation is not significant, then measuring that frequency is not beneficial, as the crack can be present in any member. The reasoning behind this is that every higher order natural frequency has a zero degradation when the crack is present at specific points in each member. Lower order frequencies, with very few exceptions, exhibit the same behaviour.

The search for the natural frequencies exhibiting the zero change feature starts with discretising the frame into a number of points. The crack is placed at each point individually while calculating the degradations of the first 100 natural frequencies, given by:

$$\Delta\omega_i = \omega_{io} - \omega_{ic} \tag{5.5}$$

where ω_{io} and ω_{ic} are the natural frequencies in the uncracked and cracked cases, respectively. When ‘as measured’ natural frequencies are contaminated with noise, then any natural frequency can be considered as possessing the zero change feature when the calculated degradations in all points are less than twice the measurement error, i.e. have zero lower limits when measured. This calculation procedure has been programmed into MATLAB.

5.5. Numerical example

The example used in Section 5.3 is considered, along with the two cases for the crack location. The beams and columns of the frame are discretised into points distanced at {0.01, 0.10, 0.20, 0.30…2.70, 2.80, 2.90, 2.99} m and {0.01, 0.10, 0.20, 0.30…5.70, 5.80, 5.90, 5.99} m, respectively from the ends. A single crack having $d/h = 0.4$ is placed at each point individually while calculating the degradations of the first 100 natural frequencies using the MATLAB code. Table 5.4 shows some of the natural frequencies exhibiting the zero change feature and unique to each member, on the basis that the maximum calculated noise free degradation, $\Delta\omega_{i\max}$, of each frequency is less than twice the measurement error, assumed to be ±0.005 Hz. The maximum degradations are also reported. For each frequency, the degradation plots along the whole frame are shown in Figs. 5.6 and 5.7, noting that Member C (F) requires additional discretisation points when plotting the degradations of the 77th natural frequency. Simulated degradations $\Delta\omega_{im}$ and their lower limits $\Delta^L\omega_{im}$, corresponding to the two crack cases, are reported in Table 5.5. Considering Case 1, when the crack is present in Member A (H), it can be seen that the lower limits for the degradations of frequencies 2 and 29 ($\Delta^L\omega_{2m}$ and $\Delta^L\omega_{29m}$) are greater than the reported values in Table 5.4 for their maximum noise free degradations, $\Delta\omega_{2\max}$ and $\Delta\omega_{29\max}$, respectively. Thus, Members D and I (J) can be marked as uncracked and excluded from any subsequent analysis. In a similar manner, considering Case 2, when the crack is present in Member I (J), it can be seen that the lower limits for the degradations of frequencies 3 and 29 are greater than $\Delta\omega_{3\max}$ and $\Delta\omega_{29\max}$, respectively. Members D and E can thus be marked as uncracked and excluded from any subsequent analysis.

Table 5.4. Zero change natural frequencies unique to each frame member and their maximum noise free degradations.

Member	A (H)	B (G)	C (F)	D	E	I (J)
i	77	-	-	29	3	2
$\Delta\omega_{i\max}$ (Hz)	0.0025	-	-	0.0000	0.0036	0.0040

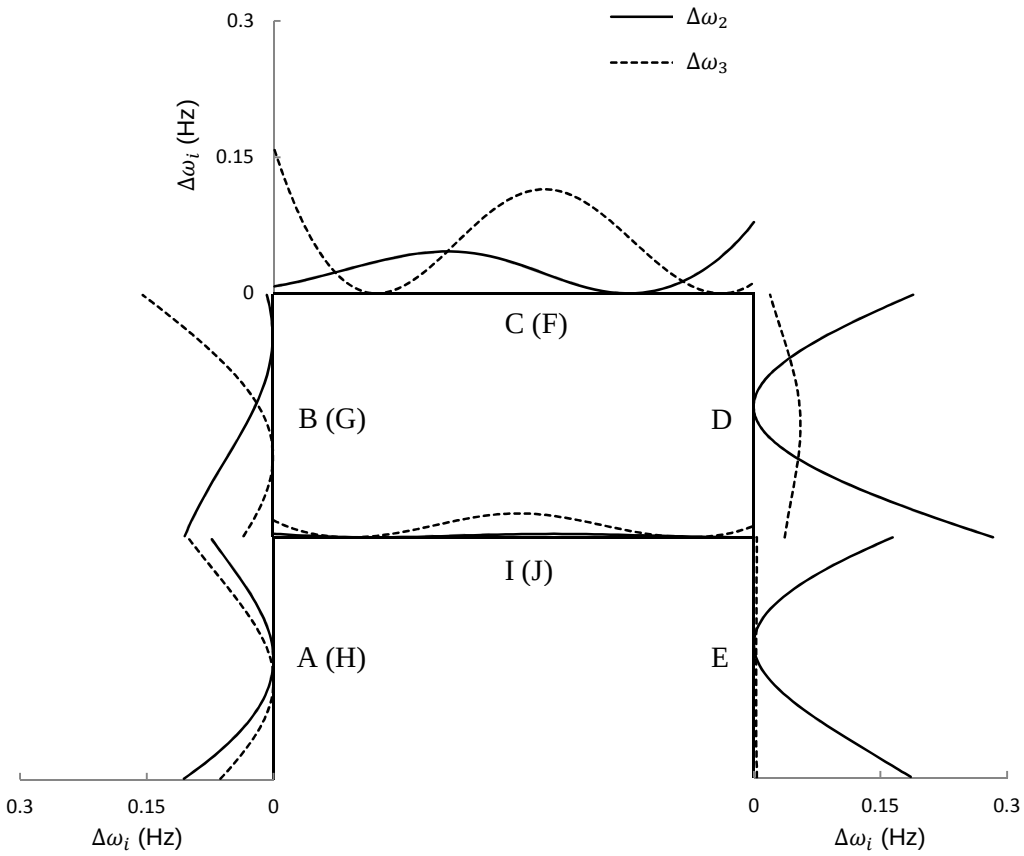

Fig. 5.6. Variation of the second and third natural frequencies of the two bay, two storey frame with the crack location when $d/h = 0.4$.

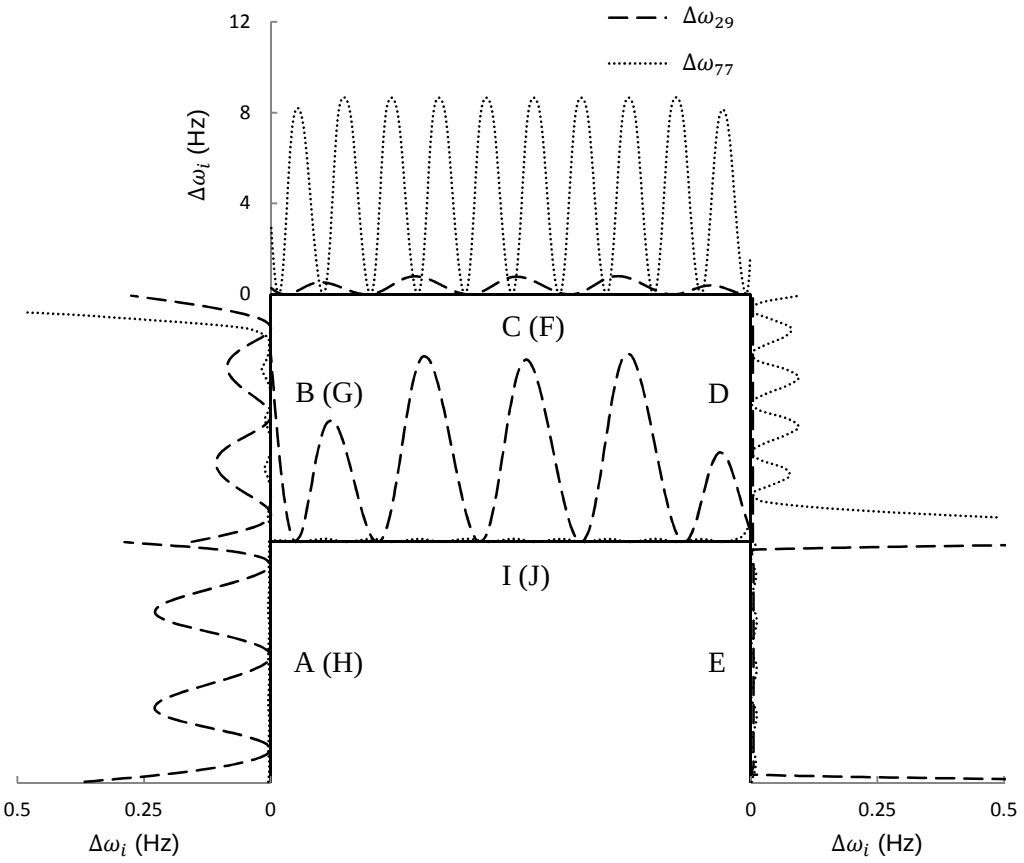

Fig. 5.7. Variation of the twenty ninth and seventy seventh natural frequencies of the two bay, two storey frame with the crack location when $d/h = 0.4$ (the vertical scale on Member C (F) is different from that on the other members).

Table 5.5. Frequency variations and their lower limits for $i = 2$, 3, 29 and 77.

i		2	3	29	77
Crack case 1	$\Delta\omega_{im}$ (Hz)	0.0180	0.0080	0.0860	0.0000
	$\Delta^L\omega_{im}$ (Hz)	0.0080	0.0000	0.0760	0.0000
Crack case 2	$\Delta\omega_{im}$ (Hz)	0.0020	0.0150	0.0970	0.0020
	$\Delta^L\omega_{im}$ (Hz)	0.0000	0.0050	0.0870	0.0000

5.6. Discussion

The two devised methods for enhancing the crack detection procedure reduce the number of falsely detected crack location ranges. The method based on the arrangement of the natural frequency variations results in the narrowing down and elimination of some of the false ranges. The reasoning behind the

selection of the two natural frequencies having the highest variations from a group of frequencies is illustrated with the help of Figs. 5.8–5.15. The lightly shaded areas represent the detected ranges corresponding to each frequency, while the hatched darkly shaded areas represent the combined ranges, if any, for all frequencies used.

For crack case 1, the simulated variations of the fifth and ninth natural frequencies are almost zero, contrary to the first three natural frequencies. Referring to Eqs. (5.3) and (5.4), this results in the zero lower limits of the normalised variations $\overline{\delta}_{5m}^{L}$ and $\overline{\delta}_{9m}^{L}$, along with the upper limits $\overline{\delta}_{5m}^{U}$ and $\overline{\delta}_{9m}^{U}$ being low (< 0.5). $\overline{\delta}_{1m}^{U}$, $\overline{\delta}_{2m}^{U}$ and $\overline{\delta}_{3m}^{U}$ remain unchanged, while $\overline{\delta}_{1m}^{L}$, $\overline{\delta}_{2m}^{L}$ and $\overline{\delta}_{3m}^{L}$ lower slightly. The large variations of the fifth and ninth natural frequencies, based on which, these two additional frequencies were chosen, are pronounced in the $\overline{\delta}_{5}$ and $\overline{\delta}_{9}$ curves, within at least two of the falsely detected crack location ranges. One of these false ranges is in Member C (F), around $x/l = 0.9$, and the other is in Member I (J), around $x/l = 0.7$. According to Table 5.2, the fifth and ninth natural frequencies have the two highest variations around these two locations, respectively. Referring to Figs. 5.8 and 5.9, it can be seen that the high values of $\overline{\delta}_{5}$ around $x/l = 0.9$ in Member C (F), cause the values of $\overline{\delta}_{1}$ and $\overline{\delta}_{2}$ to lower. Coupled with the low value of $\overline{\delta}_{5m}^{U}$, the overall outcome is the elimination of the false range around $x/l = 0.9$. A similar pattern is observed for Member I (J) (Figs. 5.10 and 5.11), where as a result of using the ninth natural frequency, the false range around $x/l = 0.7$ is eliminated. Using the fifth and ninth natural frequencies can eliminate or narrow down other false ranges. The false range in Member C (F) around $x/l = 0.15$ is significantly narrowed down, while the false range around the middle of Member E is eliminated, as shown in Figs. 5.2 and 5.3.

For crack case 2, the simulated variations of the fourth and fifth natural frequencies are high, contrary to the first two natural frequencies. As the fourth natural frequency has the highest variation, both the lower and the upper limits, $\overline{\delta}_{4m}^{L}$ and $\overline{\delta}_{4m}^{U}$, respectively, are high. $\overline{\delta}_{1m}^{U}$, $\overline{\delta}_{2m}^{U}$ and $\overline{\delta}_{3m}^{U}$ lower significantly, while $\overline{\delta}_{1m}^{L}$, $\overline{\delta}_{2m}^{L}$ and $\overline{\delta}_{3m}^{L}$ remain unchanged (= 0.0). This results in $\overline{\delta}_{im}^{L}$ and $\overline{\delta}_{im}^{U}$ for all

frequencies being close. The overall outcome in this crack case is the elimination of all false ranges in every member despite the highest variation in the fourth natural frequency being in Member I (J) and in the fifth frequency being in Member C (F), as shown in Table 5.3. The effect of using the additional fourth and fifth natural frequencies is illustrated by comparing Figs. 5.12 with 5.13, concerned with Member C (F), and Figs. 5.14 with 5.15, concerned with Member D. In this particular crack case, all false ranges are eliminated mainly due to the high values of the lower and upper limits $\overline{\delta}_{4m}^{L}$ and $\overline{\delta}_{4m}^{U}$ being above the $\overline{\delta}_4$ curve.

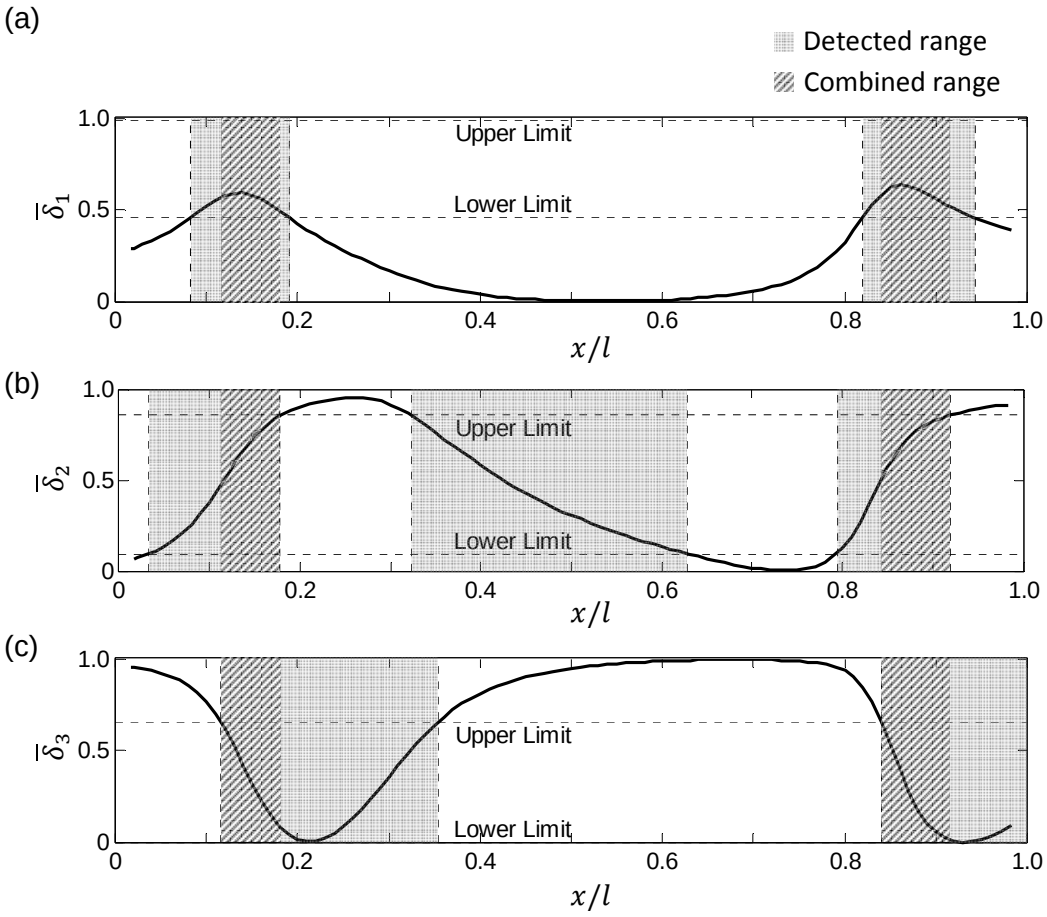

Fig. 5.8. Variation of $\overline{\delta}_i$ with the crack location in Member C (F) and the detected crack location ranges assuming a simulated error of ±0.005 Hz and the actual crack location in Member A (crack case 1), with $d/h = 0.3$. (a) $i = 1$; (b) $i = 2$; (c) $i = 3$.

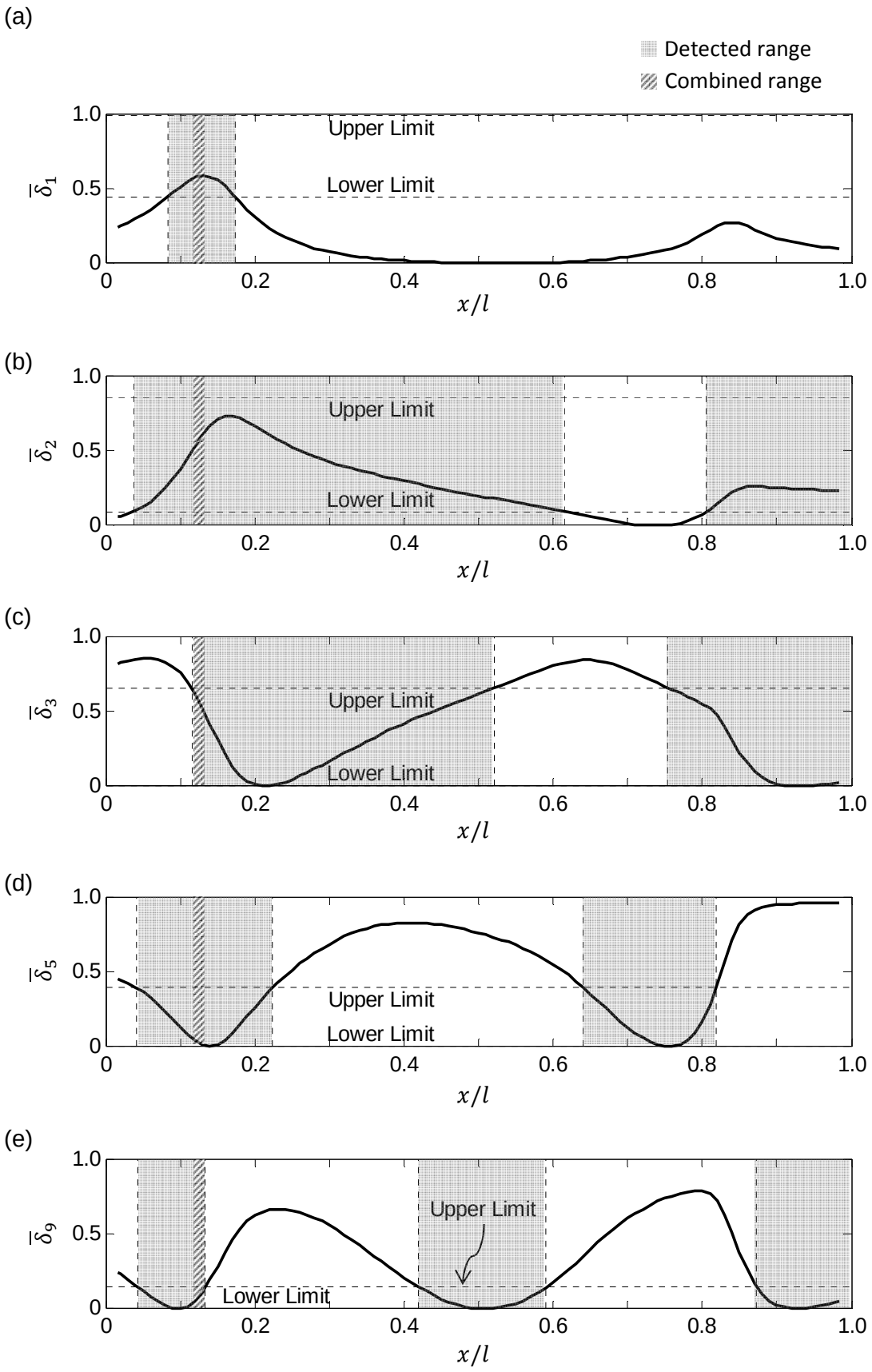

Fig. 5.9. Variation of $\overline{\delta}_i$ with the crack location in Member C (F) and the detected crack location ranges assuming a simulated error of ±0.005 Hz and the actual crack location in Member A (crack case 1), with $d/h = 0.3$. (a) $i = 1$; (b) $i = 2$; (c) $i = 3$; (d) $i = 5$; (e) $i = 9$.

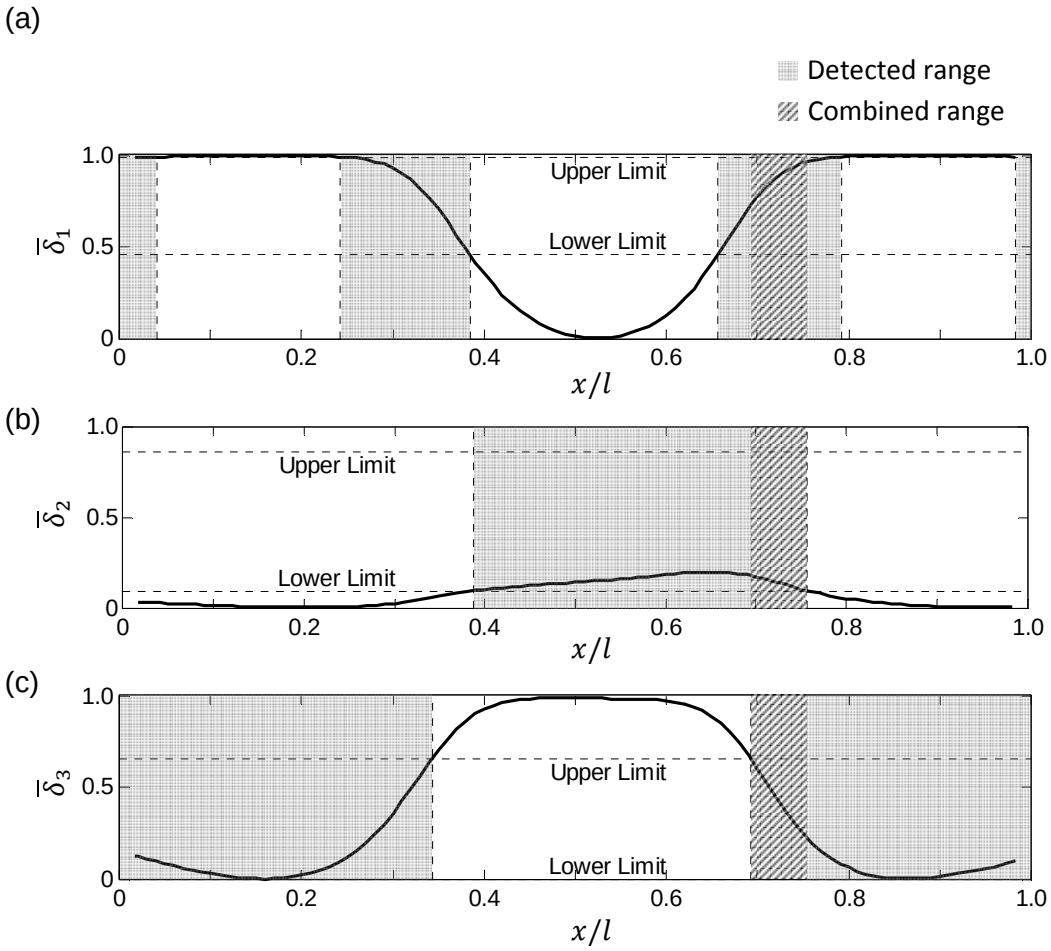

Fig. 5.10. Variation of $\overline{\delta}_i$ with the crack location in Member I (J) and the detected crack location ranges assuming a simulated error of ±0.005 Hz and the actual crack location in Member A (crack case 1), with $d/h = 0.3$. (a) $i = 1$; (b) $i = 2$; (c) $i = 3$.

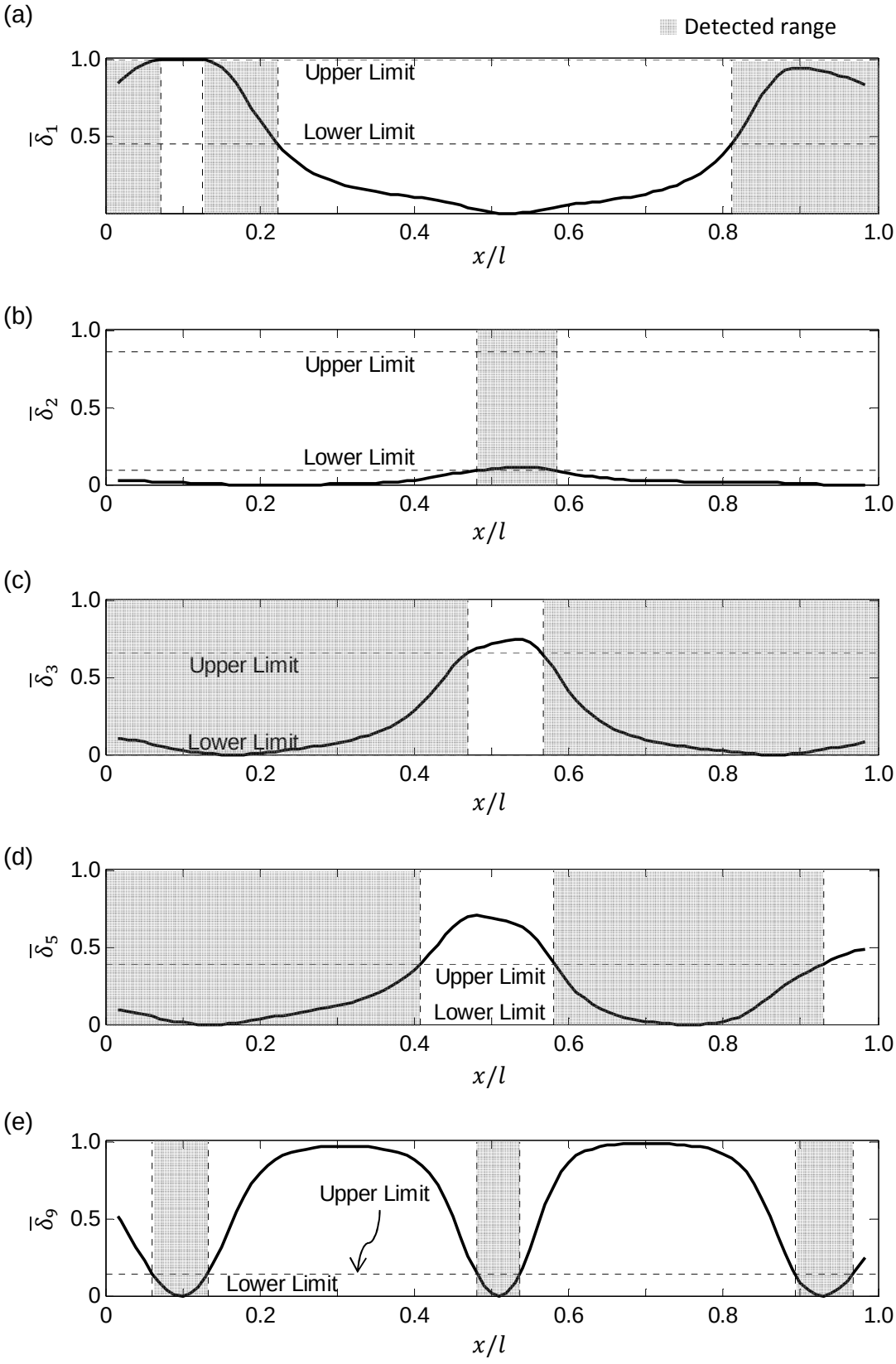

Fig. 5.11. Variation of $\overline{\delta}_i$ with the crack location in Member I (J) and the detected crack location ranges assuming a simulated error of ±0.005 Hz and the actual crack location in Member A (crack case 1), with $d/h = 0.3$. (a) $i = 1$; (b) $i = 2$; (c) $i = 3$; (d) $i = 5$; (e) $i = 9$.

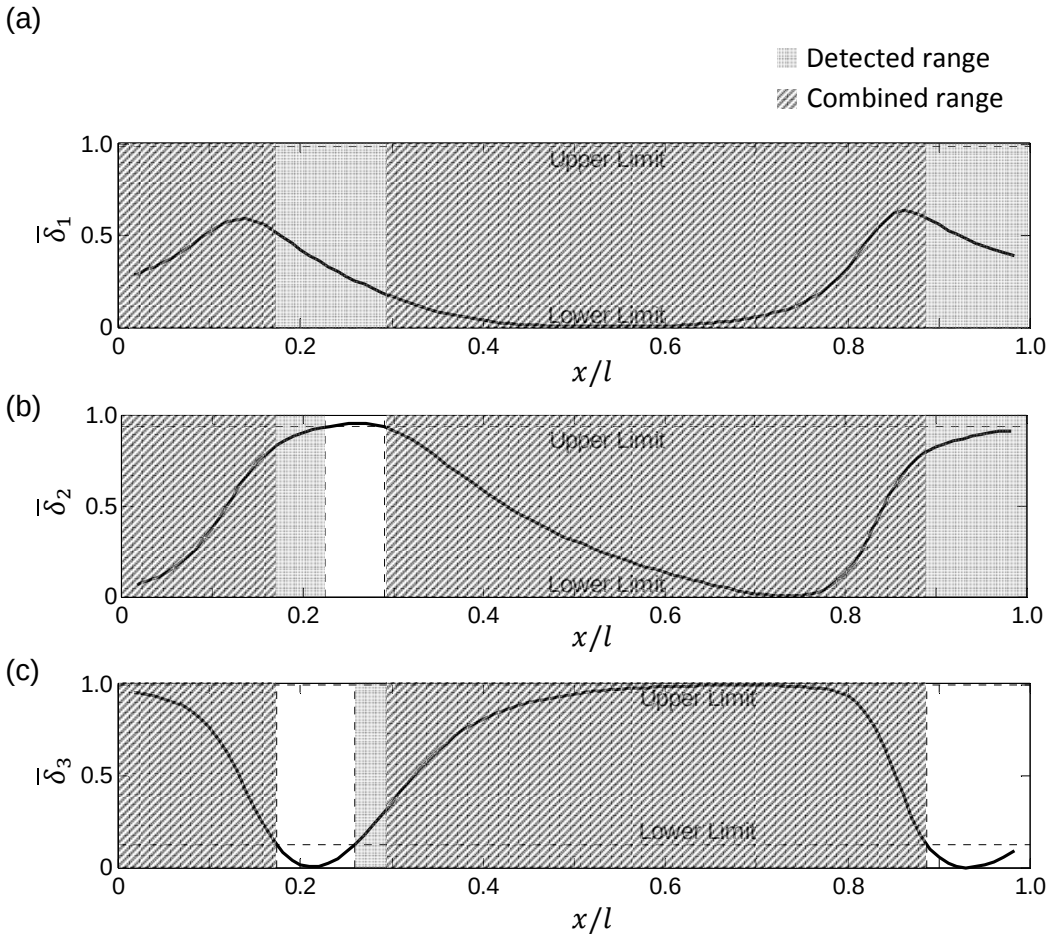

Fig. 5.12. Variation of $\overline{\delta}_i$ with the crack location in Member C (F) and the detected crack location ranges assuming a simulated error of ±0.005 Hz and the actual crack location in Member I (crack case 2), with $d/h = 0.3$. (a) $i = 1$; (b) $i = 2$; (c) $i = 3$.

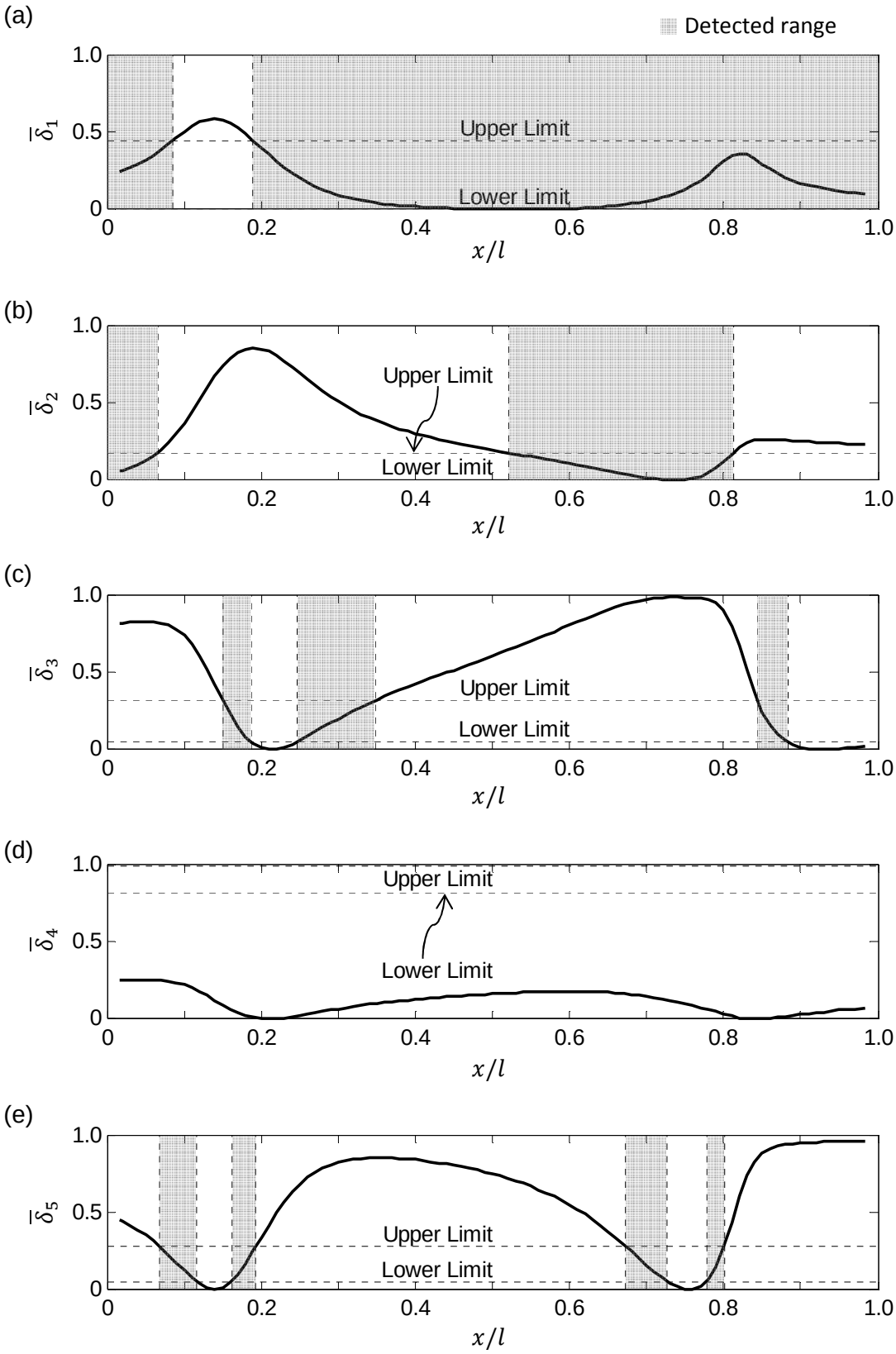

Fig. 5.13. Variation of $\overline{\delta}_i$ with the crack location in Member C (F) and the detected crack location ranges assuming a simulated error of ±0.005 Hz and the actual crack location in Member I (crack case 2), with $d/h = 0.3$. (a) $i = 1$; (b) $i = 2$; (c) $i = 3$; (d) $i = 4$; (e) $i = 5$.

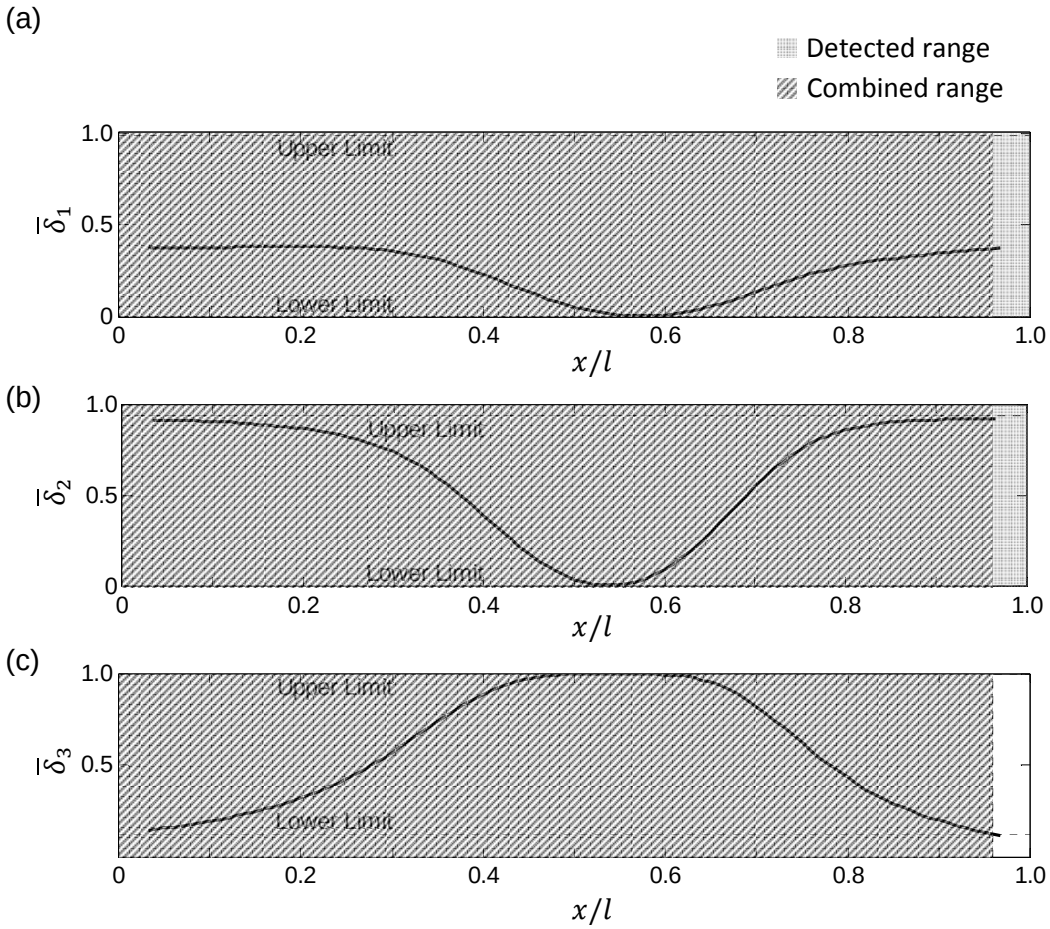

Fig. 5.14. Variation of $\overline{\delta}_i$ with the crack location in Member D and the detected crack location ranges assuming a simulated error of ±0.005 Hz and the actual crack location in Member I (crack case 2), with $d/h = 0.3$. (a) $i = 1$; (b) $i = 2$; (c) $i = 3$.

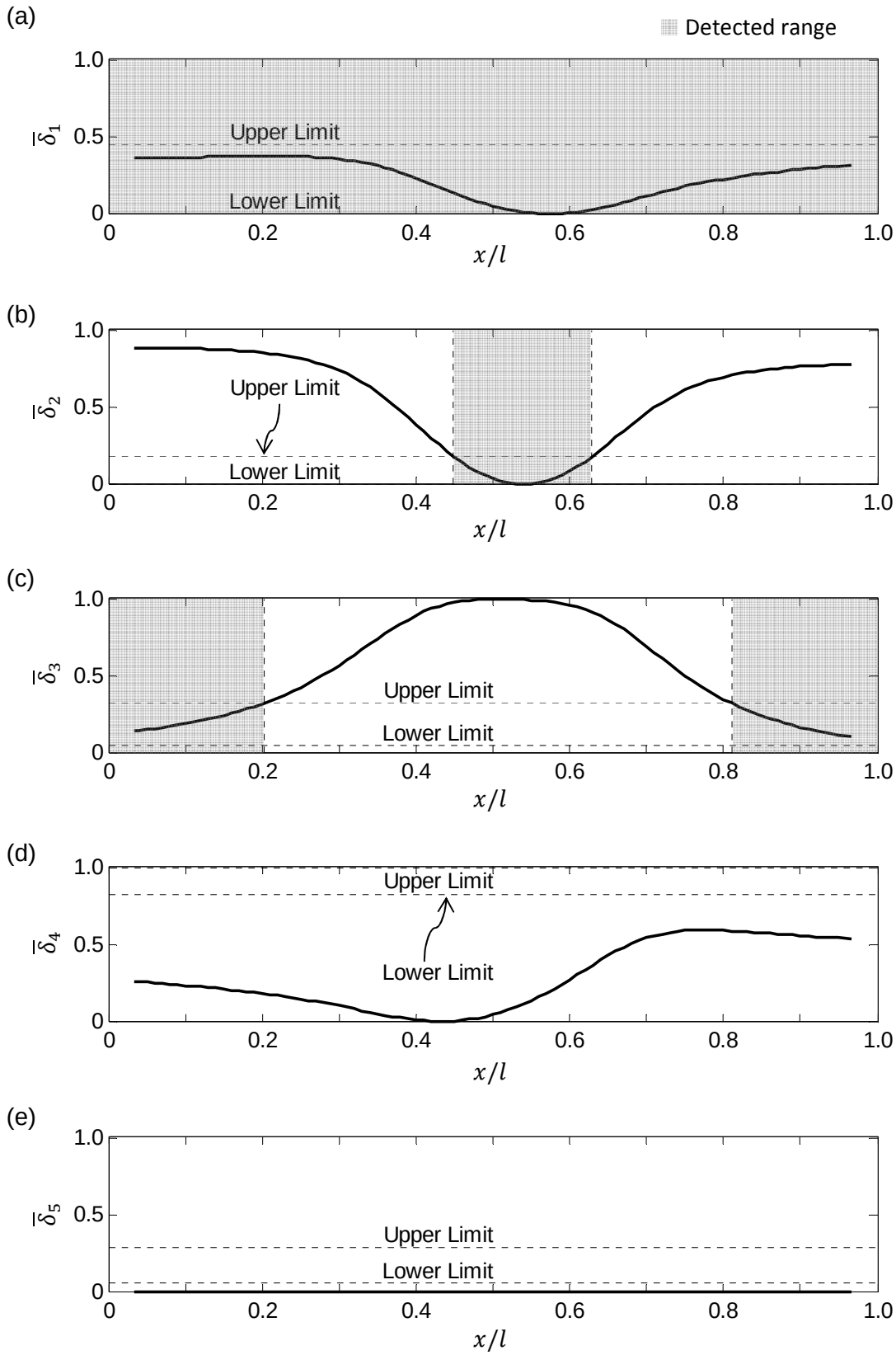

Fig. 5.15. Variation of $\bar{\delta}_i$ with the crack location in Member D and the detected crack location ranges assuming a simulated error of ±0.005 Hz and the actual crack location in Member I (crack case 2), with $d/h = 0.3$. (a) $i = 1$; (b) $i = 2$; (c) $i = 3$; (d) $i = 4$; (e) $i = 5$.

The natural frequencies exhibiting the zero change feature can help in eliminating falsely detected crack location ranges in whole members, before applying any thorough crack detection procedure. However, using the zero change feature has limitations. The frame under consideration must only have a single crack. The example in Section 5.5 shows that the method requires the use of higher order natural frequencies, up the 77th. This is attributed to the relative complexity of the frame. Some frame Members, B (G) and C (F), cannot be associated with a zero change natural frequency within the first one hundred frequencies. All members of the simple frame shown in Fig. 5.16, cannot be associated with a zero change frequency. This frame has the same material properties as that in Section 5.5, but with one column having double the value of Young's modulus of the other members.

Using the higher order natural frequencies may have a fundamental limitation concerned with the rotational spring model employed in the calculations. According to Morassi (2008), in the case of axial vibrations, the linear spring model does not allow accurate calculations of the axial natural frequencies of high order. Studies have yet to be carried out on the accuracy of the rotational spring model in calculating the higher order natural frequencies of frames. Practical application may currently be limited as the ability of measurement devices to pick up natural frequencies, as high as the 77th frequency, is questionable.

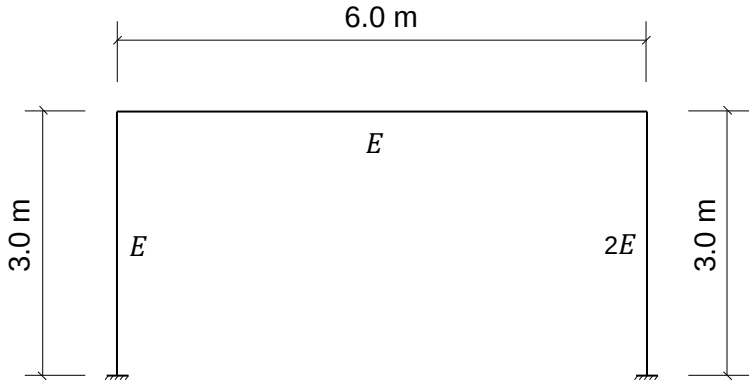

Fig. 5.16. One bay, one storey frame.

5.7. Conclusions

This study presents two methods for enhancing the prediction of single crack locations in frames using natural frequency measurements in the presence of noise. The first method is based on selecting the two natural frequencies having the highest variations within the detected crack location ranges after a first iteration. The method does not require the two natural frequencies to have high simulated variations due to the crack presence. The second method eliminates false ranges in frame members as a whole, making use of the zero change feature unique to some lower and higher order modes.

Chapter 6 – Conclusions and suggestions for future work

6.1. Conclusions

Chapter 2 develops a new method for calculating the natural frequencies of beams and frames with multiple cracks, forming the basis of the crack detection procedures presented in Chapters 3 and 5. The exact dynamic stiffness matrix of the cracked Bernoulli–Euler beam element and the Wittrick–Williams algorithm (Wittrick and Williams 1971) allow the calculation of the natural frequencies in a timely and accurate manner. The calculations must take into account the additional sign counts removed by the partial Gaussian elimination, applied to the original 7 × 7 matrix of the cracked beam element, disregarding the decoupled axial stiffness taken into account later. Otherwise, the orders of the calculated natural frequencies become erroneous and some frequencies can be missed. Lower and higher order natural frequencies of beams and frames with any number of cracks can be easily calculated without re-insertion of additional nodes in the global stiffness matrices. The calculation method does not require finite element meshing. Discretisation of beams into a large number of points is only performed if the calculation of the displacements and rotations for mode shape display is required.

The natural frequency calculation results are in close agreement with those obtained by previous authors utilising the same rotational spring model. The results of some other authors are lower, in the case of beams, due to their implementation of additional shear springs to model the crack. The developed calculation method in this thesis can be easily modified to include axial and shear springs at the crack locations.

The results obtained for the two bay, two storey frame example used throughout the thesis, show that different natural frequencies have different sensitivities to a single crack according to its location in each frame member. Some frequencies may even be insensitive to the crack present anywhere along specific frame members. These sensitivities have been used in devising the crack detection procedures in Chapters 3 and 5.

Chapter 3, the core chapter, presents a new method for single crack detection in frames, using natural frequency measurements. The method, with

great potential for practical application, is based on normalising the variations in natural frequencies between the uncracked and cracked cases. The normalised variations are largely independent of the crack depth to section height ratio, i.e. the crack severity, which can be randomly assumed, as long as the value is ≤ 0.4. At least three natural frequencies must be used. The orders of the natural frequencies are arbitrarily selected, but it is common practice to use the first three. The natural frequency calculation method developed in Chapter 2 is utilised in the detection procedure to calculate the selected natural frequencies in the uncracked case and when the crack is placed at the discretisation points in the frame members to plot the normalised variation curves essential in the detection procedure. The calculation method is also used to simulate the natural frequency measurements corresponding to two crack cases, and hence, the variations.

Noise free and noisy measurements are considered. Noise free measurements yield point crack predictions close to their actual locations. However, obtaining a location prediction is not guaranteed due to the cubic spline interpolation involved and the possibility of any spline shifting very slightly according to the randomly assumed crack severity. Therefore, a spline corresponding to a certain frequency and required to touch or cross zero at the correct location may slightly miss. If the true location is detected, then the crack depth to section height ratio can be recovered as a single value, almost matching the true value. Depending on which simulated natural frequency is used in recovering the severity, the obtained single value differs slightly.

Noisy measurements yield crack location and severity ranges. It has been demonstrated that an error in the order of ± 0.005 Hz can lead to false location ranges being detected, in addition to the true range. The numbers and width of each false range depend on the actual location of the crack and, consequently, the measured or simulated natural frequency variations. Using additional natural frequencies eliminates some of these false ranges. The severity ranges can also be useful in eliminating some of the false ranges. Illustrations have been plotted, showing that as the actual crack severity increases, the upper and lower limits of the normalised simulated frequency variations converge towards the exact (noise free) variations. However, as the

crack depth to section height ratio exceeds 0.4, the exact normalised variations become dependent on the crack severity, rendering the detection procedure unreliable for high severities, although, in some crack cases, this value can be exceeded while causing negligible difference in the exact normalised variations. In any case, the applicability of the rotational spring model is restricted to small crack depth to section height ratios ≤ 0.4. Referring to the previous paragraph, regarding the unguaranteed possibility of obtaining a point location prediction, it can be argued that having a small amount of measurement noise, leading to an upper and lower limit around the actual crack location, is better than pure noise free measurements.

Empirical probability distributions can be plotted for each location range. These can be used in practice to set up an in situ visual inspection procedure in which the inspection areas are prioritised according to the relative probabilities of each detected range. The detection procedure is efficient when the measurement noise is relatively lower than the variations in at least one of the utilised natural frequencies. For frames with inclined members, the loss of axial stiffness through the crack should be taken into account.

The experimental work described in Chapter 4 validates the devised method for single crack detection in frames. The third to sixth natural frequencies of a two bay, two storey frame with scaled down dimensions, were measured using the fast Fourier transform (FFT). A single crack, with depth to section height ratio as low as 0.2, was successfully detected, in terms of both location and severity.

Two enhancement techniques for single crack detection in frames are described in Chapter 5, with the purpose of eliminating some of the falsely detected crack location ranges. One technique considers the use of the first three natural frequencies as a first iteration of the detection procedure established in Chapter 3. It then requires the selection of two additional natural frequencies out of a group of higher order ones. A search is made within the detected crack location ranges from the first iteration, for the two natural frequencies having the highest variations among that group of frequencies. The two additional frequencies, together with the first three, are used in a second iteration of the crack detection procedure. The high variations do not have to be

exhibited in the simulated (or measured) variations. Some false ranges will be eliminated, nevertheless, due to the manner in which the high variations of the two additional frequencies affect the normalised variation curves within the false crack location ranges.

The second technique serves to exclude some frame members from any crack identification procedure, by making use of the zero change feature exhibited in some of the low and higher order natural frequencies. These frequencies are insensitive to single cracks present anywhere along specific frame members. If the lower limit of the simulated (or measured) variations in any frequency exhibiting the zero change feature is significantly high, then the corresponding frame member can be marked as uncracked, as long as the frame contains only a single crack. Thus, any falsely detected crack location range within that member becomes irrelevant and the member can even be excluded from any identification procedure.

Some limitations regarding the second enhancement technique should be highlighted. Identifying the natural frequencies exhibiting the zero change feature involves carrying out low and high order frequency calculations, and hence the variations, while varying the crack location along whole member lengths. The rotational spring model used in these calculations may not be applicable in case of higher order natural frequencies due to the loss of accuracy (Morassi 1993, 2008). It can be argued that as only frequency variations are of interest, and, more specifically, zero variations, then any inaccuracy is irrelevant. Another limitation is that the measuring device may not be able to pick up natural frequencies of very high order.

6.2. Suggestions for future work

Single crack detection in frames has been tackled in this thesis. Normalising the variations in the utilised natural frequencies, due to the crack presence, facilitates locating the crack as the normalised variations do not depend on the crack severity, except when the crack is severe. With the help of the curve fitting toolbox in MATLAB, the crack locations can be pinpointed in case of noise free simulations, or evaluated as ranges when the noise is introduced. The crack severity is then evaluated by a simple modification in the

Wittrick–Williams algorithm (Wittrick and Williams 1971). However, in the presence of multiple cracks, the normalisation does not eliminate the dependency on any of the unknown crack severities. This can be explained by referring to the following equation describing the frequency variations in the case of two cracks:

$$\delta_i = \tilde{s}_1 . f_{1i}(x_1/l) + \tilde{s}_2 . f_{2i}(x_2/l), \tag{6.1}$$

which, when normalised, take the form:

$$\overline{\delta}_i = \frac{\delta_i}{\sqrt{\sum_i \delta_i^2}} = \frac{\tilde{s}_1 . f_{1i}(x_1/l) + \tilde{s}_2 . f_{2i}(x_2/l)}{\sqrt{\sum_i \left(\tilde{s}_1 . f_{1i}(x_1/l) + \tilde{s}_2 . f_{2i}(x_2/l)\right)^2}}. \tag{6.2}$$

Eqs. (6.1) and (6.2) are expanded versions of Eqs. (3.2) and (3.3), respectively. It can be seen that Eq. (6.2) offers no benefit, except when the cracks have equal severities. It can be seen from Eq. (6.1) that there are four unknowns, two crack severities and two locations, requiring four natural frequencies to be solved. The crack location functions f_1 and f_2 can be interpolated, but to a high degree polynomial. Efficient solution techniques are yet to be established for this system of equations, to produce rational results. This will save the need for resorting to mode shape measurements, which may be highly inaccurate or even impossible to obtain, especially in large structures. An important area to be explored is the manner in which the natural frequencies degrade when multiple cracks are present in the frame, whether it is linearly accumulative, or otherwise. Some of the published studies in the literature, concerned with multiple crack detection, can be used as background information (Hu and Liang 1993; Patil and Maiti 2003; Lee 2009; Ghadami et al. 2013; Maghsoodi et al. 2013; Caddemi and Caliò 2014; Khiem and Tran 2014; Nandakumar and Shankar 2014; Rubio et al. 2014). The detection of diffused damage while using the concentrated damage model is yet to be studied.

Another aspect, needing further studies, is obtaining the probability distributions for the detected crack location ranges, from those of the normalised frequency variations. Rather than the empirical method described in this thesis and applied directly on the locations ranges, attempts have been made by the author to accurately calculate the required probability distributions,

starting with those of the natural frequency variations (unnormalised). The methods described by Meyer (1965) for obtaining the probability distributions corresponding to functions of random variables were used. However, these methods to obtain the probability distributions for the normalised variations, given by Eq. (3.3), were inapplicable for hand calculations or MATLAB programming. Other attempts have been made at using the software package MAPLE (Maplesoft 2013). However, the package was left running for more than twelve hours. It was apparent that it gets stuck when the denominator containing a summation inside a square root was inputted.

The most important aspect needing further studies, is the accuracy of the rotational spring model in describing the behaviour of the crack, especially in higher order vibration modes. The applicability of nonlinear crack models for the devised crack detection method in this thesis, is yet to be studied. These models, for example, the bilinear crack model (Shen and Chu 1992; Chati et al. 1997), take into account the opening and closing of the crack during vibration. Other aspects are the technological limitations of the current measuring devices to pick up higher order natural frequencies.

6.3. Inspired research

Research into crack detection in frames is currently being carried out by the PhD student Julian DeLosRios in the University of Waikato, Hamilton, New Zealand. An alternate detection method, inspired by the published part of this thesis (Labib et al. 2014, 2015), is currently being explored. The method is based on the determinant of the dynamic stiffness matrix. The following equation applies at any frequency of vibration ω:

$$\tilde{s}.\det.\{\mathbf{K}(\tilde{s},x,\omega)\} = \det.\{\mathbf{K}(\omega)\} + \tilde{s}.\det.\{\mathbf{K}(x,\omega)\}, \tag{6.3}$$

where $\tilde{s}$ is a function of the crack severity, x is the crack location, $\mathbf{K}(\tilde{s},x,\omega)$ is the dynamic stiffness matrix of the cracked frame, $\mathbf{K}(\omega)$ is the dynamic stiffness matrix of the uncracked frame, i.e. $\tilde{s} = 0.0$, and $\mathbf{K}(x,\omega)$ is the dynamic stiffness matrix when the crack depth covers the whole cross-section thickness, i.e. $\tilde{s} = \infty$. At any natural frequency ω_i, $\det.\{\mathbf{K}(\tilde{s},x,\omega_i)\} = 0.0$. Using two natural frequencies, $\tilde{s}$ can be easily eliminated. The crack location x is then calculated. The method is currently being extended to multiple crack detection.

The effect of temperature changes on crack detection is also being explored. Referring to Fig. 6.1, an increase in temperature causes axial compression in the constrained member. The relation between the natural frequencies and the axial load is given by the equation (Galef 1968):

$$\frac{P}{P_o} + \frac{\omega_{i\mathrm{a}}^2}{\omega_{i\mathrm{u}}^2} = 1, \tag{6.4}$$

where P_o is the critical buckling load, $\omega_{i\mathrm{a}}$ is the natural frequency of the axially loaded member, and $\omega_{i\mathrm{u}}$ is the natural frequency of the unloaded member.

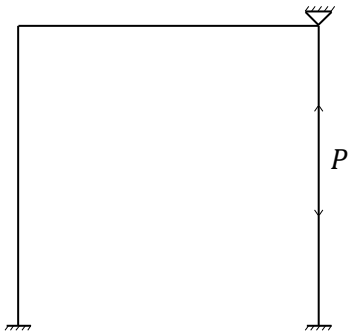

Fig. 6.1. Frame with axially constrained member undergoing an increase in temperature.

The frequency variations due to the axial load can thus be written in the form:

$$\delta_i = 1 - \frac{\omega_{i\mathrm{a}}}{\omega_{i\mathrm{u}}} = 1 - \sqrt{1 - \frac{P}{P_o}}. \tag{6.5}$$

The relation between the frequency variations δ_i and the temperature change ΔT takes the form:

$$\delta_i = \emptyset_i \, \Delta T, \tag{6.6}$$

where $\emptyset$ is a constant. The combined problem in which the natural frequency variations are due to a series of cracks and also due to temperature change, can be described by the equation:

$$\delta_i^t = \emptyset_i \, \Delta T + \sum_c \tilde{s}_c \delta_i(x_c), \tag{6.7}$$

where c is the crack number. The solution requires a multi-dimensional search for $\tilde{s}_c$, x_c and ΔT.

Appendix – MATLAB codes

- MATLAB function file for performing Gaussian elimination without row interchange:

```
function [ge] = genre(x) %Code to be stored in a file named
'genre.m'
for i=1:(length(x)-1);
    for j=(i+1):length(x);
        x(j,:)=x(j,:)-((x(j,i)/x(i,i))*x(i,:));
    end;
end;
ge=x;
```

- MATLAB function file for applying the Wittrick–Williams algorithm considering no loss of axial stiffness:

```
function [WTWLfDKAG] = WWfDKAG(w, nodes, sup, conn, angle, L,...
                                E, A, I, m, ks, mem, fe)
%Code to be stored in a file named 'WWfDKAG.m'.
%'w' is the trial frequency in rad s^-1.
%'nodes' is the total number of nodes in the frame.
%'sup' is a vector of the suppressed degrees of freedom at the
nodes. The input numbers 1, 4, 7,... correspond to suppressed
displacements in the global horizontal direction for nodes 1, 2,
3,.... The vertically supressed displacements take the numbers 2,
5, 8,..., while the suppressed rotations take the numbers 3, 6,
9,...
%'conn' is a matrix of the two nodes connecting each member,
ignoring the cracks.
%'angle' is a vector of the angle of each member, measured from a
horizontal axis, counter clock-wise positive. The longitudinal
axis of any individual member starts from the first defined node
to the second one, regardless of the global node numbering.
%'L' is a matrix of the length of each uncracked portion of every
member.
%'E', 'A', 'I', 'm' are vectors of Young's modulus, cross-
sectional area, second moment of area, and mass per unit length
of each member.
%'ks' is the stiffness of the rotational springs in each cracked
member.
%'mem' is a vector of the number of uncracked portions of each
member.
%'fe' is the total number of frame members, ignoring the cracks.
Jm=0; ng=0; Jc=0; %Initial values for the terms of the Wittrick–
Williams algorithm, where 'Jm' is the number of fixed end natural
frequencies below the trial frequency 'w', 'ng' is the number of
negative leading diagonal elements of the upper triangular matrix
formed from the global stiffness matrix after performing Gaussian
elimination without row interchange, 'Jc' is the additional sign
count due to the partial Gaussian elimination performed as result
of the crack presence to reduce the order of the stiffness
matrix.
DFGstiff=zeros(3*nodes,3*nodes); %Global dynamic stiffness matrix
of the frame
DFstiff=zeros(6,6);  %Dynamic  stiffness  matrix  of  individual
members
for f=1:fe
```

```
estiff=zeros(4*mem(f),4*mem(f)); %Dynamic stiffness matrix of
individual members in local coordinates, ignoring the decoupled
axial stiffness
mu=w*(sum(L(f,:)))*((m(f,1)/(E(f,1)*A(f,1)))^0.5);     %Frequency
function related to the axial stiffness of the whole member
Jm=Jm+int16(fix(mu/pi));
ax=E(f,1)*A(f,1)*mu*cot(mu)/sum(L(f,:));
ax2=-E(f,1)*A(f,1)*mu*csc(mu)/sum(L(f,:)); % 'ax' and 'ax2' are
the dynamic stiffness matrix terms related to the axial stiffness
DFstiff(1:2,1:2)=[ax ax2;ax2 ax];
for i=1:mem(f)
    lambda=L(f,i)*((m(f,1)*(w^2)/(E(f,1)*I(f,1)))^0.25);
%Frequency function related to the bending stiffness of
individual uncracked member portions
    Jm=Jm+int16(fix(lambda/pi))-(0.5*(1-...
        (((-1)^int16(fix(lambda/pi)))*...
        sign(1-cos(lambda)*cosh(lambda)))));
    a=lambda*((cosh(lambda)*sin(lambda))-...
        (sinh(lambda)*cos(lambda)))/...
        (1-(cosh(lambda)*cos(lambda)));
    b=lambda*(sinh(lambda)-sin(lambda))/...
        (1-(cosh(lambda)*cos(lambda)));
    n=(lambda^2)*sinh(lambda)*sin(lambda)/...
        (1-(cosh(lambda)*cos(lambda)));
    d=(lambda^2)*(cosh(lambda)-cos(lambda))/...
        (1-(cosh(lambda)*cos(lambda)));
    g=(lambda^3)*((cosh(lambda)*sin(lambda))+...
        (sinh(lambda)*cos(lambda)))/...
        (1-(cosh(lambda)*cos(lambda)));
    ep=(lambda^3)*(sinh(lambda)+sin(lambda))/...
        (1-(cosh(lambda)*cos(lambda)));
    %Dynamic stiffness matrix for uncracked member portions
    estiff(((4*i)-3):(4*i),((4*i)-3):(4*i))= E(f,1)*I(f,1)*...
        [g/(L(f,i)^3) n/(L(f,i)^2) -ep/(L(f,i)^3) d/(L(f,i)^2);
           n/(L(f,i)^2) a/L(f,i) -d/(L(f,i)^2) b/L(f,i);
         -ep/(L(f,i)^3) -d/(L(f,i)^2) g/(L(f,i)^3) -n/(L(f,i)^2);
           d/(L(f,i)^2) b/L(f,i) -n/(L(f,i)^2) a/L(f,i)];
end;
if mem(f)>1
for i=1:(mem(f)-1) % If the member is cracked
    fs=1/ks(f,i);   %Flexibility   of   the   rotational   spring
corresponding to the crack
    %Delta variables
    Delta1=1/(1+(estiff((4*i),(4*i))*fs));
    Delta2=1/(estiff((4*(i+1))-2,(4*(i+1))-2)+...
        (estiff((4*i),(4*i))*Delta1));
    q1=Delta1*(fs+(Delta1*Delta2));
    Delta3=1/(estiff((4*i)-1,(4*i)-1)+...
        estiff((4*(i+1))-3,(4*(i+1))-3)-...
        (((-estiff((4*i)-1,4*i))^2)*q1)-...
        (((estiff((4*(i+1))-3,(4*(i+1))-2))^2)*Delta2)+...
        (2*(-estiff((4*i)-1,4*i))*...
        (estiff((4*(i+1))-3,(4*(i+1))-2))*Delta1*Delta2));
    %Additional   sign   counts   due   to   the   partial   Gaussian
elimination
    if Delta1<0
        Jc=Jc+1;
    end;
    if Delta2<0
        Jc=Jc+1;
    end;
```

```
    if Delta3<0
        Jc=Jc+1;
    end;
    %Calculation of the dynamic stiffness matrix for the cracked
member in the local coordinates
    q2=(-estiff((4*i)-1,4*i)*q1)-(estiff((4*(i+1))-3,...
        (4*(i+1))-2)*Delta1*Delta2);
    q3=Delta2*(estiff((4*(i+1))-3,(4*(i+1))-2)-...
        (-estiff((4*i)-1,4*i)*Delta1));
    p1=estiff((4*i)-3,(4*i)-1)+(estiff((4*i)-3,4*i)*q2);
    p2=estiff((4*i)-2,(4*i)-1)+(estiff((4*i)-2,4*i)*q2);
    p3=estiff((4*(i+1))-3,(4*(i+1))-1)+...
        (-estiff((4*(i+1))-2,(4*(i+1))-1)*q3);
    p4=estiff((4*(i+1))-3,(4*(i+1)))-...
        (estiff((4*(i+1))-2,(4*(i+1)))*q3);
    am=(estiff((4*i)-3,(4*i)-3)-...
        ((estiff((4*i)-3,(4*i))^2)*q1)-((p1^2)*Delta3));
    bm=(estiff((4*i)-3,(4*i)-2)-(estiff((4*i)-3,(4*i))*...
        estiff((4*i)-2,(4*i))*q1)-(p1*p2*Delta3));
    dm=(-estiff((4*i)-3,(4*i))*...
        (-estiff((4*(i+1))-2,(4*(i+1))-1))*...
        Delta1*Delta2)+(p1*p3*Delta3);
    em=(-estiff((4*i)-3,(4*i))*...
        estiff((4*(i+1))-2,(4*(i+1)))*...
        Delta1*Delta2)-(p1*p4*Delta3);
    cm=(estiff((4*i)-2,(4*i)-2)-...
        ((estiff((4*i)-2,4*i)^2)*q1)-((p2^2)*Delta3));
    epsm=(-estiff((4*i)-2,(4*i))*...
        (-estiff((4*(i+1))-2,(4*(i+1))-1))*...
        Delta1*Delta2)+(p2*p3*Delta3);
    fm=(-estiff((4*i)-2,(4*i))*...
        estiff((4*(i+1))-2,(4*(i+1)))*...
        Delta1*Delta2)-(p2*p4*Delta3);
    alpham=(estiff((4*(i+1))-1,(4*(i+1))-1))-...
        (((-estiff((4*(i+1))-2,(4*(i+1))-1))^2)*...
        Delta2)-((p3^2)*Delta3);
    betam=(-estiff((4*(i+1))-1,(4*(i+1)))-...
        (-estiff((4*(i+1))-2,(4*(i+1))-1)*...
        estiff((4*(i+1))-2,(4*(i+1)))*Delta2)+(p3*p4*Delta3));
    gammam=(estiff(4*(i+1),4*(i+1))-...
        ((estiff((4*(i+1))-2,4*(i+1))^2)*Delta2)-...
        ((p4^2)*Delta3));
    Dstiff=[am bm -dm em; bm cm -epsm fm;
        -dm -epsm alpham -betam;
        em fm -betam gammam];
    estiff(((4*(i+1))-3):(4*(i+1)),...
        ((4*(i+1))-3):(4*(i+1)))=Dstiff;
end;
DFstiff(3:6,3:6)=Dstiff;
else
DFstiff(3:6,3:6)=estiff; %If the member is uncracked
end;
%Regular form of the dynamic stiffness matrix in local
coordinates
DFstiff=[DFstiff(1,1) 0 0 DFstiff(1,2) 0 0;
         0 DFstiff(3,3) DFstiff(3,4) 0 DFstiff(3,5) DFstiff(3,6);
         0 DFstiff(4,3) DFstiff(4,4) 0 DFstiff(4,5) DFstiff(4,6);
         DFstiff(2,1) 0 0 DFstiff(2,2) 0 0;
         0 DFstiff(5,3) DFstiff(5,4) 0 DFstiff(5,5) DFstiff(5,6);
         0    DFstiff(6,3)    DFstiff(6,4)    0    DFstiff(6,5)
DFstiff(6,6)];
```

```
%Transformation into global coordinates
t=[cos(angle(f)) sin(angle(f)) 0; -sin(angle(f)) cos(angle(f)) 0;
    0 0 1]; T=[t zeros(3,3);zeros(3,3) t];
DFstiff=T'*DFstiff*T;
%Assembling the global dynamic stiffness matrix of the frame
n1=conn(f,1); n2=conn(f,2);
DFGstiff(((3*n1)-2):(3*n1),((3*n1)-2):(3*n1))=...
    DFGstiff(((3*n1)-2):(3*n1),((3*n1)-2):(3*n1))+...
    DFstiff(1:3,1:3);
DFGstiff(((3*n1)-2):(3*n1),((3*n2)-2):(3*n2))=...
    DFGstiff(((3*n1)-2):(3*n1),((3*n2)-2):(3*n2))+...
    DFstiff(1:3,4:6);
DFGstiff(((3*n2)-2):(3*n2),((3*n1)-2):(3*n1))=...
    DFGstiff(((3*n2)-2):(3*n2),((3*n1)-2):(3*n1))+...
    DFstiff(4:6,1:3);
DFGstiff(((3*n2)-2):(3*n2),((3*n2)-2):(3*n2))=...
    DFGstiff(((3*n2)-2):(3*n2),((3*n2)-2):(3*n2))+...
    DFstiff(4:6,4:6);
end;
if isempty(sup) %In the case of no supports or restraints for the
whole frame
DFGstiff=genre(DFGstiff); %Perform Gaussian elimination using the
function file 'genre.m'
diagonal=diag(DFGstiff);
for i=1:length(diagonal);
    if diagonal(i)<0
        ng=ng+1; %Sign counts of the diagonal terms
    end;
end;
WTWLfDKAG=ng+Jm+Jc; %Summation of terms of the Wittrick-Williams
algorithm
else
DFGstiff([sup],:)=[]; DFGstiff(:,[sup])=[];  %Delete the rows and
columns in the stiffness matrix, corresponding to the suppressed
degrees of freedom
DFGstiff=genre(DFGstiff); diagonal=diag(DFGstiff);
for i=1:length(diagonal);
    if diagonal(i)<0
        ng=ng+1;
    end;
end;
WTWLfDKAG=ng+Jm+Jc;
end;
end
```

- MATLAB function file for calculating the mode shapes:

```
function [WTWLfDKAGModeshapes] = WWfDKAGModeshapes(w, nodes,...
    sup, conn, angle, L, E, A, I, m, ks, mem, fe)
%Code to be stored in a file named 'WWfDKAGModeshapes.m'
%This code is similar to the previous, except there are no sign
counts and the input frequency 'w' should correspond to a
calculated natural frequency of the considered frame. All the
other input data should correspond to the same frame, but divided
into a large number of points for a smooth output plot of the
mode shape.
DFGstiff=zeros(3*nodes,3*nodes);
DFstiff=zeros(6,6);
for f=1:fe
estiff=zeros(4*mem(f),4*mem(f));
```

```
mu=w*(sum(L(f,:)))*((m(f,1)/(E(f,1)*A(f,1)))^0.5);
ax=E(f,1)*A(f,1)*mu*cot(mu)/sum(L(f,:));
ax2=-E(f,1)*A(f,1)*mu*csc(mu)/sum(L(f,:));
DFstiff(1:2,1:2)=[ax ax2;ax2 ax];
for i=1:mem(f)
    lambda=L(f,i)*((m(f,1)*(w^2)/(E(f,1)*I(f,1)))^0.25);
    a=lambda*((cosh(lambda)*sin(lambda))-...
        (sinh(lambda)*cos(lambda)))/...
        (1-(cosh(lambda)*cos(lambda)));
    b=lambda*(sinh(lambda)-sin(lambda))/...
        (1-(cosh(lambda)*cos(lambda)));
    n=(lambda^2)*sinh(lambda)*sin(lambda)/...
        (1-(cosh(lambda)*cos(lambda)));
    d=(lambda^2)*(cosh(lambda)-cos(lambda))/...
        (1-(cosh(lambda)*cos(lambda)));
    g=(lambda^3)*((cosh(lambda)*sin(lambda))+...
        (sinh(lambda)*cos(lambda)))/...
        (1-(cosh(lambda)*cos(lambda)));
    ep=(lambda^3)*(sinh(lambda)+sin(lambda))/...
        (1-(cosh(lambda)*cos(lambda)));
    estiff(((4*i)-3):(4*i),((4*i)-3):(4*i))= E(f,1)*I(f,1)*...
        [g/(L(f,i)^3) n/(L(f,i)^2) -ep/(L(f,i)^3) d/(L(f,i)^2);
         n/(L(f,i)^2) a/L(f,i) -d/(L(f,i)^2) b/L(f,i);
        -ep/(L(f,i)^3) -d/(L(f,i)^2) g/(L(f,i)^3) -n/(L(f,i)^2);
         d/(L(f,i)^2) b/L(f,i) -n/(L(f,i)^2) a/L(f,i)];
end;
if mem(f)>1
for i=1:(mem(f)-1)
    fs=1/ks(f,i);
    Delta1=1/(1+(estiff((4*i),(4*i))*fs));
    Delta2=1/(estiff((4*(i+1))-2,(4*(i+1))-2)+...
        (estiff((4*i),(4*i))*Delta1));
    q1=Delta1*(fs+(Delta1*Delta2));
    Delta3=1/(estiff((4*i)-1,(4*i)-1)+...
        estiff((4*(i+1))-3,(4*(i+1))-3)-...
        (((-estiff((4*i)-1,4*i))^2)*q1)-...
        (((estiff((4*(i+1))-3,(4*(i+1))-2))^2)*Delta2)+...
        (2*(-estiff((4*i)-1,4*i))*...
        (estiff((4*(i+1))-3,(4*(i+1))-2))*Delta1*Delta2));
    q2=(-estiff((4*i)-1,4*i)*q1)-...
        (estiff((4*(i+1))-3,(4*(i+1))-2)*Delta1*Delta2);
    q3=Delta2*(estiff((4*(i+1))-3,(4*(i+1))-2)-...
        (-estiff((4*i)-1,4*i)*Delta1));
    p1=estiff((4*i)-3,(4*i)-1)+(estiff((4*i)-3,4*i)*q2);
    p2=estiff((4*i)-2,(4*i)-1)+(estiff((4*i)-2,4*i)*q2);
    p3=estiff((4*(i+1))-3,(4*(i+1))-1)+...
        (-estiff((4*(i+1))-2,(4*(i+1))-1)*q3);
    p4=estiff((4*(i+1))-3,(4*(i+1)))-...
        (estiff((4*(i+1))-2,(4*(i+1)))*q3);
    am=(estiff((4*i)-3,(4*i)-3)-...
        ((estiff((4*i)-3,(4*i))^2)*q1)-((p1^2)*Delta3));
    bm=(estiff((4*i)-3,(4*i)-2)-(estiff((4*i)-3,(4*i))*...
        estiff((4*i)-2,(4*i))*q1)-(p1*p2*Delta3));
    dm=(-estiff((4*i)-3,(4*i))*...
        (-estiff((4*(i+1))-2,(4*(i+1))-1))*...
        Delta1*Delta2)+(p1*p3*Delta3);
    em=(-estiff((4*i)-3,(4*i))*...
        estiff((4*(i+1))-2,(4*(i+1)))*...
        Delta1*Delta2)-(p1*p4*Delta3);
    cm=(estiff((4*i)-2,(4*i)-2)-...
        ((estiff((4*i)-2,4*i)^2)*q1)-((p2^2)*Delta3));
```

```
    epsm=(-estiff((4*i)-2,(4*i))*...
        (-estiff((4*(i+1))-2,(4*(i+1))-1))*...
        Delta1*Delta2)+(p2*p3*Delta3);
    fm=(-estiff((4*i)-2,(4*i))*...
        estiff((4*(i+1))-2,(4*(i+1)))*...
        Delta1*Delta2)-(p2*p4*Delta3);
    alpham=(estiff((4*(i+1))-1,(4*(i+1))-1))-...
        (((-estiff((4*(i+1))-2,(4*(i+1))-1))^2)*...
        Delta2)-((p3^2)*Delta3);
    betam=(-estiff((4*(i+1))-1,(4*(i+1)))-...
        (-estiff((4*(i+1))-2,(4*(i+1))-1)*...
        estiff((4*(i+1))-2,(4*(i+1)))*Delta2)+(p3*p4*Delta3));
    gammam=(estiff(4*(i+1),4*(i+1))-...
        ((estiff((4*(i+1))-2,4*(i+1))^2)*Delta2)-...
        ((p4^2)*Delta3));
    Dstiff=[am bm -dm em; bm cm -epsm fm;
        -dm -epsm alpham -betam; em fm -betam gammam];
    estiff(((4*(i+1))-3):(4*(i+1)),...
        ((4*(i+1))-3):(4*(i+1)))=Dstiff;
end;
DFstiff(3:6,3:6)=Dstiff;
else
DFstiff(3:6,3:6)=estiff;
end;
DFstiff=[DFstiff(1,1) 0 0 DFstiff(1,2) 0 0;
     0 DFstiff(3,3) DFstiff(3,4) 0 DFstiff(3,5) DFstiff(3,6);
     0 DFstiff(4,3) DFstiff(4,4) 0 DFstiff(4,5) DFstiff(4,6);
     DFstiff(2,1) 0 0 DFstiff(2,2) 0 0;
     0 DFstiff(5,3) DFstiff(5,4) 0 DFstiff(5,5) DFstiff(5,6);
     0 DFstiff(6,3) DFstiff(6,4) 0 DFstiff(6,5) DFstiff(6,6)];
t=[cos(angle(f)) sin(angle(f)) 0; -sin(angle(f)) cos(angle(f)) 0;
    0 0 1]; T=[t zeros(3,3);zeros(3,3) t];
DFstiff=T'*DFstiff*T;
n1=conn(f,1); n2=conn(f,2);
DFGstiff(((3*n1)-2):(3*n1),((3*n1)-2):(3*n1))=...
    DFGstiff(((3*n1)-2):(3*n1),((3*n1)-2):(3*n1))+...
    DFstiff(1:3,1:3);
DFGstiff(((3*n1)-2):(3*n1),((3*n2)-2):(3*n2))=...
    DFGstiff(((3*n1)-2):(3*n1),((3*n2)-2):(3*n2))+...
    DFstiff(1:3,4:6);
DFGstiff(((3*n2)-2):(3*n2),((3*n1)-2):(3*n1))=...
    DFGstiff(((3*n2)-2):(3*n2),((3*n1)-2):(3*n1))+...
    DFstiff(4:6,1:3);
DFGstiff(((3*n2)-2):(3*n2),((3*n2)-2):(3*n2))=...
    DFGstiff(((3*n2)-2):(3*n2),((3*n2)-2):(3*n2))+...
    DFstiff(4:6,4:6);
end;
if isempty(sup)  %In the case of no supports or restraints for
the whole frame
dis(1:((3*nodes)-length(sup)-1))=...
    (inv(DFGstiff(1:((3*nodes)-length(sup)-1),...
    1:((3*nodes)-length(sup)-1))))*...
    DFGstiff(1:((3*nodes)-length(sup)-1),...
    ((3*nodes)-length(sup)));
dis(((3*nodes)-length(sup)))=-1; %The highest numbered degree of
freedom is assumed to have a unit displacement (or rotation)
WTWLfDKAGModeshapes=dis;
else
DFGstiff([sup],:)=[]; DFGstiff(:,[sup])=[];
dis(1:((3*nodes)-length(sup)-1))=...
    (inv(DFGstiff(1:((3*nodes)-length(sup)-1),...
```

```
    1:((3*nodes)-length(sup)-1))))*...
    DFGstiff(1:((3*nodes)-length(sup)-1),...
    ((3*nodes)-length(sup)));
dis(((3*nodes)-length(sup)))=-1;
WTWLfDKAGModeshapes=dis;
end;
end
```

- MATLAB function file for calculating the ranges of the normalised natural frequency variations:

```
function[NormalisedFreq]=interval(reqnfreq,freqs,merror)
% 'reqnfreq' is the index of the natural frequency for which the
normalised variation is required, 'freq' are the simulated or
measured natural frequency inputs, 'merror' is the measurement
error in each frequency
LLUL=[freqs'-merror freqs'+merror];
  for i=1:((length(LLUL(:,1)))/2)
      if (1-(LLUL(2*i,2)/LLUL(((2*i)-1),1))) >= 0
          %Delta Squared
          dsq(i,:)=[(1-(LLUL(2*i,2)/LLUL(((2*i)-1),1)))^2 ...
              (1-(LLUL(2*i,1)/LLUL(((2*i)-1),2)))^2];
      else
          dsq(i,:)=[0  (1-(LLUL(2*i,1)/LLUL(((2*i)-1),2)))^2];
      end;
  end;
sumsqu=[(sum(dsq(1:((length(LLUL(:,1)))/2),1))-...
    dsq(reqnfreq,1))/dsq(reqnfreq,2)...
    (sum(dsq(1:((length(LLUL(:,1)))/2),2))-...
    dsq(reqnfreq,2))/dsq(reqnfreq,1)];...
    %sum(di^2/(d^2 of the required normalised freq.))
NormalisedFreq=[(1+sumsqu(2))^-0.5  (1+sumsqu(1))^-0.5];
End
```

- MATLAB code for calculating the natural frequencies and mode shapes:

```
clear; clear all; format long;
fe=10;   %Number of frame elements
Ec=206e9; %Young's modulus in N m-2
Ic=0.198*((0.122)^3)/12; %Second moment of area in m4
mc=185.3973; %Mass per unit length in Kg m-1
Ac=0.198*0.122; %Cross-sectional area in m2
h=0.122; %Cross-sectional height in m
E(1:fe,1)=Ec; A(1:fe,1)=Ac; I(1:fe,1)=Ic; m(1:fe,1)=mc; %Vectors
of properties for each and every frame member
conn=[1 2; 2 3; 3 4; 4 5; 5 6; 4 7; 7 8; 8 9; 2 5; 5 8];
nodes=9; angle=[pi/2 pi/2 0 -pi/2 -pi/2 0 -pi/2 -pi/2 0 0];
sup=[1 2 3 16 17 18 25 26 27]; %Nodes 1, 6, and 9 are clamped
mem=[1 1 1 1 1 1 1 1 1]; %Frame is uncracked
L=[3 0; 3 0; 6 0; 3 0; 3 0; 6 0; 3 0; 3 0; 6 0; 6 0]; %The column
of zeros can be deleted if all members are uncracked.
B=0.3; %Crack depth to section height ratio
CB=B*(2-B)/(0.9*((B-1)^2));  %Function corresponding to the
rotational spring model implemented by Caddemi and Caliò
ksc=Ec*Ic/(h*CB); ks(9,1)=ksc; %Equivalent spring stiffness for a
crack in Member 9.
reqmodes=[1  2  3  4]; %Required natural frequencies, must be
arranged in ascending order of modes
fr=length(reqmodes);  %Total  number  of  required  natural
frequencies
```

```
fe350=350; %Number of short elements the frame is divided into
for mode shape calculation
E350(1:fe350,1)=Ec; A350(1:fe350,1)=Ac;...
    I350(1:fe350,1)=Ic;  m350(1:fe350,1)=mc;  %Properties  of  the
short elements
L350(1:fe350,1)=0.12; L350(275,1)=0.03;...
    L350(275,2)=0.12-L350(275,1); %Each short element is 0.12 m
in length. Cracked element no. 275 is part of Member 9
mem350(1:fe350)=1; mem350(275)=2; %Lengths and number of portions
of the small elements
%X and Y Coordinates of the small elements' nodes, required for
mode shape plotting
coorx(1:51)=0.0; coorx(52:101)=0.12:0.12:6.0; coorx(102:151)=6.0;
coorx(152:201)=6.12:0.12:12.0; coorx(202:251)=12.0;
coorx(252:300)=0.12:0.12:5.88; coorx(301:349)=6.12:0.12:11.88;
coory(1:51)=0.0:0.12:6.00; coory(52:101)=6.0;
coory(102:151)=5.88:-0.12:0.0; coory(152:201)=6.0;
coory(202:251)=5.88:-0.12:0.0; coory(252:300)=3.0;
coory(301:349)=3.0;
%Node connectivity for the small elements
for i=1:fe350
    conn350(i,:)=[i i+1];
end;
conn350(151,:)=[101 152]; conn350(251,:)=[26 252];
conn350(300,:)=[300 126]; conn350(301,:)=[126 301];
for i=302:349
    conn350(i,:)=[i-1 i];
end;
conn350(350,:)=[349 226];
nodes350=349; %Total number of nodes for the small elements
%Angles of the small elements
angle350(1:50)=pi/2;
angle350([101:150 201:250])=-pi/2;
angle350([51:100 151:200 251:350])=0;
%Suppressed degrees of freedom for the small elements
sup350=[1 2 3 451 452 453 751 752 753]; %Nodes 1, 151, and 251
are  clamped  (these  correspond  to  Nodes  1,  6,  and  9  of  the
undivided frame
ks350(275,1)=ksc; %Equivalent spring stiffness for the crack in
Element 275, part of Member 9
w=0.000001; %Trial value for 'w'
J=WWfDKAG(w, nodes, sup, conn, angle, L, E, A, I, m, ks,...
    mem, fe);
for r=reqmodes %Calculating the required natural frequencies, the
orders of which are defined by 'reqmodes'
    while r>J %Establishing the lower and upper limits around the
required natural frequency
        wl=w; w=2*w; wu=w;
        J=WWfDKAG(w, nodes, sup, conn, angle, L, E,...
            A, I, m, ks, mem, fe);
    end;
    while (wu-wl)>0.000000000001  %Required accuracy
        w=(wu+wl)/2; %Bisection
        J=WWfDKAG(w, nodes, sup, conn, angle, L, E,...
            A, I, m, ks, mem, fe);
        if r>J
            wl=w;
        else
            wu=w;
        end;
    end;
```

```
    wr(r)=w;
end;
EUfHz(1:fr,1)=wr(reqmodes)./(2*pi)   %Exact   uncracked   natural
frequencies in Hz
UfHz(1:fr,1)=fix(EUfHz*1000)/1000; %Uncracked natural frequencies
considered up to three decimal places, to be used for crack
detection simulations
mem=[1 1 1 1 1 1 1 1 2 1]; %Member 9 has one crack
L=[3 0; 3 0; 6 0; 3 0; 3 0; 6 0; 3 0; 3 0;
    6*0.485 6*(1-0.485); 6 0];
w=0.000001;
J=WWfDKAG(w, nodes, sup, conn, angle, L, E, A, I, m, ks,...
    mem, fe);
for r=reqmodes
    while r>J
        wl=w; w=2*w; wu=w;
        J=WWfDKAG(w, nodes, sup, conn, angle, L, E,...
            A, I, m, ks, mem, fe);
    end;
    while (wu-wl)>0.000000000001
        w=(wu+wl)/2;
        J=WWfDKAG(w, nodes, sup, conn, angle, L, E,...
            A, I, m, ks, mem, fe);
        if r>J
            wl=w;
        else
            wu=w;
        end;
    end;
    wr(r)=w;
    modeshape(r,:)=WWfDKAGModeshapes(w, nodes350,...
        sup350, conn350, angle350, L350, E350,...
        A350, I350, m350, ks350, mem350, fe350);
end;
fHz(1:fr,1)=wr(reqmodes)./(2*pi)      %Natural      frequencies
corresponding to a crack in Member 9, having a crack depth to
section height ratio of 0.3
MfHz(1:fr,1)=fix(fHz*1000)/1000;  %Cracked  natural  frequencies
considered up to three decimal places, to be used for crack
detection simulations
for mode=reqmodes; %Mode shape calculations and plotting
dx([1 151 251])=0.0; %Zero horizontal displacements at clamped
nodes 1, 151, and 251 of the divided frame
dx([2:150 152:250 252:349])=0.2*modeshape(mode,1:3:1036); %0.2 is
an arbitrary scaling factor, 1036 is the horizontal degree of
freedom of node no. 346
dy([1 151 251])=0.0; %Zero vertical displacements at clamped
nodes 1, 151, and 251 of the divided frame
dy([2:150 152:250 252:349])=0.2*modeshape(mode,2:3:1037);
figure %Plotting the coordinates of each node + displacements
plot(coorx(1:151)+dx(1:151), coory(1:151)+dy(1:151))
hold all
plot(coorx([101 152:251])+dx([101 152:251]),...
    coory([101 152:251])+dy([101 152:251]))
hold all
plot(coorx([26 252:300 126 301:349 226])+...
    dx([26 252:300 126 301:349 226]),...
    coory([26 252:300 126 301:349 226])+...
    dy([26 252:300 126 301:349 226]))
end;
```

- MATLAB code for detecting crack location ranges in frames:

```
clear; clear all; format long;
fe=10;
Ec=206e9; Ic=0.198*((0.122)^3)/12; mc=185.3973; Ac=0.198*0.122;
h=0.122;
E(1:fe,1)=Ec; A(1:fe,1)=Ac; I(1:fe,1)=Ic; m(1:fe,1)=mc;
conn=[1 2; 2 3; 3 4; 4 5; 5 6; 4 7; 7 8; 8 9; 2 5; 5 8];
nodes=9; angle=[pi/2 pi/2 0 -pi/2 -pi/2 0 -pi/2 -pi/2 0 0];
sup=[1 2 3 16 17 18 25 26 27];
B=0.1; %Randomly assumed crack depth to section height ratio
CB=B*(2-B)/(0.9*((B-1)^2));
ksc=Ec*Ic/(h*CB); ks(1:10,1)=ksc;
reqmodes=[1 2 3 4]; fr=length(reqmodes);
UfHz=[3.267; 10.852; 12.084; 14.320]; %Simulated or measured
uncracked natural frequencies in Hz
MfHz=[3.267; 10.850; 12.069; 14.223]; %Simulated or measured
cracked natural frequencies in Hz
mem=[1 1 1 1 1 1 1 1 1 1];
L=[3 0; 3 0; 6 0; 3 0; 3 0; 6 0; 3 0; 3 0; 6 0; 6 0];
w=0.000001;
J=WWfDKAG(w, nodes, sup, conn, angle, L, E, A, I, m, ks,...
    mem, fe);
for r=reqmodes %Calculation of accurate uncracked natural
frequencies
    while r>J
        wl=w; w=2*w; wu=w;
        J=WWfDKAG(w, nodes, sup, conn, angle, L, E,...
            A, I, m, ks, mem, fe);
    end;
    while (wu-wl)>0.000000000001
        w=(wu+wl)/2;
        J=WWfDKAG(w, nodes, sup, conn, angle, L, E,...
            A, I, m, ks, mem, fe);
        if r>J
            wl=w;
        else
            wu=w;
        end;
    end;
    wr(r)=w;
end;
EUfHz(1:fr,1)=wr(reqmodes)./(2*pi)
d=[1 2 3 4 5 9]; %Crack is placed at each discretisation point in
the symmetric frame while calculating the cracked natural
frequencies and normalising the frequency variations
for di=1:length(d)
    mem=[1 1 1 1 1 1 1 1 1 1];
    L=[3 0; 3 0; 6 0; 3 0; 3 0; 6 0; 3 0; 3 0; 6 0; 6 0];
    %Discretisation points
    if L(d(di),1)==3
        p=[0.1 0.15:0.15:2.85 2.9]; location=p./L(d(di),1);
    else p=[0.1 0.15:0.15:5.85 5.9]; location=p./L(d(di),1);
    end;
    mem(d(di))=2;
    for dp=1:length(p)
        if sum(L(d(di),:))==3.0
            L(d(di),:)=[p(dp) 3.0-p(dp)];
        else L(d(di),:)=[p(dp) 6.0-p(dp)];
        end;
```

```
            w=0.000001;
            J=WWfDKAG(w, nodes, sup, conn, angle, L, E, A,...
                I, m, ks, mem, fe);
            for r=reqmodes
                while r>J
                    wl=w; w=2*w; wu=w;
                    J=WWfDKAG(w, nodes, sup, conn, angle,...
                        L, E, A, I, m, ks, mem, fe);
                end;
                while (wu-wl)>0.000000000001
                    w=(wu+wl)/2;
                    J=WWfDKAG(w, nodes, sup, conn, angle,...
                        L, E, A, I, m, ks, mem, fe);
                    if r>J
                        wl=w;
                    else
                        wu=w;
                    end;
                end;
                wr(r)=w;
            end;
            format long;
            dltafHz(((fr*d(di))-(fr-1)):(fr*d(di)),dp)=...
                (EUfHz-(wr(reqmodes)./(2*pi))')./EUfHz;
            ndltafHz(((fr*d(di))-(fr-1)):(fr*d(di)),dp)=...
                dltafHz(((fr*d(di))-(fr-1)):(fr*d(di)),dp)./...
                norm(dltafHz(((fr*d(di))-(fr-1)):(fr*d(di)),dp));
            %Exact normalised natural frequency variations
        end;
        intervalinput(1,1:2:(2*fr))=UfHz';
        intervalinput(1,2:2:(2*fr))=MfHz'; %Preparing inputs to be
used for the 'interval' function
        %Error in uncracked freq.
        error(1:2:(2*fr),1)=[0.005; 0.005; 0.005; 0.005];
        %Error in cracked freq.
        error(2:2:(2*fr),1)=[0.005; 0.005; 0.005; 0.005];
        for i=1:fr
            intervalindex(i:fr:(fr*fe),1)=i; %Required input for the
function 'interval' where each natural frequency is assigned an
index number 1, 2, 3,...etc.
        end;
        figure('DefaultAxesFontName','Arial',...
            'DefaultAxesFontSize',11)
        icounter=((fr*d(di))-(fr-1)):(fr*d(di));
        for  i=1:length(icounter)  %Loop  for  detecting  the  crack
location ranges by calculating the intervals for the simulated or
measured normalised natural frequency variations then calculating
their intersections with the interpolated normalised frequency
variation curves while plotting the results
            rdloc(icounter(i),:)=interval(intervalindex...
                (icounter(i),1),intervalinput,error);
            v(icounter(i))=csapi(location,...
                ndltafHz(icounter(i),1:length(location)));
            LocLLtempv=fnzeros(fncmb(v(icounter(i)),...
                '-',rdloc(icounter(i),1)));
            LocLL(icounter(i),1:length(LocLLtempv(1,:)))=...
                LocLLtempv(1,:);
            LocULtempv=fnzeros(fncmb(v(icounter(i)),'-',...
                rdloc(icounter(i),2)));
            LocUL(icounter(i),1:length(LocULtempv(1,:)))=...
                LocULtempv(1,:);
```

```
            format short
            srange(icounter(i),1:length([LocLLtempv(1,:)...
                LocULtempv(1,:)]))=sort([LocLLtempv(1,:)...
                LocULtempv(1,:)]) %sorted ranges
            subplot(fr,1,i);
            if L(d(di),1)==2.9
            xx=[0.1/3 0.04:0.01:0.95 2.9/3];
            else xx=[0.1/6 0.02:0.01:0.97 5.9/6];
            end; %Extra points for curve plotting
            yy=[]; yy(1:length(xx))=0;
            for pl=1:length(xx)
                yy(pl)=csapi(location,ndltafHz(...
                    icounter(i),1:length(location)),xx(pl));
                if csapi(location,ndltafHz(icounter(i),...
                        1:length(location)),xx(pl))<0
                    yy(pl)=0;
                end;
                if csapi(location,ndltafHz(icounter(i),...
                        1:length(location)),xx(pl))>1
                    yy(pl)=1;
                end;
            end;
            plot(xx,yy,'-k','LineWidth',2),hold on,...
                plot([0 1],[rdloc(icounter(i),1) ...
                rdloc(icounter(i),1)] ,':k'), hold on,...
                plot([0 1],[rdloc(icounter(i),2) ...
                rdloc(icounter(i),2)],':k'), hold on
            for j=1:length(LocLL(icounter(i),:))
                if LocLL(icounter(i),j)~=0
                    plot([LocLL(icounter(i),j) ...
                        LocLL(icounter(i),j)],[0 1],':k'),hold on
                end;
            end;
            for j=1:length(LocUL(icounter(i),:))
                if LocUL(icounter(i),j)~=0
                    plot([LocUL(icounter(i),j) ...
                        LocUL(icounter(i),j)],[0 1],':k'),hold on
                end;
            end;
            daspect([1 5 1]);    %To control the axes width
            text(0.3,rdloc(icounter(i),1),'Lower Limit',...
                'HorizontalAlignment','right',...
                'VerticalAlignment','Bottom','fontsize',...
                11,'fontname','Arial')
            text(0.3,rdloc(icounter(i),2),'Upper Limit',...
                'HorizontalAlignment','right',...
                'VerticalAlignment','Top','fontsize',11,...
                'fontname','Arial')
            xlabel('                  ','fontsize',11,...
                'fontname','Arial','fontangle','italic');
            axis([0 1.0 0 1.005])
            set(gca,'XTick',0:0.1:1.0)
            set(gca,'XTickLabel',{'0','','0.2','','0.4',...
                '','0.6','','0.8','','1.0'})
            set(gca,'YTick',0:0.5:1.0)
            set(gca,'YTickLabel',{'0','0.5','1.0'})
        end;
    end;
```

- MATLAB code for detecting crack severity ranges in frames:

```
clear; clear all;
fe=10; %Number of frame members
Ec=206e9; Ic=0.198*((0.122)^3)/12; mc=185.3973; Ac=0.198*0.122;
h=0.122; E(1:fe,1)=Ec; A(1:fe,1)=Ac; I(1:fe,1)=Ic; m(1:fe,1)=mc;
conn=[1 2; 2 3; 3 4; 4 5; 5 6; 4 7; 7 8; 8 9; 2 5; 5 8];
nodes=9; angle=[pi/2 pi/2 0 -pi/2 -pi/2 0 -pi/2 -pi/2 0 0];
sup=[1 2 3 16 17 18 25 26 27];
UfHz=[3.267; 10.852; 12.084; 14.320]; %Simulated or measured
uncracked natural frequencies in Hz
MfHz=[3.267; 10.850; 12.069; 14.223]; %Simulated or measured
cracked natural frequencies in Hz
uerror=[0.005; 0.005; 0.005; 0.005]; %Error in uncracked freq.
merror=[0.005; 0.005; 0.005; 0.005]; %Error in cracked freq.
freq=[1 2 3 4]; %Mode numbers
loc=[0.003:0.003:5.997]; %Detected crack location range in Member
9
for iloc=1:length(loc)
    mem=[1 1 1 1 1 1 1 1 2 1];
    L=[3 0; 3 0; 6 0; 3 0; 3 0; 6 0; 3 0; 3 0;
       loc(iloc) 6-loc(iloc); 6 0];
    for ifreq=1:length(freq)
        %Two Possible cases for the uncracked and cracked natural
frequency ranges corresponding to one mode
        if MfHz(ifreq)+merror(ifreq) <=...
                UfHz(ifreq)-uerror(ifreq)     %No     overlapping
frequency ranges
                w=(MfHz(ifreq)+merror(ifreq))*2*pi;
                %Frequency in rad s-1
                 Bl=0.0001; Bu=1.0; %Lower and upper limits for
the crack depth to section height ratio B
                for r=freq(ifreq)
                    while (Bu-Bl)>0.000000000001
                        B=(Bu+Bl)/2; %Bisection
                        CB=B*(2-B)/(0.9*((B-1)^2));
                        ksc=Ec*Ic/(h*CB); ks(1:10,1)=ksc;
                        J=WWfDKAG(w, nodes, sup, conn, angle,...
                            L, E, A, I, m, ks, mem, fe);
                        if r>J
                            Bl=B;
                        else
                            Bu=B;
                        end;
                    end;
                    Br=B;
                end;
                LLBfinal(ifreq)=Br; %Lower limit for the crack
severity
                ULfHz(ifreq)=w/(2*pi); %Upper limit for the
frequency
                w=(MfHz(ifreq)-merror(ifreq))*2*pi;
                Bl=0.0001; Bu=1.0;
                for r=freq(ifreq)
                    while (Bu-Bl)>0.000000000001
                        B=(Bu+Bl)/2; CB=B*(2-B)/(0.9*((B-1)^2));
                        ksc=Ec*Ic/(h*CB); ks(1:10,1)=ksc;
                        J=WWfDKAG(w, nodes, sup, conn, angle,...
                            L, E, A, I, m, ks, mem, fe);
                        if r>J
                            Bl=B;
```

```
                        else
                            Bu=B;
                        end;
                    end;
                    Br=B;
                end;
                ULBfinal(ifreq)=Br;  %Upper  limit  for  the  crack
severity
                LLfHz(ifreq)=w/(2*pi);   %Lower   limit   for   the
frequency
        else %In the case of overlapping frequency ranges
            w=(MfHz(ifreq)-merror(ifreq))*2*pi;
            Bl=0.0001; Bu=1.0;
            for r=freq(ifreq)
                while (Bu-Bl)>0.000000000001
                    B=(Bu+Bl)/2; CB=B*(2-B)/(0.9*((B-1)^2));
                    ksc=Ec*Ic/(h*CB); ks(1:10,1)=ksc;
                    J=WWfDKAG(w, nodes, sup, conn, angle, L,...
                        E, A, I, m, ks, mem, fe);
                    if r>J
                        Bl=B;
                    else
                        Bu=B;
                    end;
                end;
                Br=B;
            end;
            ULBfinal(ifreq)=Br; LLfHz(ifreq)=w/(2*pi);
            LLBfinal(ifreq)=0; ULfHz(ifreq)=w/(2*pi);
        end;
    end;
    RBfinal(((length(freq)*iloc)-(length(freq)-1)):...
             (length(freq)*iloc),1)=loc(iloc);
    RBfinal(((length(freq)*iloc)-(length(freq)-1)):...
             (length(freq)*iloc),2:5)=...
             [ULfHz' LLBfinal' LLfHz' ULBfinal'];
    CRBfinal(iloc,:)=[loc(iloc) max(LLBfinal) min(ULBfinal)];
    %Final Common Ranges for B
end;
RBfinal
delindex=0;  %delete incorrect ranges and replace with zero
for i=1:length(CRBfinal(:,1))
    if CRBfinal(i,2)>=CRBfinal(i,3)
        delindex=delindex+1;
        del(delindex)=i;
    end;
end;
if delindex>0
    CRBfinal(del,:)=[];
end;
if isempty(CRBfinal)
else
    xlswrite('Branges.xlsx',CRBfinal)
    figure
    plot(CRBfinal(:,1), CRBfinal(:,2),...
        CRBfinal(:,1), CRBfinal(:,3))
end;
CRBfinal
```

References

Adams, R.D., Cawley, P., Pye, C.J. and Stone, B.J. 1978. A vibration technique for non-destructively assessing the integrity of structures. *Journal of Mechanical Engineering Science*, 20(2), pp. 93-100.

Banerjee, J.R. and Guo, S. 2009. On the dynamics of cracked beams. *50th AIAA/ASME/ASCE/AHS/ASC Structures, Structural Dynamics, and Materials Conference*. American Institute of Aeronautics and Astronautics.

Berger, J. and Wilson, D. 2011. Hole in Southwest jet attributed to cracks. *The New York Times*, 3 April 2011.

Bicanic, N. and Chen, H.-P. 1997. Damage identification in framed structures using natural frequencies. *International Journal for Numerical Methods in Engineering*, 40(23), pp. 4451-4468.

Błaszkowiak, S. and Kączkowski, Z. 1966. *Iterative methods in structural analysis*. Oxford: Pergamon Press.

Blevins, R.D. 1979. *Formulas for natural frequency and mode shape*. Florida: Robert E. Krieger.

Brasiliano, A., Doz, G.N. and de Brito, J.L.V. 2004. Damage identification in continuous beams and frame structures using the Residual Error Method in the Movement Equation. *Nuclear Engineering and Design*, 227(1), pp. 1-17.

Brigham, E.O. 1988. *The fast Fourier transform and its applications*. New Jersey: Prentice Hall.

Caddemi, S. and Caliò, I. 2008. Exact solution of the multi-cracked Euler–Bernoulli column. *International Journal of Solids and Structures*, 45(5), pp. 1332-1351.

Caddemi, S. and Caliò, I. 2009. Exact closed-form solution for the vibration modes of the Euler–Bernoulli beam with multiple open cracks. *Journal of Sound and Vibration*, 327(3–5), pp. 473-489.

Caddemi, S. and Caliò, I. 2013. The exact explicit dynamic stiffness matrix of multi-cracked Euler–Bernoulli beam and applications to damaged frame structures. *Journal of Sound and Vibration*, 332(12), pp. 3049-3063.

Caddemi, S. and Caliò, I. 2014. Exact reconstruction of multiple concentrated damages on beams. *Acta Mechanica*, 225(11), pp. 3137-3156.

Caddemi, S. and Greco, A. 2006. The influence of instrumental errors on the static identification of damage parameters for elastic beams. *Computers and Structures*, 84(26–27), pp. 1696-1708.

Caddemi, S. and Morassi, A. 2007. Crack detection in elastic beams by static measurements. *International Journal of Solids and Structures*, 44(16), pp. 5301-5315.

Caddemi, S. and Morassi, A. 2013. Multi-cracked Euler–Bernoulli beams: Mathematical modeling and exact solutions. *International Journal of Solids and Structures*, 50(6), pp. 944-956.

Cerri, M.N. and Vestroni, F. 2000. Detection of damage in beams subjected to diffused cracking. *Journal of Sound and Vibration*, 234(2), pp. 259-276.

Cerri, M.N. and Vestroni, F. 2003. Use of Frequency Change for Damage Identification in Reinforced Concrete Beams. *Journal of Vibration and Control*, 9(3-4), pp. 475-491.

Chati, M., Rand, R. and Mukherjee, S. 1997. Modal analysis of a cracked beam. *Journal of Sound and Vibration*, 207(2), pp. 249-270.

Chatzi, E.N., Hiriyur, B., Waisman, H. and Smyth, A.W. 2011. Experimental application and enhancement of the XFEM–GA algorithm for the detection of flaws in structures. *Computers and Structures*, 89(7–8), pp. 556-570.

Chinchalkar, S. 2001. Determination of crack location in beams using natural frequencies. *Journal of Sound and Vibration*, 247(3), pp. 417-429.

Chondros, T.G., Dimarogonas, A.D. and Yao, J. 1998. A continuous cracked beam vibration theory. *Journal of Sound and Vibration*, 215(1), pp. 17-34.

Chondros, T.G., Dimarogonas, A.D. and Yao, J. 2001. Vibration of a beam with a breathing crack. *Journal of Sound and Vibration*, 239(1), pp. 57-67.

Christides, S. and Barr, A.D.S. 1984. One-dimensional theory of cracked Bernoulli-Euler beams. *International Journal of Mechanical Sciences*, 26(11–12), pp. 639-648.

Ciambella, J. and Vestroni, F. 2015. The use of modal curvatures for damage localization in beam-type structures. *Journal of Sound and Vibration*, 340, pp. 126-137.

Danai, K., Civjan, S.A. and Styckiewicz, M.M. 2012. Direct method of damage localization for civil structures via shape comparison of dynamic response measurements. *Computers and Structures*, 92–93(0), pp. 297-307.

Diaferio, M. and Sepe, V. 2015. Modal identification of damaged frames. *Structural Control and Health Monitoring*, pp. n/a-n/a.

Dimarogonas, A.D. 1996. Vibration of cracked structures: A state of the art review. *Engineering Fracture Mechanics*, 55(5), pp. 831-857.

Doebling, S.W., Farrar, C.R. and Prime, M.B. 1998. A summary review of vibration-based damage identification methods. *The Shock and Vibration Digest*, 30(2), pp. 91-105.

Escobar, J.A., Sosa, J.J. and Gómez, R. 2005. Structural damage detection using the transformation matrix. *Computers and Structures*, 83(4–5), pp. 357-368.

Ewins, D.J. 1984. *Modal testing: theory and practice*. Hertfordshire: Research Studies Press.

Fang, X., Luo, H. and Tang, J. 2005. Structural damage detection using neural network with learning rate improvement. *Computers and Structures*, 83(25–26), pp. 2150-2161.

Friswell, M.I. 2007. Damage identification using inverse methods. *Philosophical Transactions of the Royal Society A: Mathematical, Physical and Engineering Sciences*, 365(1851), pp. 393-410.

Friswell, M.I., Penny, J.E.T. and Garvey, S.D. 1998. A combined genetic and eigensensitivity algorithm for the location of damage in structures. *Computers and Structures*, 69(5), pp. 547-556.

Galef, A.E. 1968. Bending frequencies of compressed beams. *The Journal of the Acoustical Society of America*, 44(2), pp. 643-643.

Ge, M. and Lui, E.M. 2005. Structural damage identification using system dynamic properties. *Computers and Structures*, 83(27), pp. 2185-2196.

Ghadami, A., Maghsoodi, A. and Mirdamadi, H.R. 2013. A new adaptable multiple-crack detection algorithm in beam-like structures. *Archives of Mechanics*, 65(6), pp. 469-483.

Gillich, G.-R. and Praisach, Z.-I. 2014. Modal identification and damage detection in beam-like structures using the power spectrum and time–frequency analysis. *Signal Processing*, 96, Part A, pp. 29-44.

Gillich, G.R., Mituletu, I.C., Negru, I., Tufoi, M., Iancu, V. and Muntean, F. 2015. A method to enhance frequency readability for early damage detection. *Journal of Vibration Engineering and Technologies*, 3(5), pp. 637-652.

Gounaris, G. and Dimarogonas, A. 1988. A finite element of a cracked prismatic beam for structural analysis. *Computers and Structures*, 28(3), pp. 309-313.

Greco, A. and Pau, A. 2012. Damage identification in Euler frames. *Computers and Structures*, 92–93(0), pp. 328-336.

Hassiotis, S. 2000. Identification of damage using natural frequencies and Markov parameters. *Computers and Structures*, 74(3), pp. 365-373.

Hassiotis, S. and Jeong, G.D. 1993. Assessment of structural damage from natural frequency measurements. *Computers and Structures*, 49(4), pp. 679-691.

Hassiotis, S. and Jeong, G.D. 1995. Identification of stiffness reductions using natural frequencies. *Journal of Engineering Mechanics*, 121(10), pp. 1106-1113.

He, R.-S. and Hwang, S.-F. 2006. Damage detection by an adaptive real-parameter simulated annealing genetic algorithm. *Computers and Structures*, 84(31–32), pp. 2231-2243.

Hearn, G. and Testa, R. 1991. Modal analysis for damage detection in structures. *Journal of Structural Engineering*, 117(10), pp. 3042-3063.

Howson, W.P. 1979. A compact method for computing the eigenvalues and eigenvectors of plane frames. *Advances in Engineering Software (1978)*, 1(4), pp. 181-190.

Hu, J. and Liang, R.Y. 1993. An integrated approach to detection of cracks using vibration characteristics. *Journal of the Franklin Institute*, 330(5), pp. 841-853.

Jiang, S.-F., Zhang, C.-M. and Zhang, S. 2011. Two-stage structural damage detection using fuzzy neural networks and data fusion techniques. *Expert Systems with Applications*, 38(1), pp. 511-519.

Kam, T.Y. and Lee, T.Y. 1992. Detection of cracks in structures using modal test data. *Engineering Fracture Mechanics*, 42(2), pp. 381-387.

Kao, C.Y. and Hung, S.-L. 2003. Detection of structural damage via free vibration responses generated by approximating artificial neural networks. *Computers and Structures*, 81(28–29), pp. 2631-2644.

Khiem, N.T. and Lien, T.V. 2001. A simplified method for natural frequency analysis of a multiple cracked beam. *Journal of Sound and Vibration*, 245(4), pp. 737-751.

Khiem, N.T. and Tran, H.T. 2014. A procedure for multiple crack identification in beam-like structures from natural vibration mode. *Journal of Vibration and Control*, 20(9), pp. 1417-1427.

Labib, A., Kennedy, D. and Featherston, C.A. 2014. Free vibration analysis of beams and frames with multiple cracks for damage detection. *Journal of Sound and Vibration*, 333(20), pp. 4991-5003.

Labib, A., Kennedy, D. and Featherston, C.A. 2015. Crack localisation in frames using natural frequency degradations. *Computers and Structures*, 157(0), pp. 51-59.

Lee, J. 2009. Identification of multiple cracks in a beam using natural frequencies. *Journal of Sound and Vibration*, 320(3), pp. 482-490.

Lee, Y.S. and Chung, M.J. 2000. A study on crack detection using eigenfrequency test data. *Computers and Structures*, 77(3), pp. 327-342.

Liang, R., Hu, J. and Choy, F. 1992. Theoretical study of crack-induced eigenfrequency changes on beam structures. *Journal of Engineering Mechanics*, 118(2), pp. 384-396.

Liang, R.Y., Choy, F.K. and Hu, J. 1991. Detection of cracks in beam structures using measurements of natural frequencies. *Journal of the Franklin Institute*, 328(4), pp. 505-518.

Lien, T.V., Nguyen, K. and Hao, T.A. 2014. Crack identification in frame structures by using the stationary wavelet transform of mode shapes. *Jökull Journal*, 64(6).

Lin, H.P., Chang, S.C. and Wu, J.D. 2002. Beam vibrations with an arbitrary number of cracks. *Journal of Sound and Vibration*, 258(5), pp. 987-999.

Maghsoodi, A., Ghadami, A. and Mirdamadi, H.R. 2013. Multiple-crack damage detection in multi-step beams by a novel local flexibility-based damage index. *Journal of Sound and Vibration*, 332(2), pp. 294-305.

Maplesoft, 2013, *MAPLE*, version 17, computer program, Waterloo Maple Inc., Waterloo, Ontario, Canada.

MathWorks, 2012, *MATLAB*, version 7.14, computer program, The MathWorks Inc., Natick, MA, USA.

Meyer, P.L. 1965. *Introductory Probability and Statistical Applications*. Reading: Addison-Wesley.

Moore, R.E. 1979. *Methods and applications of interval analysis*. Philadelphia: Society for Industrial and Applied Mathematics.

Moradi, S., Razi, P. and Fatahi, L. 2011. On the application of bees algorithm to the problem of crack detection of beam-type structures. *Computers and Structures*, 89(23–24), pp. 2169-2175.

Morassi, A. 1993. Crack-induced changes in eigenparameters of beam structures. *Journal of Engineering Mechanics*, 119(9), pp. 1798-1803.

Morassi, A. 2008. Damage detection in vibrating beams. In: Morassi, A. and Vestroni, F. eds. *Dynamic methods for damage detection in structures*. Vol. 499. Vienna: Springer-Verlag Wien, pp. 137-182.

Morassi, A. and Rovere, N. 1997. Localizing a notch in a steel frame from frequency measurements. *Journal of Engineering Mechanics*, 123(5), pp. 422-432.

Nandakumar, P. and Shankar, K. 2014. Multiple crack damage detection of structures using the two crack transfer matrix. *Structural Health Monitoring*, 13(5), pp. 548-561.

Nikolakopoulos, P.G., Katsareas, D.E. and Papadopoulos, C.A. 1997. Crack identification in frame structures. *Computers and Structures*, 64(1–4), pp. 389-406.

Ostachowicz, W.M. and Krawczuk, M. 1991. Analysis of the effect of cracks on the natural frequencies of a cantilever beam. *Journal of Sound and Vibration*, 150(2), pp. 191-201.

Pandey, A.K., Biswas, M. and Samman, M.M. 1991. Damage detection from changes in curvature mode shapes. *Journal of Sound and Vibration*, 145(2), pp. 321-332.

Patil, D.P. and Maiti, S.K. 2003. Detection of multiple cracks using frequency measurements. *Engineering Fracture Mechanics*, 70(12), pp. 1553-1572.

Pau, A., Greco, A. and Vestroni, F. 2011. Numerical and experimental detection of concentrated damage in a parabolic arch by measured frequency variations. *Journal of Vibration and Control*, 17(4), pp. 605-614.

Perry, M.J., Koh, C.G. and Choo, Y.S. 2006. Modified genetic algorithm strategy for structural identification. *Computers and Structures*, 84(8–9), pp. 529-540.

Rao, M.A., Srinivas, J. and Murthy, B.S.N. 2004. Damage detection in vibrating bodies using genetic algorithms. *Computers and Structures*, 82(11–12), pp. 963-968.

Ratcliffe, C.P. 2000. A frequency and curvature based experimental method for locating damage in structures. *Journal of Vibration and Acoustics*, 122(3), pp. 324-329.

Rizos, P.F., Aspragathos, N. and Dimarogonas, A.D. 1990. Identification of crack location and magnitude in a cantilever beam from the vibration modes. *Journal of Sound and Vibration*, 138(3), pp. 381-388.

Rubio, L., Fernández-Sáez, J. and Morassi, A. 2014. Identification of two cracks with different severity in beams and rods from minimal frequency data. *Journal of Vibration and Control*.

Rytter, A. 1993. *Vibrational based inspection of civil engineering structures.* PhD Thesis, Aalborg University.

Sharma, D.S., Mungla, M.J. and Barad, K.H. 2015. Vibration-based non-destructive technique to detect crack in multi-span beam. *Nondestructive Testing and Evaluation*, pp. 1-21.

Shen, M.H.H. and Chu, Y.C. 1992. Vibrations of beams with a fatigue crack. *Computers and Structures*, 45(1), pp. 79-93.

Shen, M.H.H. and Pierre, C. 1990. Natural modes of Bernoulli-Euler beams with symmetric cracks. *Journal of Sound and Vibration*, 138(1), pp. 115-134.

Shifrin, E.I. and Ruotolo, R. 1999. Natural frequencies of a beam with an arbitrary number of cracks. *Journal of Sound and Vibration*, 222(3), pp. 409-423.

Solís, M., Algaba, M. and Galvín, P. 2013. Continuous wavelet analysis of mode shapes differences for damage detection. *Mechanical Systems and Signal Processing*, 40(2), pp. 645-666.

Teughels, A., Maeck, J. and De Roeck, G. 2002. Damage assessment by FE model updating using damage functions. *Computers and Structures*, 80(25), pp. 1869-1879.

Titurus, B., Friswell, M.I. and Starek, L. 2003a. Damage detection using generic elements: Part I. Model updating. *Computers and Structures*, 81(24–25), pp. 2273-2286.

Titurus, B., Friswell, M.I. and Starek, L. 2003b. Damage detection using generic elements: Part II. Damage detection. *Computers and Structures*, 81(24–25), pp. 2287-2299.

Vakil-Baghmisheh, M.-T., Peimani, M., Sadeghi, M.H. and Ettefagh, M.M. 2008. Crack detection in beam-like structures using genetic algorithms. *Applied Soft Computing*, 8(2), pp. 1150-1160.

Vestroni, F. and Capecchi, D. 2000. Damage detection in beam structures based on frequency measurements. *Journal of Engineering Mechanics*, 126(7), pp. 761-768.

Wang, Z. and Ong, K.C.G. 2008. Autoregressive coefficients based Hotelling's T^2 control chart for structural health monitoring. *Computers and Structures*, 86(19–20), pp. 1918-1935.

Werfelman, L. 2011. Crackdown on fatigue. *Aerosafety World*, March 2011.

Wickramarachi, P. 2003. Effects of windowing on the spectral content of a signal. *Sound and Vibration*, January 2003, pp. 10-11.

Williams, F.W. and Kennedy, D. 1988. Reliable use of determinants to solve non-linear structural eigenvalue problems efficiently. *International Journal for Numerical Methods in Engineering*, 26(8), pp. 1825-1841.

Williams, F.W. and Wittrick, W.H. 1970. An automatic computational procedure for calculating natural frequencies of skeletal structures. *International Journal of Mechanical Sciences*, 12(9), pp. 781-791.

Wittrick, W.H. and Williams, F.W. 1971. A general algorithm for computing natural frequencies of elastic structures. *The Quarterly Journal of Mechanics and Applied Mathematics*, 24(3), pp. 263-284.

Wolberg, G. 1988. *Fast Fourier transforms: A review*. New York: Department of Computer Science, Columbia University.

Xiang, J., Liang, M. and He, Y. 2014. Experimental investigation of frequency-based multi-damage detection for beams using support vector regression. *Engineering Fracture Mechanics*, 131, pp. 257-268.

Yang, J.C.S., Tsai, T., Pavlin, V., Chen, J. and Tsai, W.H. 1985. Structural damage detection by the system identification technique. *Shock and Vibration Bulletin*, 55, pp. 57-66.

Yoon, M.-K., Heider, D., Gillespie, J., Jr., Ratcliffe, C. and Crane, R. 2009. Local damage detection with the global fitting method using mode shape data in notched Beams. *Journal of Nondestructive Evaluation*, 28(2), pp. 63-74.

Yun, C.-B. and Bahng, E.Y. 2000. Substructural identification using neural networks. *Computers and Structures*, 77(1), pp. 41-52.

Zheng, D.Y. and Kessissoglou, N.J. 2004. Free vibration analysis of a cracked beam by finite element method. *Journal of Sound and Vibration*, 273(3), pp. 457-475.